Estimation of Stripping by Static Immersion Test using Image Processing and Machine Learning

by

Ashkan Sahari Moghaddam

A thesis
submitted to the Faculty of Graduate Studies
in partial fulfilment of the requirements for the
Degree of Master of Science
in

Civil Engineering

Supervisor
Dr. Ehsan Rezazadeh Azar
Assistant Professor – Dept. of Civil Engineering

Lakehead University
Thunder Bay, Ontario
May 2019

Author's Declaration

I hereby declare that I am the sole author of the thesis. This is a true copy of the thesis, including any required final revisions, as accepted by my examiners.

I understand that my thesis may be made electronically available to the public.

Abstract

Hot Mixed Asphalt (HMA) is one of the most common types of pavement, which exists on the surface of the roads, inside and outside of cities. One of the main destresses in HMA is moisture-related damage, which mainly occurs in the form of stripping. The process of losing adhesion and cohesion of asphalt cement due to the presence of moisture and cyclic loads is called “stripping”. Several test procedures have been designed and conducted on different types of asphaltic mixtures to identify and measure moisture damages, especially stripping. Stripping evaluations could be divided into two classes: tests on compacted mixtures and tests on loose mixtures. Test procedures for loose mixture have been adopted by different highway agencies, such as the Ministry of Transportation Ontario (MTO), and pavement industries, because they are easy to perform, cost-effective, and do not require complex equipment. But since stripping estimation is based on visual assessment, the results could be inconsistent when they are estimated by inexperienced operators. One of the most common tests on loose mixtures is static immersion test, and a modified version of the static immersion test has been used by MTO, listed as LS-285 R29. To evaluate stripping in this test procedure, 104g of loose asphaltic mixture should be immersed inside water for 24 hours and then the retained coating areas should be measured by a skilled technician as a percentage of the total surface area.

Image processing methods are proper examples of using smart agents in visual assessment problems, such as object detection and pattern recognition. In this research, a vision-based algorithm and a low-cost light improvement system were developed as an alternative for manual judgment. The system receives images of samples captured in a controlled lighting condition, which is called illumination box, and then it applies Contrast Limited Adaptive Histogram

Equalization to enhance contrast intensity of the image. In addition, the system uses inpainting to reconstruct specular highlights in the image, and then classifies the regions on the image, i.e. coated and stripped areas, using combinations of K-means clustering and K-Nearest Neighbors and Support Vector Machines classifiers. The developed system is able to overcome most of the shortcomings of prior methods, such as evaluation of the stripping on mixtures with dark-colour aggregates and processing test images without alteration of the test samples. The differences of the results in the best configuration of classifiers from manual estimations had the mean of 4.8 % and the standard deviation of 5.2 %. Moreover, application of illumination box and contrast enhancement module proved to be effective to improve the performance of this system.

Acknowledgments

Over the past two years of master study at Lakehead University, I have received support and encourage from many individuals. First and foremost, I would like to express my deepest appreciation to my supervisor, Prof. Ehsan Rezazadeh Azar, for his patient guidance. During writing, he spent countless hours on proofreading my thesis, providing constructive suggestions, and helping me whenever I had issues on my thesis. I have learned much through his teaching. I could not reach this stage without his supervision. It is such an honour to be his student. I would also like to thank Dr. Pernia and Dr. Liao for accepting to be on my examination committee.

I would also like to thank Pamela Marks, Zain Islam, Dr. Yolibeth Mejias, Heather Bell, and Heera Shakya from the Ministry of Transportation of Ontario for their great help and support during this project. This work was financially supported by the Ministry of Transportation of Ontario Highway Infrastructure Innovation Funding Program.

Especially, I would like to appreciate my parents, who are always supporting me financially and emotionally in any circumstances. They always protect me and offer the help as far as possible for many years. Thank them for giving me endless love.

At last but not least, I would also like to thank my friends and faculty members of the civil engineering department in Lakehead University for all the encouragements and supports they provided to me especially my dear friend Pooya.

Table of Contents

List of Figures

List of Tables

Nomenclature/List of Acronyms

2D	Two Dimensional
3D	Three Dimensional
AHE	Adaptive Histogram Equalization
AI	Artificial Intelligence
ATPM	Asphalt-Treated Permeable Material
BWT	Boiling Water Test
C_SVC	C-Support Vector Classification
CDF	Cumulative Distribution Function
CLAHE	Contrast Limited Adaptive Histogram Equalization
CLUT	Colour Look-Up Table
DTS	Direct Tensile Strength
EM	Expectation maximization
ENVI	Environment for Visualizing Images
F_T	Freeze-Thaw
FMM	Fast Marching Method
HMA	Hot-Mixed Asphalt
IT	Information Technology
K-NN	K-Nearest Neighbors
K-NN3	K-Nearest Neighbors performing on three clusters
K-NN4	K-Nearest Neighbors performing on four clusters
L*	Contrast Light intensity for each pixel
LED	Light-Emitted Diode
MAS	Multi-Agent System
MDF	Medium-Density Fiberboard
MTO	Ministry of Transportation Ontario
PCM	Pulse Code Modulation
PDE	Partial Differential Equation
r	Capillary action

RBT	Rolling Bottle Test
RGB	Red Green Blue
ROI	Region of Interest
SVM	Support Vector Machines
SVM3	Support Vector Machines performing on three clusters
SVM4	Support Vector Machines performing on four clusters
Ts	the surface tension of water
W_D	Wet Dry
WCSS	Within-Cluster Sum of Squares
WMA	Warm-Mixed Asphalt
α	the liquid-solid contact angle
ρ	the density of water

Chapter 1: Introduction

1.1. Background and Research Motivation

Asphalt pavements are among the most common type of pavements which could be divided into warm-mixed asphalt (WMA) and hot-mixed asphalt (HMA) pavements. There are continuous research efforts to improve the durability of asphalt pavements, which include the research on identifying causes of damages and how to assess the quality of the pavements. The durability of asphalt pavements is directly influenced by the moisture sensitivity of the mixture (Chen, 2007; Liu et al., 2014). The destructive effect of moisture in asphalt pavements was recognized in the 1930s, and highway agencies and pavement industries started to investigate the damages caused by moisture in the 1980s (Lantieri et al., 2017). Moisture damage is the degree of reduction in an asphaltic system's performance which is caused by moisture. Moisture transports into an asphaltic system by various transportation modes and causes cohesive and adhesive failure in the asphalt cement coating (Caro et al., 2008). One of the main forms of moisture damage is stripping. Stripping is a phenomenon in which the asphalt cement coating detaches from the aggregate surface, and it is mainly due to the failure in the internal texture of asphalt in the presence of moisture and cyclic traffic load (Mehrara and Khodaii, 2013).

The most common test procedures to evaluate the moisture susceptibility of loose asphalt mixtures are boiling water, rolling bottle, and static immersion tests. The Ministry of Transportation Ontario has been utilizing a modified version of static immersion test, named LS-285 R29, which is conducted using 100g of sample aggregate and 4 grams of asphalt cement (Ministry of Transportation Ontario, 1996). Static immersion and rolling bottle (EN 12697-11) methods are subjective test procedures, because the stripping is measured by evaluating the retained coating percentage based on the judgment of a technician. To overcome possible

subjectivity image processing-based algorithms were proposed to provide consistent and accurate results (Kim et al., 2012; Amelian et al., 2014).

Also, Artificial Intelligence (AI) methods have been able to facilitate informed decision making and uncover information and patterns where the traditional approaches fail to recognize. Image processing and machine learning algorithms, including supervised (classification) and unsupervised learning (e.g. clustering), are potential AI tools to improve visual assessment problems. Supervised learning methods aim at classifying test data based on the provided training data set, whereas unsupervised learning methods process test data based on predefined rules and without training data (Nemati et al., 2002).

In addition, images and videos are valuable sources of data, and numerous image and video processing methods have been developed to enhance the use of the embedded data. A digital image consists of a group of small data units, called pixels, and each unit holds the data about the intensity of colours in the pixel's location. Since human errors and inconsistency could negatively affect the manual evaluation of striping assessment test methods, researchers have tried to use image processing techniques as an alternative for human judgment. The proposed method by Amelian et al. (2014) could be mentioned as an example of image processing techniques, where the results of boiling water test were analyzed by an image analysis method, in which the samples were placed out of water on a plane background and the operator had to alter a colour value threshold to differentiate coated from uncoated pixels (Amelian et al., 2014). MATLAB image processing ToolboxTM was used to improve the moisture suitability estimations for the direct tensile strength (DTS) test on HMA and WMA. The resulting images from samples were analyzed using Colour Look-Up Table (CLUT) provided by MATLAB. Furthermore, by means of capturing a minimum of 20 images from different angles of a sample, and merging these images using Autodesk 123D

Catch software, a three-dimensional model of the sample was created to evaluate the stripping; however, the results were tend to underestimate the adhesion failure percent in some cases (Hamzah et al., 2017). Another study tried to evaluate the stripping by simple thresholding of the test images in two steps: a) a Cyan-coloured background was removed by simple thresholding and; b) stripped parts were removed using secondary thresholding. The method, however, was not able to properly evaluate stripping of dark colour aggregates and shadows also caused error in the estimations (Lantieri et al., 2017). Moreover, Image Pro-Plus software was used as a thresholding tool to detect objects of interest and to evaluate the stripping by segmenting the remained parts in the images captured from rolling bottle test samples in the controlled lighting conditions (Yuan et al., 2015).

In addition, some research efforts employed special illumination systems to improve the accuracy of computer vision-based stripping estimations, such as indirect illumination using a shooting chamber (Merusi et al., 2010), and a LED-based illumination (Light-Emitted Diode) embedded in an image acquisition system (Yuan et al., 2015), which all were either using expensive equipment or failed to detect partially coated parts. In another research by Källén et al. (2016), an illumination system consisting of a quarter circle lamp and a camera located in a particular angle with respect to the light directions and the sample was used to capture a number of images from different angles of a sample. This system identifies coated parts based on the assumption that the coated areas reflect the light more than the aggregate surfaces (Källén et al., 2016). Different colour-based segmentation methods, such as graph-cut method (Källén et al., 2012) and K-means clustering (Källén et al., 2016), were performed on the test samples to distinguish coated parts.

Despite all these advances, there are some shortcomings which need to be addressed. These methods were unable to accurately measure the stripping, on dark-colour aggregates (Hamzah et al., 2014; Lantieri et al., 2017; Källén et al., 2016), and in addition, the test samples required manual preparation, such spreading the particles on a plane background inside or outside of water (Hamzah et al., 2014; Yuan et al., 2015; Källén et al., 2016), which changes some of the original test procedures, namely MTO's LS-285, which requires the mixture to remain intact within the water container. Lastly, specular highlights and shadows could still cause error for the submerged samples (Amelian et al., 2014; Hamzah et al., 2014).

1.2. Research Objectives

The objectives of this research are to improve the recent developments in the computer vision-based stripping assessment. This research attempts to develop a system without altering the existing test procedure of MTO's LS-285 (i.e. no need to remove the particles out of the water and spread them on a plane sheet), therefore, the following objectives were determined:

- Investigate automated methods to enhance lighting and contrast of the regions of interest in the images of samples
- Reconstruct specular highlights by detection of the highlights and image inpainting
- Automatically segment the images' pixels based on the similarity of colour intensities
- Classify the detected clusters automatically to determine whether they represent coated or uncoated regions

1.3. Research Methodology

This research includes development of an especial illumination system and an automated image processing algorithm, which consists of three modules: a) image preprocessing by enhancing

contrast intensity of the image and reduction of specular highlights; b) segmenting image pixels into different clusters; and c) identifying the nature of each cluster (whether it is a coated part or not). The step by step workflow of the methodology is provided in Figure 1.

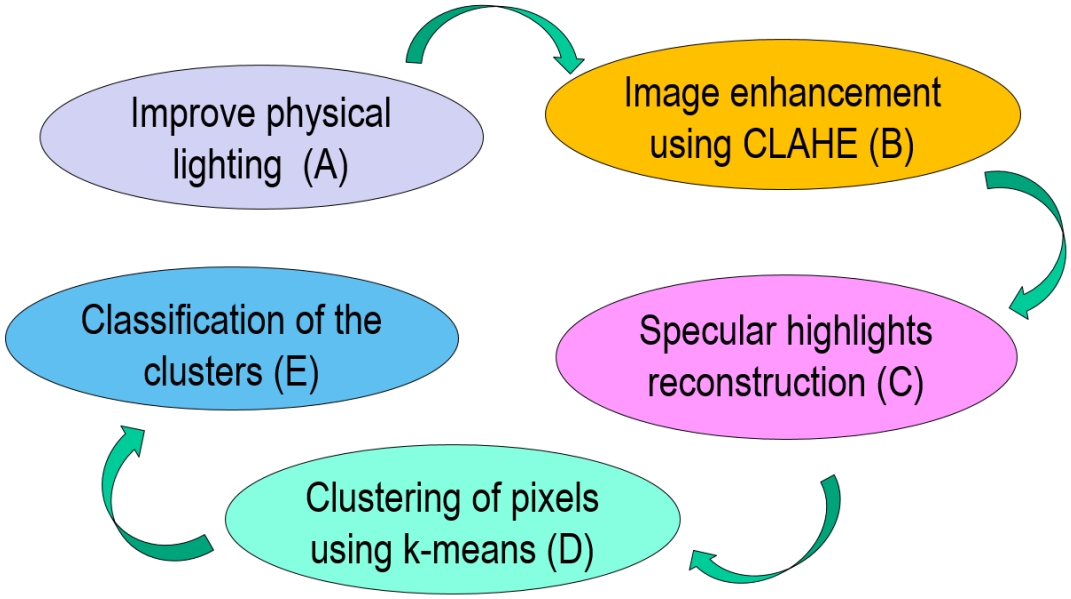

Figure 1: Research methodology

1.4. Thesis Organization

This thesis consists of five chapters. Chapter 1 provides an introduction to the research background, main concepts, and test procedures to evaluate stripping of asphalt mixtures. Then, research motivations, objectives, and methodology of this research are presented. Chapter 2 provides a comprehensive literature review on the topics related to this research. Chapter 3 explains the details of the methodology and development of the proposed system. In this chapter, the details of the designed illumination system, descriptive information regarding the employed algorithms, and the supporting concepts of the methodology are provided. Chapter 4 presents experimental results on a number of test samples from three types of aggregates and then discusses the results. In this chapter, the effects of a number of factors, including preprocessing of the input images, number of segmentation clusters, application of two supervised classifiers, and the impact

of using an illumination system, on the final results are discussed. Chapter 5 presents the conclusions for this research which summarizes the results, mentions the existing limitations, and provides recommendations for future developments.

Chapter 2: Literature Review

2.1. Introduction

This chapter presents a summary of research efforts which investigated the moisture-related damages in asphalt pavements, namely stripping of the asphalt coating, and also discusses the application of artificial intelligence in this area. Therefore, this literature review consists of two main sections. Moisture damages and their mechanisms, affecting factors, related measurement test procedures, and controlling factors are presented in part one. Part two discusses research projects related to evaluating moisture-related damages using artificial intelligence algorithms.

2.2. Part 1: Moisture-related Damages of Hot-mix Asphalt

The moisture damage sensitivity of the hot-mixed asphalt pavements is an important issue in the durability of the highway networks. One of the main factors is the precipitation in the highway location, which could be more critical in high-latitude and tropical regions (Liu et al., 2014). Moisture damage can be defined as the degree of loss in the performance of an asphaltic system due to the moisture. The damage process initiates through various moisture transportation modes and results in cohesive and adhesive failures of the asphalt cement coating (Caro et al., 2008).

Stripping phenomenon is one of the main manifestations of the moisture damage and is defined as a detachment of the asphalt cement from aggregate surface. Stripping usually occurs when the internal texture of the asphalt fails in the presence of water moisture and cyclic traffic loads. The moisture can be either water, water vapor, or both. (Mehrara and Khodaii, 2013).

In one hand, many researchers initially believed that the stripping occurs due to the loss of the bond between asphalt cement and aggregate in presence of water (Badru and Roberts, 1988; Kennedy et al., 1984). On the other hand, some other researchers have provided more comprehensive failure mechanisms. They believed that the loss of mixture adhesiveness and

cohesiveness could contribute to the moisture damage. For evaluating the moisture damages on asphalt pavements, some scholars applied cyclic traffic loads together with the moisture as a combined failure factor, but other researchers believed that the long-term presence of the moisture in asphalt voids could provide a proper and realistic presentation of damages (Mehrara and Khodaii, 2013). Based on the stripping reasons, physio-chemical incompatibility and mechanical failure were listed as the main classes of the stripping (Kandhal and Rickards, 2001). First class relates stripping to the asphalt components' sensitivity in the presence of moisture, whereas failures in the second class occur due to the cyclic hydraulic stresses in saturated conditions, which result in scouring of the asphalt binder from the aggregate surface. Also, three affecting factors for stripping were identified: the presence of water, high pressure, and high temperature (Kandhal and Rickards, 2001).

2.2.1. Moisture damage mechanisms

A mechanism is generally defined as a process that produces a new state or condition in a system by altering external and/or internal conditions (Caro et al., 2008). If a mechanism deteriorates the previous state, it is considered as a damage mechanism. Moisture damage mechanism is based on two steps, moisture transport and response of the system. Moisture transport is a process in which the moisture, in any form, penetrates to the asphalt and reaches the interface of asphalt cement and aggregate. The response of the system is the internal structural changes which reduce the load carrying capacity of the system (Caro et al., 2008). Some of the environmental conditions, including relative humidity, severe freeze-thaw cycles, intense rainfall periods, and in-service conditions, such as dynamic loads of traffic and aging, increase the damage potential (Lu and Harvey, 2006). Several pavement cores were studied to identify affecting factors in the moisture-related damages. The most important factors were identified as pavement structure,

rainfall, air void content, and ageing. The effect of cumulative truck traffic and repeated loading found to be marginal (Caro et al., 2008).

The response of an asphalt mixture system to the moisture penetration, (i.e. stripping effect), is caused by penetration of the moisture (water) into the asphalt mixture and it could decrease the durability of the mixture due to thermal stresses and traffic cyclic load in various forms (Mehrara and Khodaii, 2013). The first type is detachment, which can be defined as placement of a thin film of water in the intersection of the aggregate surface and asphalt cement. This separation is not obvious and has a thermodynamic or chemical nature. The second type is displacement which is a mechanical effect and causes the loss of bonds in an asphalt mixture and separates asphalt cement from aggregates. Third, the cohesion of the asphalt mixture becomes weak due to the long-term dispersion periods and erosion of the mixture material. This effect is mechanical failure. Forth, the film rapture and micro-crack theory investigate ruptures in the binder or aggregates, which could be thermos-dynamical or mechanical. Fifth, desorption is a random movement of the binder as the outer layer of mastic is washed away by the existing flow. This mechanical phenomenon occurs after the diffusion process. Sixth, the chemical emulsification is related to the emulsion of water droplets which are inserted into the binder (Mehrara and Khodaii, 2013).

Mechanisms of the moisture damage can also be divided into two major categories. The first category is micro-mechanisms which focuses on the bonding forces inside the mixture, such as adhesion of aggregate and asphalt cement as well as the cohesion of asphalt texture in a molecular scale. The second category discusses the failure of mixture bonds on a macro-scale through mechanical effects, known as macro-mechanisms (Mehrara and Khodaii, 2013).

2.2.1.1. Macro-Mechanism

Research on macro mechanisms studies only the effects of physical stresses, such as traffic load, thermal stresses, and voids' internal hydraulic flow. Evaluating moisture damage includes different sub-mechanisms. First sub-mechanism includes extra pressure created by traffic load, thermal stresses, or evaporation of internal water within the asphalt voids. Second sub-mechanism is the effect of cyclic traffic load on an asphaltic system that causes hydraulic scouring (pumping effect), and then the high velocity of hydraulic flows in the interior voids causes physical erosion to the system (Kringos, 2007; Kettil et al., 2005).

2.2.1.2. Micro-Mechanism

There were some studies on the adhesion theory which investigated adhesion of mixtures in a micro-mechanism scale and could be divided into five individual groups: mechanical, chemical reaction, molecular orientation, surface energy, and weak boundary. In addition, there are some research studies on stripping mechanisms which are categorized into six theories. These theories are detachment, displacement, dispersion of the mastic, film rupture and micro-crack, desorption and spontaneous emulsification. There are also other mechanisms of moisture damage that were investigated. For example, osmosis phenomenon is considered as another possible mechanism where the dissolved salts inside the droplets of water or a film of absorbed water cause osmotic pressure (Mehrara and Khodaii, 2013); however, some researchers believe that the effect of this phenomenon is negligible (Thelen, 1958).

2.2.2. Moisture Transport Modes

Moisture movement in asphalt mixtures is classified into three main modes: 1. Penetration: infiltration of the surface water; 2. Diffusion, permeation of water vapour; and 3. Subsurface

water's capillary rise (Masad et al., 2007). The main mode of moisture transport in asphalt pavements is the penetration of water from the subsurface. This mode of moisture transport is related to drainage conditions, rainfall, and material properties. All of these three modes are important in moisture transport (Caro et al., 2008).

- Permeability is the capability of the material to transmit fluids (Park and Koumoto, 2004). Three types of common asphalt mixtures were studied, and the permeability ranges were presented (Chen et al., 2004). It was demonstrated that the air voids and permeability have a correlation with each other. Voids structure in an asphalt mix provides measures of the effective permeability value. Construction factors, such as lift thickness, density, homogeneity, and compaction effort also affect the air void content. For example, lift thickness has an inverse relationship with permeability (St Martin et al., 2003; Mohammad et al., 2003). Since there is a lack of clear relationship between the field and laboratory permeability measurements, the laboratory results could not substitute actual field permeability outcomes (Cooley et al., 2002; Caro et al., 2008).
- Subsurface water is transported into the interconnected paths and capillaries due to the capillary action phenomenon. The rate and the height of the capillary rise is controlled by the r (capillaries geometric characteristics), ρ (the water density), α (the liquid-solid contact angle), and T_s (the surface tension of water). The capillary rise in an asphalt pavement hypothetically should not occur, but it sometimes happens; because water is in contact with mastic, mixture of fine aggregate and binder, instead of pure binder (Masad et al., 2007; Caro et al., 2008).
- The volume of water vapour and its storage rate inside a mixture are determined by relative humidity and material properties. Holding potential with storage rate, capacity, and diffusion coefficient are the controlling material properties. There are many studies in terms of moisture

diffusion. The relationship between storage capacity, vapour transport, and moisture damage was demonstrated (Sasaki et al., 2006). A new method, which was able to measure the suction value using thermocouple psychrometers, was developed and moisture diffusion was studied on samples, which were resulted from suction value test. A direct relation between the size of air void and the suction value was observed, where the smaller air voids had higher suction values (Kassem et al., 2006). Also, it was observed that moisture damage could be minimized in an optimal suction value (Kassem et al., 2006). Moreover, suction values and moisture damage level have inverse relation due to the direct relation of relative humidity gradients inside voids and suction values (Caro et al., 2008).

2.2.3. Controlling Moisture Damage

2.2.3.1. Moisture Damage Controlling Factors

Based on the mentioned mechanisms, moisture damage can be controlled by two types of factors. The first type includes internal factors, which are related to the nature of the mixture and properties of its components. The second type includes external factors, which depend on external stresses and the surrounding environment (Mehrara and Khodaii, 2013).

Internal factors include properties of asphalt cement, aggregate, and the mixture. Asphalt cement properties are determined by its viscosity, thickness of asphalt film, the water-bearing capacity, which is the volume of water that can be kept inside the material, and its chemical structure (Birgisson et al., 2003; Kanitpong and Bahia, 2003; Caro et al., 2009). Aggregate properties can be determined by surface texture, coating, moisture, chemical characteristics, mineralogy, porosity, and content of mineral fillers (Kandhal, 1992; Bahia and Ahmad, 1999; Terrel et al., 1993). Asphalt mixture properties are affected by void ratio, distribution and the

average size of voids, permeability, asphalt content, asphalt age, gradation, additives, and type of mixture's fine aggregates (Caro et al., 2008; Kim and Coree, 2005; Kanitpong and Bahia, 2005).

External factors can be varied by the conditions during and after pavement's construction. Conditions during the construction of pavement such as precipitation, compaction, temperature, and the time gap between friction layer construction and the new layer (Kandhal and Rickards, 2001; Bahia and Ahmad, 1999; Tunnicliff and Root, 1982). Conditions of after construction are listed as precipitation, temperature, freeze-thaw cycles, drainage condition, wet-dry cycles, traffic load, sub grade water content, micro-organisms activity, and the PH level of the water flowing through the pavement (Cheng et al., 2003; Kandhal and Rickards, 2001; Bahia and Ahmad, 1999). Table 1 illustrates the favourable conditions for these characteristics in which the asphalt pavement performs as designed and it is the most durable condition due to the related factors (Mehrara and Khodaii, 2013).

Table 1: External factors contribute to the moisture sensitivity of the asphalt mixture (Mehrara and Khodaii, 2013)

Component condition	Affecting factors	Favourable condition
During the construction	Environmental temperature	Warm
	Precipitation	None
	Compaction	Enough
	Time interval between the construction of new HMA and the old pavement	Roughly two summers
After construction	Precipitation	None + dry season after
	F_T cycle	None
	Temperature	Mild- low day and night temperature fluctuation
	W-D cycle	None at high temperature
	Sub-grad water content	Low
	Drainage condition	Good
	Traffic load	Low
	Activity of micro-organisms	Using additives which are compatible with the micro-organisms
	PH of through-pavement-flowing water	Acidic conditions

Initially, some transportation agencies, such as MTO (Ministry of Transportation of Ontario), tried to limit the moisture damage by lowering the air void percentage (El Hussein et al., 1993). In contrast, it was demonstrated that just the air void content is not a proper measure for asphalt mixture's moisture transport (Masad et al., 2007). Investigation of asphalt pavement structure with different techniques revealed a better understanding of the void structures. For instance, obtaining

2D (two dimensional) images of materials' cross-section with electron microscopy or spectroscopic scanning techniques determined the chemical composition of the mixture (Kosek et al., 2005). Moreover, 3D (three dimensional) imaging techniques, such as nuclear magnetic resonance, x-ray computed tomography, and transmission electron microscopy visualization (Kosek et al., 2005; Barrie, 2000), facilitated studying characteristics of voids structure, such as distribution, tortuosity of the flow path, connectivity, and their sizes. Aggregate properties, the process of compaction, and mix design are the controlling factors in the distribution and size of the air voids in an asphalt mixture. Air voids in asphalt mixture are categorized into effective (top-down connections), impermeable (scattered without any connection with borders), and semi-effective (not fully connected through the material) (Chen et al., 2004). The air void structure and tortuosity were determined for 14 samples with different total air-void percentages to measure their permeability (Al Omari, 2005). The Pessimum air void size is referred to the average air void size in which the moisture sensitivity of the asphalt mixture is maximum. The penetration of moisture in the mix is low when the air voids are small. Although penetration of the moisture is high in large air voids, the drainage rate is also high. Thus, Pessimum air void size is the worst scenario which traps water inside the material and provides a suitable environment for the progress of moisture damage. The Pessimum air void size range for limestone was estimated at 0.8 mm to 1.0 mm and for granite was 1.2 mm to 1.4 mm (Masad et al. 2006). There was some more research on characterizing the internal air void structure of the asphalt mixtures. They limited the air void content to 6-7 percent for the same material samples and examined the structure through analyzing X-ray CT images. It was observed that different samples have different susceptibility based on the air void structure of the sample (Caro et al., 2008; Arambula et al., 2007).

It was found that the cracks, termed as checks, are generated in some compaction processes, such as in conventional steel-wheeled compaction in the first two passes. The length and apart sizes of the checks usually vary from 1 inch to 4 inches and 1 inch to 3 inches, respectively (El Hussein et al., 1993). These checks ease the access of moisture and air in the mixture. Cracks increase the air void content and affect the moisture resistance of the mixture in the same manner as the air void, because cracks are able to make new connected paths and create links through the air voids (Chen et al., 2004; Caro et al., 2008; St Martin et al., 2003).

There are two types of cracks in the asphalt mixture. The first type is cohesive cracks and grows in the binder. The second type includes adhesive cracks which expand through the binder-aggregate interface. The former type occurs typically in asphalt mixtures with a very thick binder. The latter cracking, the more important in moisture damage, usually happens in very thin asphaltic binders (Lytton et al., 2004).

2.2.3.2. Preventing Procedures

To minimize moisture-related damages, some practical recommendations were proposed (Kandhal and Rickards, 2001). The moisture content of the pavement could be examined by visual observation and by dry sampling using a jack hammer. A saturated asphalt mixture is highly vulnerable to the stripping phenomenon (Kandhal and Rickards, 2001). Inadequate pavement subsurface drainage also allows the moisture to move upward via capillary action and makes the asphalt course saturated. By utilizing Asphalt Treated Permeable Material (ATPM) to replace the base course, which is expanded through the drainage edges of the asphalt pavement, moisture penetration could be restricted. Experiments on a dense-graded HMA with a maximum of 8% air voids showed that the air void percentage gradually decreases to 4-5% through the first three years

of serviceability due to the application of traffic load. If this reduction does not occur, the thermal pumping of moisture has a high potential (Kandhal and Rickards, 2001).

2.2.3.2.1. Additives

Many research projects focused on identifying additives which can affect the moisture susceptibility of asphalt mixtures (Palit, 2001; Pundhir et al., 2005; ASTM, 1996). The tests for the moisture damage susceptibility are mostly carried on the loose mixtures, such as static immersion and boiling water tests, and compacted samples like tensile strength and retained-strength ratio tests. The modification of the mixture with crumb rubber showed about 50% and 10% less stripping in boiling and static immersion tests, respectively (Palit et al., 2004; Pundhir et al., 2005; ASTM. 1996). Five different aggregate types, two antistripping agents, and 60/70 penetration graded asphalt binder were used for the moisture susceptibility experiments. It was observed that high carbonate material, such as limestone and slag-limestone, provide a stronger bond with asphalt binder. In contrast, granite, quartzite and andesite containing a high amount of silica are vulnerable to stripping (Amelian et al., 2014). Antistripping binder filler, namely hydrated lime and liquid anti-stripping agent (e.g. Nano-based material termed as Zycosoil), are highly effective in moisture susceptibility reduction, restricting the stripping to less than 3.5 percent (Kim and Moore, 2009).

2.2.4. Moisture Damage Assessments

The destructive effect of moisture in asphalt pavements was firstly identified in the 1930s and highway agencies and pavement industries laboriously investigated moisture-related damages in the 1980s (Taylor and Khosla, 1983). As a result, a number of tests procedures were developed to assess the susceptibility of mixture designs to the moisture-related damages (Terrel et al., 1993; Aschenbrener et al., 1995). Although these tests are mostly simple and adopted by most of the

highway agencies, there have been some instances of poor correlation between laboratory results and the field observations. Experimental studies on the effects of air voids distribution and connectivity, moisture movements, mixture adhesive bond, and materials physical characteristics provide great opportunities to understand moisture damage causes and mechanisms (Bhasin et al., 2006a; Bhasin et al., 2006b; Copeland and Kringos, 2006: Kassem et al., 2006).

In addition, test methods were proposed with better correlation with field performance results, which also used for evaluation of the antistripping agents' effects on moisture-vulnerable mixtures (Atud et al., 2007; Kvasnak and Williams, 2007; Wasiuddin, 2007). Moisture damage has been investigated in three main ways: laboratory investigation, field studies, and modeling and numerical analysis (Mehrara and Khodaii, 2013).

The field studies mostly focused on observing pavement performance exposed to moisture damage in actual conditions. These studies tried to estimate potential moisture damage of the mixture or effectiveness of the additives in asphalt. Kandhal and Rickards (2001) are among the scholars who conducted research in the field to investigate stripping causes. It was observed that the lack of proper drainage results in some undesirable moisture effects in asphalt pavements. The prevailing mechanism for initiation and propagation of these effects, and some pre-diagnostic symptoms to detect the moisture damage were introduced (Kandhal and Rickards, 2001).

However, most of the research projects for studying moisture-related damages have been conducted in a laboratory setting. These laboratory-based studies aimed at evaluation of anti-stripping additives effectiveness, development of new experimental methods and comparison of new methods with existing methods. A comprehensive literature review studied parameters and criteria of different test methods. They grouped existing experimental tests by dividing them into a single parameter and multi-parameter tests (Caro et al., 2008; Reinke et al., 2010). Tests can also

be categorized into five main groups based on their performance. These groups include tests on loose mixtures, destructive mechanical tests on loose mixtures, non-destructive mechanical tests on the compacted mixture, energy-based methods, and non-destructive non-mechanical tests (Mehrara and Khodaii, 2013). Destructive tests on compacted mixtures assess stripping potential via fatigue index, permanent deformation index, and indirect tensile strength test. Energy based test methods measure adhesion and cohesion potentials in a mixture using energy-based indexes fracture mechanics, which are measured by means of mechanical and non-mechanical tests on materials in the mixture. Non-destructive non-mechanical test methods evaluate the stripping potential using two types of parameters: permeability and moving velocity of the mechanical waves. There are also many tests investigating stripping on compacted and loose asphalt mixture (Mehrara and Khodaii, 2013). Direct Tensile Strength (DTS) provides the most representative measurement for the tensile properties of the materials (Azari, 2010). A comprehensive list of tests on compact asphalt mixture, the required parameters, criteria, and their application was gathered by Mehrara (2013). Detailed discussions about the test methods on loose mixtures are available in the literature (Mehrara and Khodaii, 2013).

Another field of the study investigated parameters independent of size, which could demonstrate actual behaviour of the material and mixtures. The parameters should reflect the main environmental conditions and loading stresses. Analytical models were also developed to simulate the behaviour of mixtures (Mehrara and Khodaii, 2013). For instance, a model was developed by Kettil (2005) which used fracture energy analysis method by establishing mass and momentum conservation to model water velocity, pressure, and related deformation in a pavement mixture (Kettil et al., 2005).

2.2.4.1. Tests on Loose Asphalt Mixture

There are many different test methods for assessment of moisture-related damages on the loose asphalt mixtures. Some of these tests are focused on calculating cohesive energy using surface energy theory or cohesive failures such as Time Temperature Superposition (TTS) (Kanitpong and Bahia, 2005) and Wilhelmy plate (Cheng et al., 2002; Cheng et al., 2003). Some other investigate additive and mineral effects, such as Methylene blue (Kandhal et al., 1989) and bottle test (Tunnicliff and Root, 1982; Williams and Breakah, 2010). Some others are concentrating on adhesive energy such as Universal Sorption Device (USD) (Mehrara and Khodaii, 2013) and Pneumatic Adhesion Test (PATTI) (Kanitpong and Bahia, 2005). There is another group of test method which investigates adhesion bond failures such as Static immersion (Tunnicliff and Root, 1982), Dynamic immersion, Chemical immersion (Williams and Breakah, 2010), Boiling water (Badru and Roberts, 1988) and Surface reaction (Williams and Breakah, 2010). Qualitative or quantitative estimations can be obtained directly or indirectly from these tests. In one hand, the main shortcoming of these tests is that the limited range of granules' sizes is considered to measure the stripping. This approach may not fully indicate the coupling effect of load or moisture. On the other hand, these tests are easy, low-cost, quick, and do not require complex equipment (Mehrara and Khodaii, 2013).

Static immersion, RBT (Rolling Bottle Test), total water immersion, BWT (Boiling Water Test), and ultrasonic test methods are some examples of test procedures on loose mixtures and are used to assess the susceptibility of mixtures of aggregate and asphalt cement against moisture damages (Mehrara and Khodaii, 2013).

The most common tests on loose mixtures for evaluation of stripping percentage are static immersion, rolling bottle, and boiling water tests. LS-285 is a modified version of static immersion

test developed by MTO, which conducts the experiment on 100g of aggregate which is sieved in three sizes (Ministry of Transportation Ontario, 1996). Four grams of hot asphalt cement is mixed with the preheated aggregate in the mixing temperature of 141℃ and the asphalt mixture is transferred into a 600ml beaker. The sample rests till it reaches the ambient room temperature and then the beaker is filled to three-quarter of its capacity. After 24 hours, the stripping percentage of the sample is evaluated by a skilled operator (Ministry of Transportation Ontario, 1996). Moreover, the rolling bottle test could be used to measure the stripping percentage through the manual evaluation of the mixture by a skilled technician (Paliukaitė et al., 2016). According to the test procedure EN 12697-11(clause 5) (Estonian Centre for Standardisation, 2019), mechanical stringing action is introduced to the non-compact sample in the presence of water by rolling bottle. The aggregate particles are fully coated with asphalt cement and are immersed inside distilled water. After the mixture cools down, the sample is rolled in a bottle and the remained coating is evaluated in different time intervals. Both static immersion and rolling bottle are subjective tests (Estonian Centre for Standardisation, 2019) and stripping is characterized by a coating index which evaluates the retained coating degree for each sample.

Boiling water is another test procedure, in which the asphalt cement is preheated for 24-26 hours and is fully mixed with 100g of aggregate, which is preheated for 1.5 hours prior to the test. Then, the loose mixture is placed in 500cc of boiling water and after a specific time, the sample is cooled down and is dried and will be ready to be evaluated manually (Paliukaitė et al., 2016; Kennedy et al., 1984).

Most of the test methods on loose mixtures use aggregate grains ranging from 6.3 to 9.5 mm. It was observed that the static immersion test is subjective, and no performance strength qualifying tests are involved in the test (Liu et al., 2014). Moreover, the image-based algorithm was utilized

to improve the stripping measurement of static immersion test for asphalt mixtures (Kim et al., 2012; Amelian et al., 2014). In the other research same approach was utilized to evolve the estimation of stripping for HMA with a diverse synthetic wax modifier (Merusi et al., 2010; Amelian et al., 2014).

2.3. Part 2: Artificial Intelligence Integrated Asphalt Quality Control

2.3.1. Artificial Intelligence

2.3.1.1. Smart Agents

Advances in Information Technology (IT) storage, reuse, and its execution integrated with internet provide ample opportunities to implement IT into various processes and make industries more productive. Therefore, meaningful and precise data collection and appropriate analysis have become important, but these efforts rise challenges, such as big data management and analysis (Demirkan and Delen, 2013). The initial step for a better understanding of multi-agent systems is to define intelligent agents, the fundamental cell of MAS (Multi_Agent System). An intelligent agent could be defined as ''*a self-contained program capable of controlling its own decision-making and acting based on its perception of its environment, in pursuit of one or more objectives*'' (Ren and Anumba, 2004). To have a smart agent, the agent should have at least two out of three behavioural attributes which are illustrated with blue circles in Figure 2. These behavioural attributes are (Ren and Anumba, 2004):

- Autonomy: Independent operation of the agent without the interference of human. Each agent has a specific objective(s) and acts to achieve it(them). The key factor in this attribute is pro-activeness; for example, the capability to interactively respond, instead of a simple reaction to the environment.

- Co-operation: Interactive capability is required to achieve this main feature; such as interaction with human or other agents involved in the system.
- Learning: In the process of interacting with the surrounding environment, the agent should be able to learn to be considered as a smart agent (Ren and Anumba, 2004).

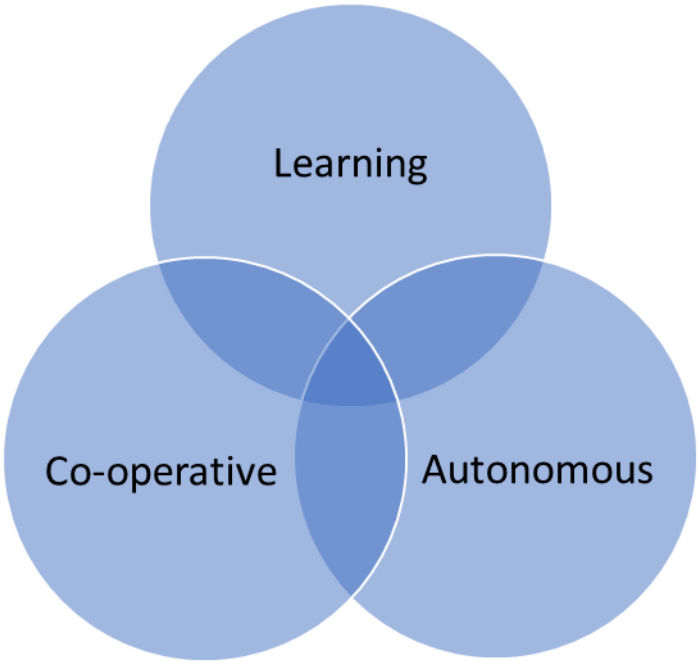

Figure 2: Requirements to have a smart agent (Ren and Anumba, 2004)

AI is vital in modern problem-solving processes because traditional techniques failed to discover and interpret various types of information and patterns in data sources, and utilization of AI methods facilitates informed decision making.

Data mining is an important field in the AI domain; a process which is categorized into verification-driven and discovery-driven. In the first category, a prior hypothesis is formed about the nature of relationships among data. The result of the data mining process is then used to reach a conclusion about the validity of the hypothesis. The methods in the second category, however, initiate without a fixed hypothesis about the nature of relationships in the dataset. It is the duty of the data mining algorithm to discover important patterns among the data. Discovery-driven data

mining can be categorized into two main types: classification (supervised learning) and clustering (unsupervised learning). Supervised learning includes construction of a model for certain objectives and to optimally classify test datasets based on the patterns in the training dataset. In contrast, unsupervised learning does not require a specific goal or historical data to predict. Clustering and detection of associated rules could be considered as unsupervised learning types (Nemati et al., 2002).

2.3.1.2. Agent Learning

An agent interacts in a complex environment. The complexity of the environment is due to a number of factors, such as environmental uncertainty, the degree of clustering, the density of the solution constraints and space, time obligations, the existence of multi-goals, the verity of comparing options and preferences, knowledge level of each individual agent and agents' skills (Ren and Anumba, 2004). It is critical for an agent to have the ability of adaptation and learning. Agent learning has main two reasons: to automatically improve its performance and to gain a more appropriate understanding of the learning processes in a MAS (Ren and Anumba, 2004). From the operational point of view, learning in MAS is the ability to do new tasks which it could not do before or to improve its performance. Learning process begins when an agent starts to communicate with other agents and the environment and receives some responses. Based on the prescribed criteria, it decides the next required action to obtain proper results. To achieve an effective learning process, some parameters should be determined before and after the process; such as the goals and scope of learning, and the methods of learning. Knowledge compilation, explanation-based learning, support vector machines, concept and multi-strategy learning, neural networks, reinforcement learning, deep learning and genetic algorithm are some examples of agent learning methods (Ren and Anumba, 2004).

2.3.2. Image Processing

Digital images and videos are heavily used in different sectors of service and industry, and numerous algorithms have been developed to facilitate processing these valuable sources of information. Machine learning and statistical methods have been adopted in the field of computer vision research to enable automated data extraction from images and videos. Object detection, classification, tracking, and segmentation in images and videos provide a better and deeper understanding of the captured items and events. Many fields, such as medical imaging, search engines, photo management, robot navigation, and quality control in production lines, benefit from computer vision-based methods (Jalled et al., 2016).

Image processing is related to signal processing where the input is an image (i.e. matrix or matrices of pixel intensities) and the output could be a modified image or some numerical results, or in other words, image processing extracts required information or modifies an image. These operations usually use signal processing methods which consider an image as a 2D signal. There are three main steps for image processing.

- Input: capturing and importing images with an image capturing device, such as a digital camera.
- Analyze and modify: data compression, image alteration, and detection of patterns.
- Output: modified image or the information of interest from the input image (Jalled et al., 2016).

Digital images are comprised of small units, called pixels, and an alteration in an image is the reflection of changes on the related pixels. Each pixel contains the intensity of colours and a digital image is represented as a matrix, or matrices in multi-channel images, and each matrix element is the related pixel value.

2.3.2.1. Application of Image processing in Striping Assessments

Some of the main stripping measurement test procedures, such as static immersion and boiling water, are subjective and could be unreliable when assessed by inexperienced technicians. To overcome this major shortcoming, many research efforts have employed image processing techniques. For example, water boiling test results were improved with the use of an image analysis method (Amelian et al., 2014).

Digital images were captured from the boiling water test specimens and two image processing software were used to replace manual evaluation. First, captured images were imported to the Image-Pro Plus software and then the green background and glares were segmented and removed from the images. Then the software converts the images into an 8-bite grayscale format and a thresholding process was applied to create binary images. The thresholding value was set to 65 to isolate stripped areas and their percentage was calculated by counting the number of remained pixels. Due to the glares on the surface of the coated areas, major errors were observed. Two approaches were proposed to overcome this issue (Amelian et al., 2014). First, using special cameras and lighting systems, which require an expert operator and expensive equipment. Second, using image enhancing software to reduce the glares. Uniform and indirect lighting could reduce glares and then the rest of the reduction could be made by using image enhancement software. Moreover, the samples should be manually spread on a plain background and the thresholding was hardcoded (Amelian et al., 2014).

There are two main types of classifications in image processing: supervised (with training dataset) and unsupervised (automatically clustered) classification (Hamzah et al., 2014). Two main phases for supervised classification are training and testing, in which specific training dataset is created and then the test samples are classified based on the training samples (Karathanassi et al.,

2000). Using this approach, a method was proposed to estimate the moisture susceptibility of compacted HMA and WMA in the direct tensile strength test procedure (Hamzah et al., 2014). The adhesion failures of 48 cylindrical mixture samples were investigated by ENVI (environment for visualizing image) image analysis software and MATLAB image processing ToolboxTM. The software transformed the colour-structure of images based on CLUT, Colour Look-Up Table. A 10 mega pixel high-resolution digital camera was used to capture images from samples, which included three mix designs and compaction temperatures, and three conditioning and two anti-stripping fillers. In particular, ENVI, as a supervised training platform, provided a tool for classification of ROI (region of interest), which was used to restrict fusion of marked area with other classes. Two ROIs, including failure in the coating (stripped parts) and failure in aggregate (broken aggregate), were defined in this research. The presented results were promising, but classification based on greyscale images may result in potential inaccuracies, namely in the samples with close grayscale colour intensities. DTS test samples are not inside water which does not suffer from the errors (such as glares and shades) that occur in images of the submerged samples, such as the samples in static immersion and rolling bottle tests.

The adhesion failure on the fractured surface of WMA samples in DTS test was quantified by a 3D image processing technique (Hamzah et al., 2017). Minimum of 20 images, which were captured from equally distributed spots in different angels, were required to create a 3D model, which also enabled consistent lighting within the image. The gray pixel values in the model varied from low to high (from 0 to 255) which represented coated and stripped areas, respectively. Then the model was processed with a certain threshold value which was determined through a trial and error process (Hamzah et al., 2017). One of the main challenges in using this method was that the image and the fracture plane were not parallel with each other which could underestimate the

adhesion failure (Hamzah et al., 2017).) Autodesk 123D catch software was utilized to merge 2D pictures in order to create a 3D model of the sample for stripping evaluation (Chandler and Fryer, 2013). The images were converted from RGB (red, green and blue) to the grayscale colour space (Turner et al., 2015).

A simple, cost-efficient method was proposed to evaluate the stripping percentage of the loose asphalt mixture samples which were resulted from rolling bottle test (Lantieri et al., 2017) procedure. The images were processed by an open-source image processing program, named ImageJ, in YUV colour space. The method was conducted on mixture particles which were placed separately from each other on a plane sheet. The method was applied on three types of aggregate (porphyry, basalt and limestone) as well as different binders which consisted of different combinations of a 70/100 based bitumen and two waxes in the amount of 1%, 2%, and 3% of the weight of bitumen. This vision-based system firstly removed the background via using a simple threshold function; therefore, the aggregate particles were separately identified in images. Then the stripped parts were detected by another thresholding as well, but the aggregates' shadows caused inaccuracy in the results. The method was tested by comparing the machine results with three skilled operator estimations, and by pixel by pixel manual-clustering. The comparison of the machine-measured results with operator estimations revealed differences in the range of 0-32.84%. Moreover, the results showed smaller differences from the manual evaluation than the skilled operators' estimations. It was also observed that the method provides results closer to the ground-truth for aggregates with lighter colour comparing to the darker ones (Lantieri et al., 2017).

Image illumination could also significantly affect the image analysis outcomes. To implement digital image processing more efficiently in measuring the stripping areas, many image processing techniques have been developed together with specialized physical lighting systems (Amelian et

al., 2014; Rombi, 2014). Some examples, such as indirect illumination through a shooting chamber (Amelian et al., 2014) and image acquisition system combined with a LED-based illumination (Yuan et al., 2015), were used for improvement of the illumination; however, all these illumination systems included complex equipment and may still produce inaccuracy when the stripping is measured in the partially stripped samples.

When light arrays hit opaque material, some portion of lights are absorbed, and the rest is reflected. For example, darker colours absorb more than lighter ones. The direction of light, and shapes, angels, texture or any pattern on the surface of the material affect the reflections (Yuan et al., 2015). A lighting system was developed to improve the vision-based evaluation of stripping percentage on loose mixture samples (rolling bottle test). Six red-coloured LED lights with 660 nm wavelength were installed on the side-walls of a black box, and a white plane surface was provided at the bottom, as a platform for placing the scattered specimens, to adjust and control the light conditions (Yuan et al., 2015). Mixture particles were separated from other objects in the resulted image by using a thresholding tool in Image Pro-Plus software. The method was tested on three types of aggregates, such as basalt and two types of limestone, and the results revealed lower measured values than visual estimations (Yuan et al., 2015). Research efforts on the stripping measurement by computer vision mostly focus on classifying pixels based on their colours. For example, a graph-cut segmentation method was used to detect the stripped parts of the samples (Källén et al., 2012; Källén et al., 2016). In the graph-cut method, a graph consisting of different nodes, which are determined based on the colour histograms, is created and the weights for the graph is calculated with respect to the smallest distance between the aggregate and the asphalt cement colours. As a result, in the cases where the colour of aggregate and the asphalt cement were

too close to each other, the colour distances were small which made the method impractical for those samples (Källén et al., 2012; Källén et al., 2016).

Considering the fact that reflection on the surface of asphalt cement is typically more than the uncoated aggregate surfaces, a colour-independent method was developed using a rotating table which was illuminated by a quarter-circle light to maximize the reflections. Retained coating percentages of samples, which were produced by a rolling bottle test, were measured using this illumination system (Källén et al., 2016; Mulsow and Marschke, 2011). The quarter-circle light and the camera had a particular angle from the sample, which directed light arrays to hit the coated parts and reflect toward the camera. This system spun around the sample to capture images from different angles. The coated parts appeared with as bright spots on a few images, but they appeared with a dark colour on the rest of the images (Källén et al., 2016) and the same approach was utilized using two laser lines illumination system which still had issues to fully determine the stripping part (Mulsow and Marschke, 2011). The mixture particles were placed separately on a plain (such as cyan) background and a simple threshold function was used to remove the background (Källén et al., 2016). In addition, check point shapes were prepared and placed on the plane surface where the aggregates had already been placed, and then by rotating the table, images were taken and then were combined using these check points. The stripped percentage was determined by classifying the combined image using K-means clustering in a gray scale space with K (number of clusters) equal to 5. The results of the technique were evaluated for the light-coloured aggregates and were compared with graph-cut method results (Källén et al., 2016). The K-means segmented the particle surfaces into different clusters with promising accuracy, but it was not able to determine which classes represent the stripped areas, and the labelling process for the created clusters was done manually. This manual classification could result in potential subjectivity.

2.4. Summary

Summary of the research efforts related to computer vision-based assessment of moisture-related damages, namely stripping, was presented. There has been considerable progress in the application of image processing techniques, especially on the loose asphalt mixtures. Performance of the developed methods is mainly affected by the employed image processing algorithms and the illumination systems. These studies used digital cameras to capture images of samples which were then analyzed by different image processing methods, such as simple thresholding and more sophisticated clustering algorithms. In addition, illumination of the samples was modified by some digital (Hamzah et al., 2017; Källén et al., 2016; Mulsow and Marschke, 2011) and physical (Merusi et al., 2010; Amelian et al., 2014; Yuan et al., 2015) alterations. Although promising results were obtained using these methods; However, some shortcomings still exist and could be addressed, which include:

- These methods had difficulty in evaluation of dark-coloured aggregates as well as in some partially coated areas (Hamzah et al., 2014; Lantieri et al., 2017; Källén et al., 2016).
- Samples were usually altered prior to capturing of the images. In all of the research works on loose mixtures, aggregates were spread on a plane platform, which some were inside water and some others were removed out of water (Amelian et al., 2014; Yuan et al., 2015; Källén et al., 2016). This could change some of the original test procedures. For example, static immersion test procedure requires the samples to remain in the container.
- Glares and shadows in the samples caused errors in some of the estimations (Amelian et al., 2014; Hamzah et al., 2014; Lantieri et al., 2017). Some portion of the errors were due to the glares, and the shadows for out of water samples could be removed by using complex illumination systems (Amelian et al., 2014; Yuan et al., 2015; Källén et al., 2016).

- Most of the studies used greyscale images which may hinder the quality of the results, namely on the edges of the particles or aggregates with specific patterns on their surfaces (Hamzah et al., 2014; Hamzah et al., 2017; Källén et al., 2016).

Chapter 3: System Development

3.1. Static Immersion Test

As discussed in the literature, the static immersion test is a common method for evaluation of the susceptibility of asphalt mixtures exposed to moisture. This test can determine the stripping potential of the mixtures made of different bitumen grades, aggregate from different types and sources, and effectiveness of antistripping additives. The details of the Ministry of Transportation Ontario's static immersion test are available in test method LS-285 R29 (Ministry of Transportation of Ontario, 2018). Method A in this test procedure was used in this research, which is used for asphalt cement mixtures. This test procedure is designed for a single grade asphalt cement with up to one antistripping additive. All the test samples should be conducted in duplicate, where two samples are made in each test. In this test procedure, 4 grams of asphalt cement and 100 grams of aggregate in three different size ranges are required. The 100-gram aggregate should contain 50 grams, 35 grams, and 15 grams of 9.5 mm, 6.7 mm, and 4.75mm sieve sizes, respectively. The aggregate should be dried in an oven with a temperature of about 141°C for 24 hours. Then the aggregate sample should be heated for 10 minutes in a quick heat oven to reach the surface temperature range of 149°C to 177°C for mixing. The heated aggregate and mixing tools (metal container and spatula) are transferred into an oven with a temperature of 143°C for 15 min. Then the preheated aggregate is mixed with the 4.0 ± 0.1 grams of 143°C asphalt cement using the preheated mixing tools till the surface of aggregate particles are fully coated (the aggregates' surface should become fully coated with bitumen). The mixture is immediately transferred into a 600 ml container (beaker) and it will rest there until it reaches the ambient room temperature. In the final preparation step, the beaker is slowly filled with water up to three-quarter of the container volume. The beaker should be covered with a lid to prevent evaporation of water

and then it is placed in a water bath with a temperature of 49 ± 0.5°C for 24 hours. The beaker should be taped until the removal of almost all the trapped bubbles.

Finally, the beaker is removed from the water bath and the surface of the mixture is evaluated. This visual evaluation is based on manual percentage estimation of the total remaining aggregate's visible coated area. The operator should estimate the retained coating area via comparing the observation with Figure 3 (Ministry of Transportation of Ontario, 2018). The fundamental issue with this procedure is the subjectivity of the estimates in different labs and by inexperienced technicians. This could result in inconsistent assessments.

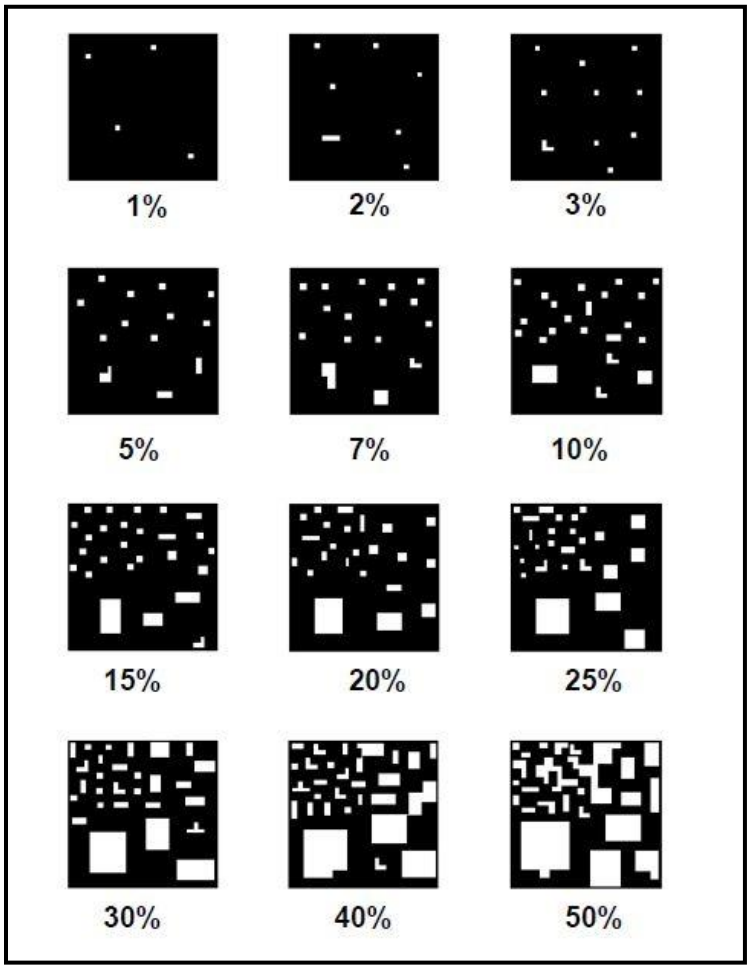

Figure 3: Percentage estimation chart for visual evaluation (Ministry of Transportation of Ontario, 2018)

3.2. Test Improvement

Image processing and machine learning methods have demonstrated strong visual assessment results in different sectors and this project intends to develop a system that can provide consistent and reliable results for assessment of the static immersion test samples. In this approach, a system could be created through the process of training, where the data will be collected from different experiments. Some visual aspects of the samples, resulting from experiments, could help in the differentiation of the samples, such as colour intensity or texture of the samples. These visual aspects are called “features”, and each could be labelled individually. The proposed system includes five main modules to enhance, extract, and analyze these features, which are illustrated in Figure 4. The following sections describe the details of each step and their implementation in this research.

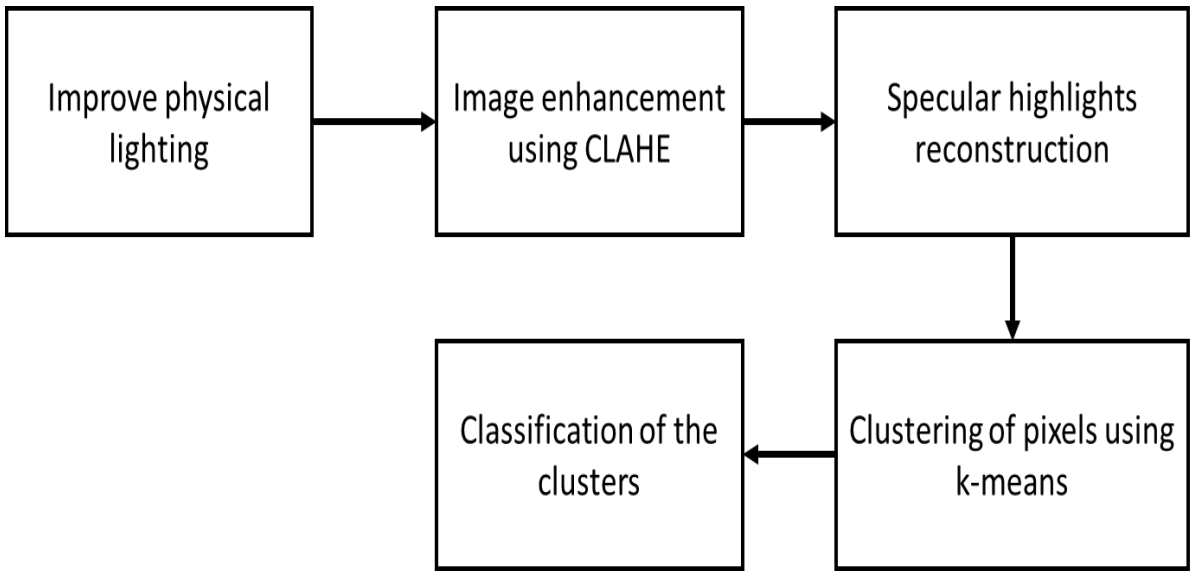

Figure 4: The process of problem-solving in this research consisting of different methods that are chosen to complete the model

3.2.1. Physical Illumination

A number of sample images are required for development, training and evaluation of this system. For instance, high-quality images (noise-free) could result in accurate and reliable outcomes. Specular highlights and shaded areas (too dark because of the shadows) were identified as important challenges in previous research. Specular highlights are light reflections on the surface of the sample, which mainly occur on the coated surfaces, air bubbles (Figure 5), and water surface (Figure 6). In the process of making test samples, the container should be slightly knocked (hit) from different sides. This process releases a considerable amount of air bubbles which were trapped inside the sample, and therefore eliminates them from the images. Despite this process, some bubbles may remain in the sample. The top view of the container holding the sample was chosen as the best view for evaluating the sample. All the analysis was carried out on this view and the striping percentage will be calculated based on this view. Also, it should be noted that the vision in an underwater environment is limited due to light absorption and scattering phenomenon (Fabio et al., 2014).

Illuminated samples with ambient room lighting could have sever specular highlights. Moreover, direct illumination from above creates a bright layer on the image (due to the surface reflection of water), which blocks large parts of the sample (see Figure 6). Another issue is the "specular highlights" which sometimes occur on the coated areas. In addition, illumination from the sides could create shadows on the opposite side of the illumination source. Even, illumination of the samples with indirect diffuse ring light could not provide ideal illumination for the images (Figure 6.b and Figure 7).

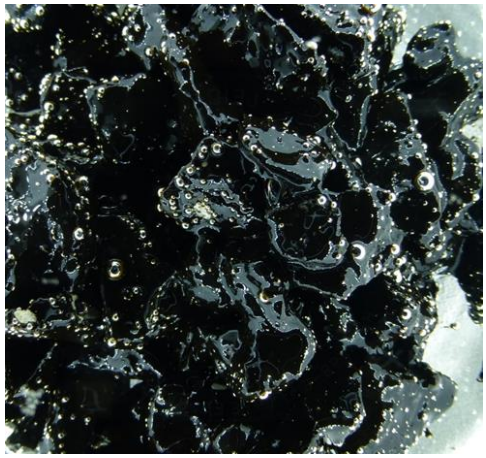

Figure 5: Trapped-bubbles in the sample after immersion inside water (without tapping)

The lighting from the bottom does not improve the conditions due to over-illumination of the bubbles and low contrast on the surface of the captured images. Quality of the image mostly depends on the camera's quality, a method of capturing, and lighting conditions. This project aims at using regular digital cameras and also to offer a practical and user-friendly approach. Therefore, complex and expensive illumination systems and sophisticated cameras were set aside. Although certain digital camera models were used in this research (e.g. Panasonic DMC-ZS20), any regular digital camera could be utilized for this purpose.

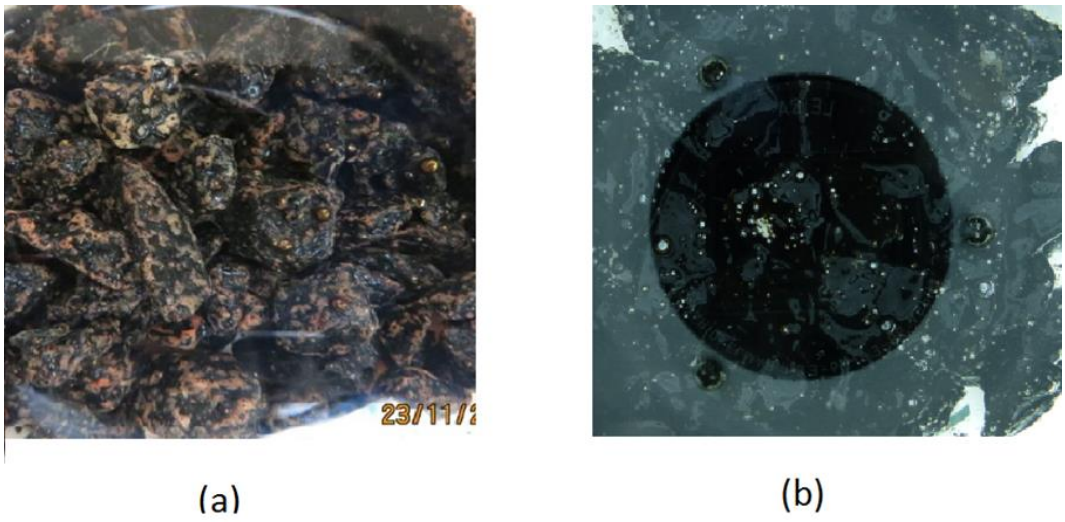

Figure 6: A bright layer on the image due to the surface reflection of the water: a) sample provided by MTO (room illumination); and b) sample illuminated by a diffuse lamp

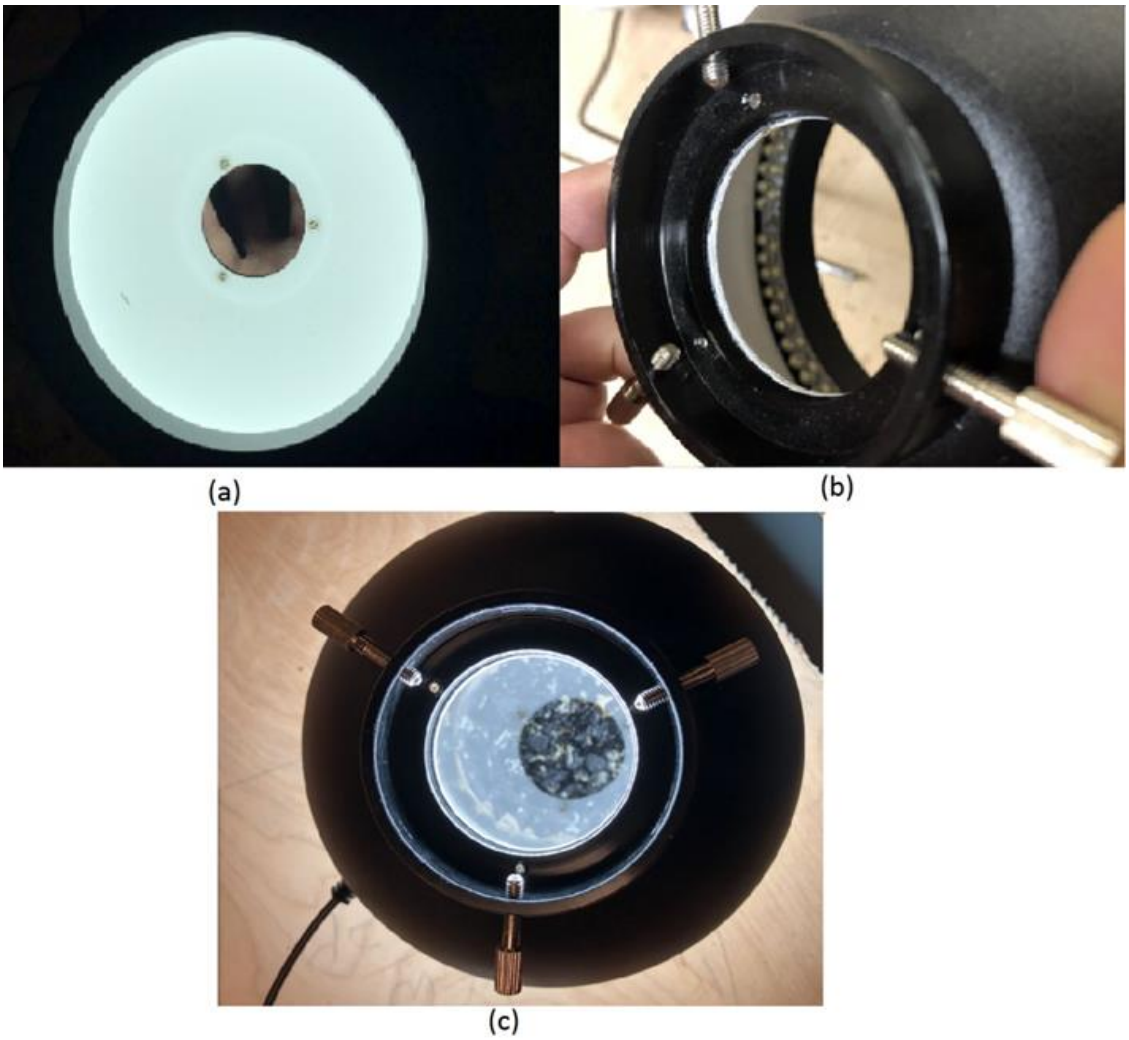

Figure 7: Illumination of static immersion samples with diffuse light: a) the indirect light reflected from the inner surface of the illumination system; b) the LEDs which provide the illumination; c) sample image using diffuse illumination

Thus, the quality of the images should be improved by using a low-cost illumination system, which provides uniform and indirect (to minimize specular highlights) lighting for the entire sample. A simple but novel approach was designed to create this lighting system, which is described in the following subsection.

3.2.1.1. Illumination box

The illumination box is a melamine box with specific characteristics to provide a uniform and indirect lighting for capturing images from samples. The beakers should be filled to at least 500ml to avoid reflections on the surface of the water. The overall size of the illumination box is 19 cm × 19 cm × 19 cm, consisting of five 19 cm × 19 cm × 0.3 cm melamine boards, where four boards are used for the sides walls (Figure 8) and one board is used for the top of the box with a hole in the center (Figure 9). The illumination box consists of three main parts: First part is the illumination source and L-shaped pieces, which were designed to direct the emitted light toward the inner surfaces of the box. This part is installed at the top surface of the box surrounding the sides of the lighting source (Figure 8 section C). Since the box is symmetric and there is no outside lighting disruption, the inner surfaces of the box uniformly reflect the light toward the sample (Figure 10). The uniform lighting was tested using a lux meter. The light receiver (sensor) of the lux meter was placed on different spots within the box and all spots recorded the light intensity as 1214 lux (Figure 11). The light source is a LED string, which is attached inside the L-shaped piece. The L-shaped pieces direct the lights into the walls in order to keep the specimen away from direct illumination (Figure 8 section C and Figure 10. b). The second part consists of four 19 cm × 19 cm × 0.3 cm melamine white board walls which distribute the light uniformly inside the box (Figure 8 and Figure 10. a). The boards are made of high-quality MDF with a white melamine surface bonded on one side. The box material is known as white melamine backing boards. The White Melamine Backing offers both the strength of an MDF (Medium-Density Fiberboard) product combined with a smooth Melamine finish. With a clean, hard-wearing surface, melamine backing boards are suitable for internal cabinetry, draw and lining. The surface material has plastic texture, so it can reflect the light as well as disturbing it; this material does not absorb the light and

due to its uneven surface, it diffuses the reflected arrays in different angles (Figure 12). This is suitable for the designed illumination box because regular reflections might create bright spots in some parts of the specimen. The third part is the board on the top of the box. This part has a square shape and there is a hole, with radius of 2.5 cm, at the center of the board. The hole is provided to allow the camera's lens to capture an image from the samples (Figure 9). The non-reflective (dark) side of the lid should face toward the inside of the box because reflections from the top-inner surface of the box could create reflections on the surface of the water. All the pieces of the box are made from the same material and the box could be placed easily on the top of the specimen container. The illumination box and a sample inside it are illustrated in Figure 13.

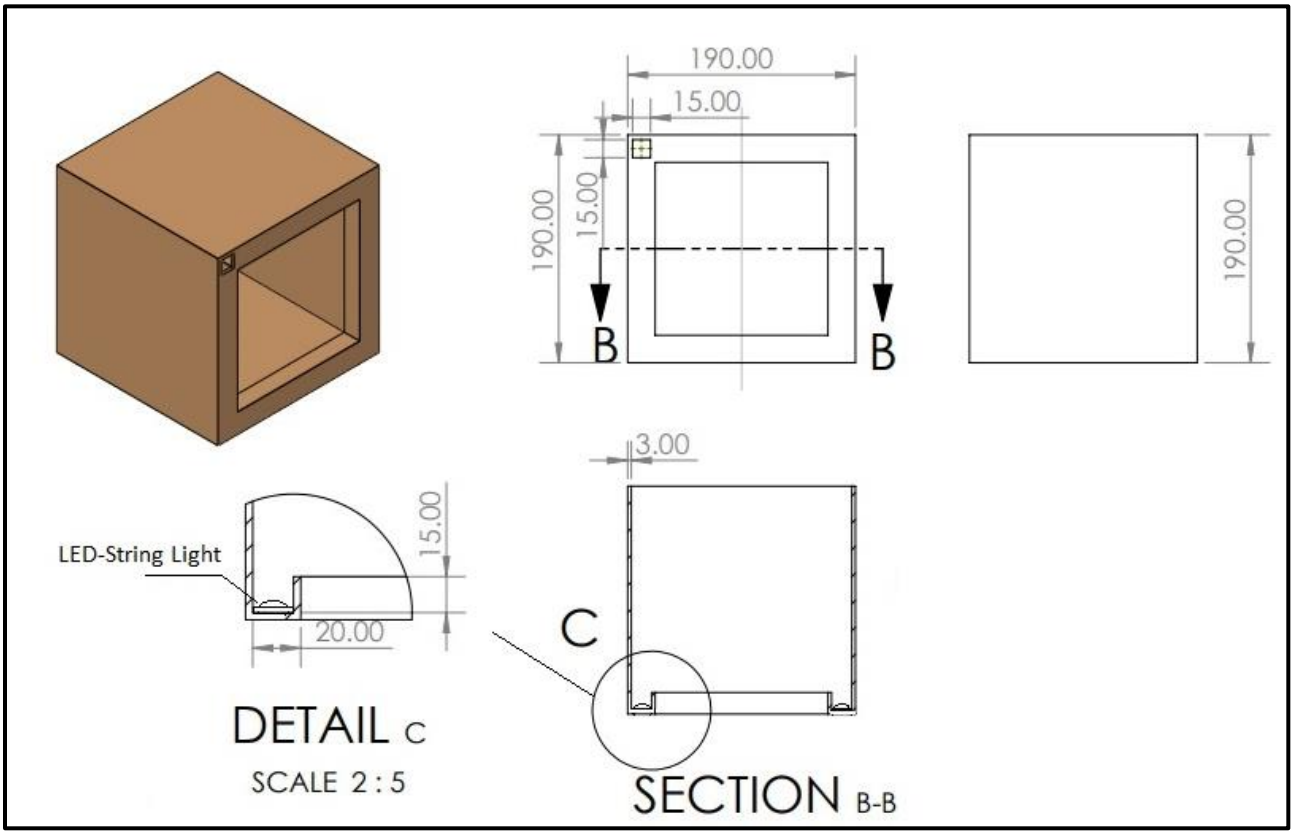

Figure 8: Illumination box drawings

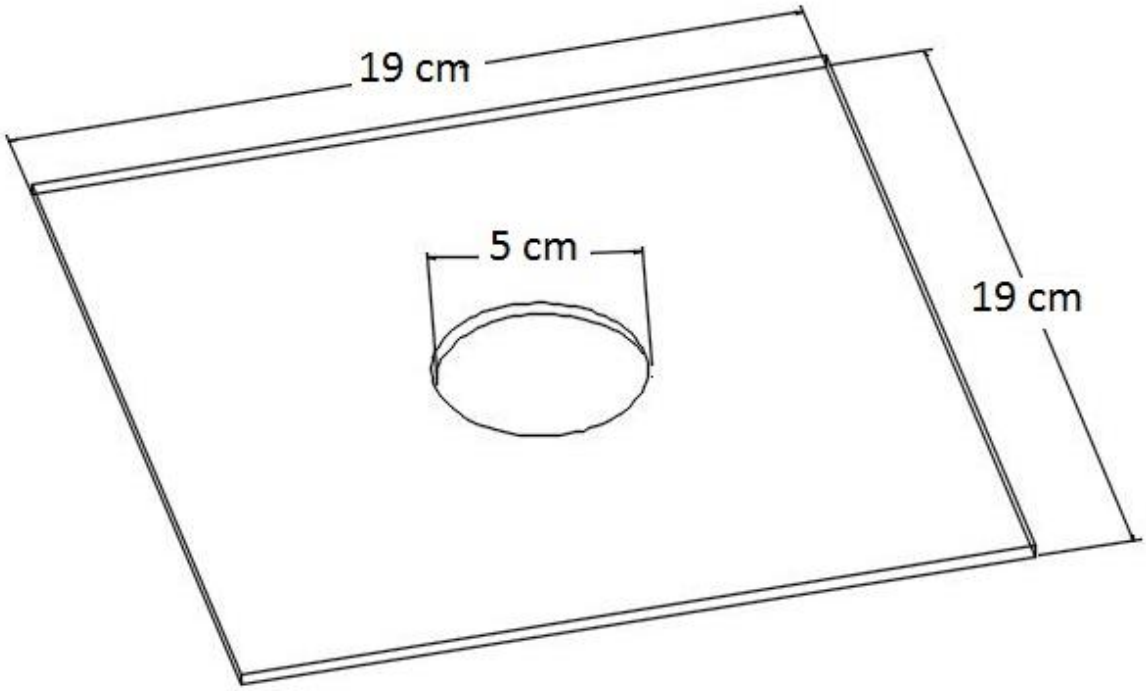

Figure 9: The top part of the illumination box

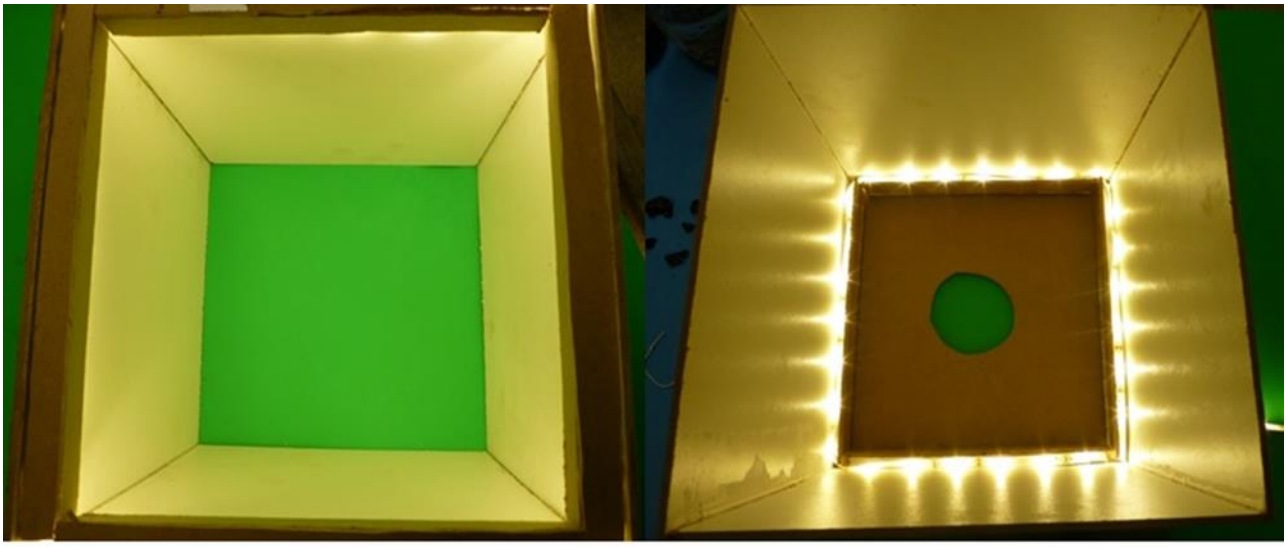

Figure 10: Illumination box: a) top view: diffusion of the light reflecting from the side walls; b) bottom view: The illumination source for the box is provided by an LED string on L shaped covers

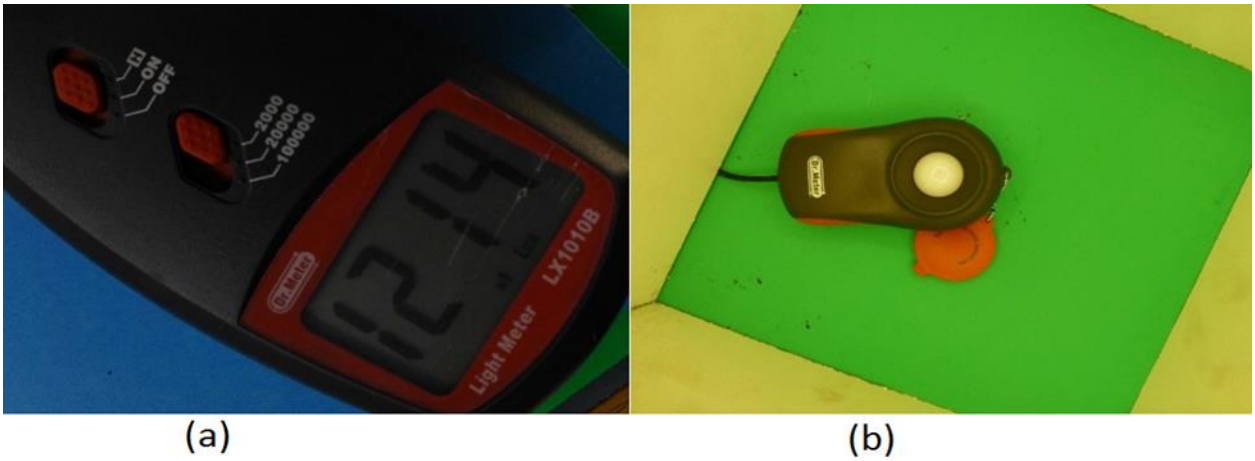

Figure 11: (a) Lux meter used for measuring the light intensity; (b) The receiver sensor of the Lux meter

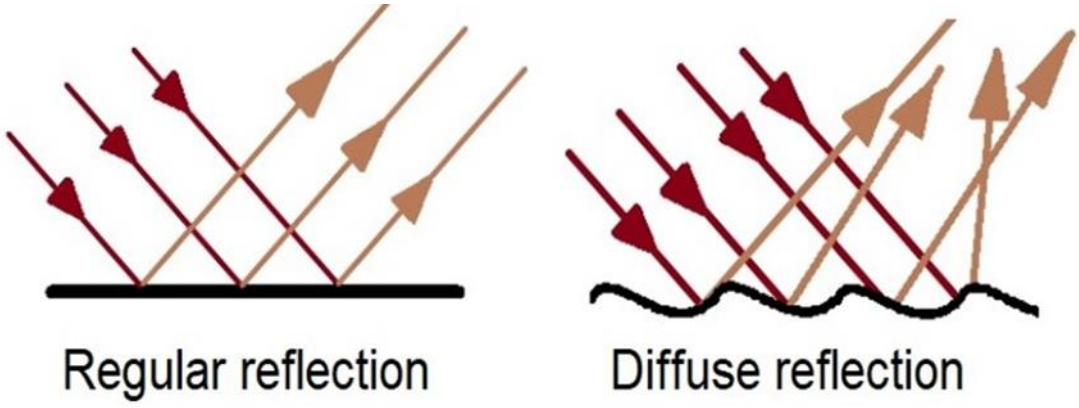

Figure 12: Schematic illustration of light reflections on different types of surfaces. A smooth surface reflects the lights regularly (on the left), but the melamine white board diffuse the reflections (on the right side)

Figure 13: The illumination box placed on the top of a sample

3.2.2. Image Enhancement (preprocessing data)

Despite using the light-box, underwater samples still might suffer from a reduction of light dispersion. The light directions will be changed and the light energy will be decreased inside the water. As a result, images of the samples in water suffer from poor contrast, because some of the light arrays are reflected when they enter the water (Ancuti et al., 2012).

The original images could be enhanced to improve the outcome of this system. A suitable image for subsequent processing (e.g. clustering and classification) is the one with distributed colour intensities, illumination contrast, and low level of noise. The enhancement process in this research consists of regional contrast enhancement of the images using CLAHE (Contrast Limited Adaptive Histogram Equalization) method and correction of the specular highlights occurring on the surface of the coated areas (Figure 14). These enhancement processes could reduce errors in the subsequent clustering and classification of test images.

This system was implemented using the open-source OpenCV 3.3.0 library ("OpenCV library", 2017) in C++ Visual Studio Community 2015 environment. OpenCV library includes more than

2500 machine learning and computer vision algorithms, which includes both state of the art and classic algorithms and is aimed to offer a platform for application of computer vision methods and to establish machine perception for practical uses. The fast operation of C++ and the availability of various algorithms make OpenCV as a suitable platform for the development of computer vision-based applications.

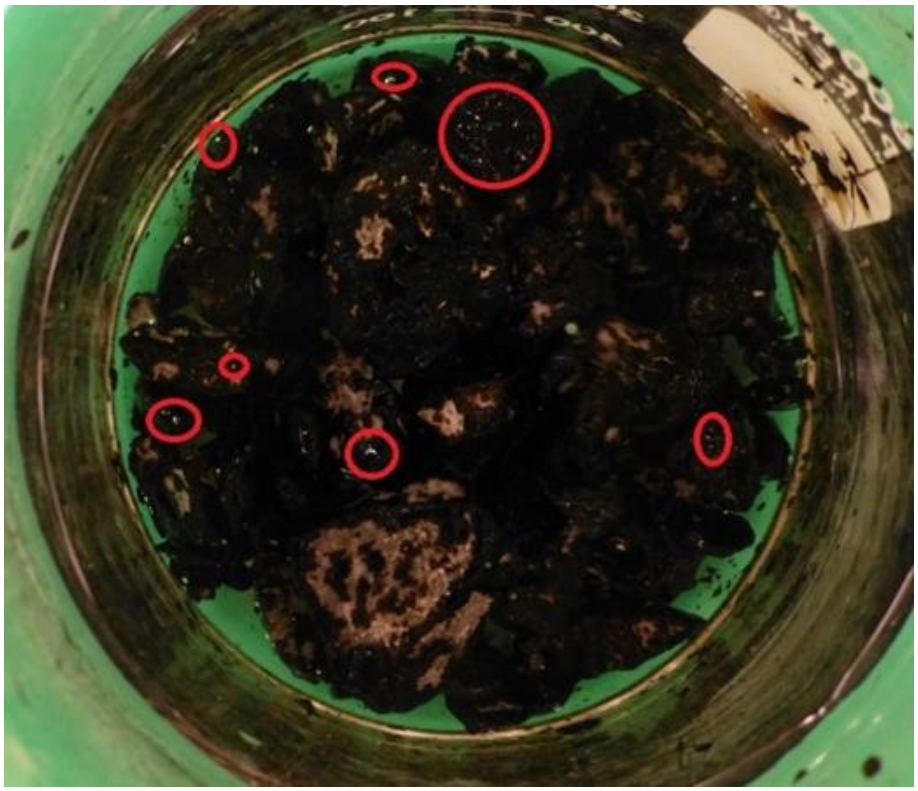

Figure 14: A sample image inside the illumination box. Some specular highlights are marked with red circles

3.2.2.1. Image Cropping

Since the samples are placed in a beaker, the region of interest in the images is usually a circle surrounding the actual mixture. The other parts of the image are useless in this research and should be removed and set to zero (their pixel intensity). The assumption is that the cropped area represents the attributes of the entire sample. A function was developed to select a circular area in the image manually. This function enables the operator to draw a circle around the area of interest,

and a circle could be drawn by clicking and holding the left button of the mouse and dragging the mouse pointer till the circle covers the desirable area. The circle is visible to the user through the process of the drawing (Figure 15). The codes of this process are provided in Figure 16.

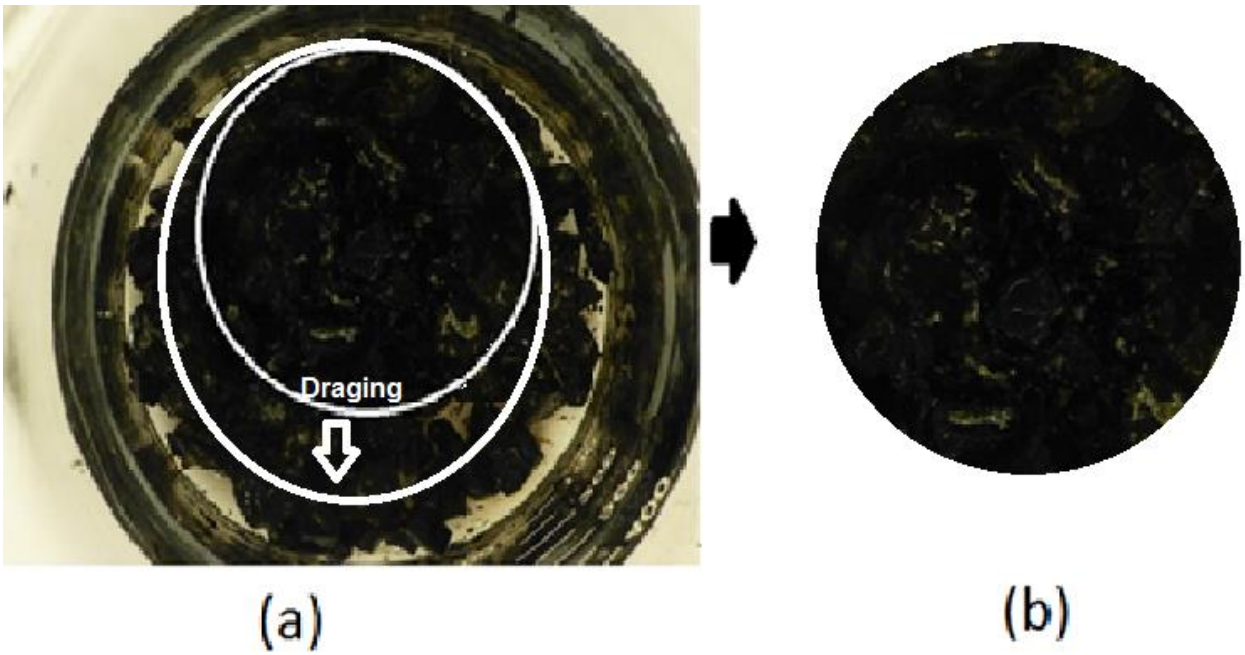

Figure 15: a) Circular cropping process; b) Resulted image after cropping

```
14  static void onMouse(int event, int x, int y, int flags, void*)
15  {
16      Mat temp_frame;
17
18      Point center;
19      if (event == EVENT_LBUTTONDOWN && clicked == false)
20      {
21          cout << "here" << endl;
22          prevPt.x = x;
23          prevPt.y = y;
24          cout << "prevPt x and y: " << prevPt.x << " " << prevPt.y << endl;
25          clicked = true;
26      }
27
28      else if (clicked == true && event == EVENT_MOUSEMOVE)
29      {
30          pt = Point(x, y);
31
32          double res = norm(pt - prevPt);
33          int radius = res / 2;
34          center.x = (pt.x + prevPt.x) / 2;
35          center.y = (pt.y + prevPt.y) / 2;
36          img.copyTo(temp_frame);
37          circle(temp_frame, center, radius, Scalar::all(255), 3, 8, 0);
38          imshow("image", temp_frame);
39      }
40      else if (event == EVENT_LBUTTONUP && clicked == true)
41      {
42          pt = Point(x, y);
43
44          double res = norm(pt - prevPt);
45          int radius = res / 2;
46          Point center;
47          center.x = (pt.x + prevPt.x) / 2;
48          center.y = (pt.y + prevPt.y) / 2;
49
50          //circle(img, center, radius, Scalar::all(255), 3, 8, 0);
51          circle(mask, center, radius, Scalar(255, 255, 255), -1, 8, 0);
52          imshow("image", img);
53          imshow("mask", mask);
54          clicked = false;
55          img.copyTo(result, mask);
56          imshow("result", result);
57          imwrite("C:\\Users\\sony\\Desktop\\9.1.jpg", result);
58      }
59  }
```

Figure 16: Circular cropping code developed in C++ environment

The drawing of the circle is defined as a sub-function which should be recalled in the main system via *setMouseCallback()* command as presented in Figure 17.

```
63      img = imread("C:\\Users\\sony\\Desktop\\9.jpg");
64      mask = Mat::zeros(img.size(), CV_8UC1);
65      //result = Mat::zeros(img.size(), CV_8UC3);
66      namedWindow("image", 1);
67      imshow("image", img);
68      setMouseCallback("image", onMouse, 0);
```

Figure 17: The callback function for cropping

A proper view of the object inside the water should be obtained to address the difficulties of the lighting conditions. Images of objects inside water usually suffer from back-scattered lighting and limited contrast. The undesirable conditions could be even worse due to the existence of suspended particles (Fabio et al., 2014). Next subsections describe methods to enhance the lighting conditions.

3.2.2.2. Histogram Equalization

Histogram equalization is a technique for pixel intensity adjustment to enhance the contrast of images. Histogram equalization could be implemented on single-channel images. For example, an 8-bit single-channel image has pixel values between 0 and 255, varying from black at the weakest intensity (0) to white at the strongest (255). Histogram of an image could be drawn by plotting intensity vs frequency of the pixel intensity or probabilities of the pixel intensity. The total number of pixels associated with each pixel intensity is calculated and the frequency of each pixel intensity in the image metrics is then measured (Hum et al., 2014; Kim, 1997).

The histogram equalization aims at the reconstruction of an image with a better contrast, which is an important characteristic of this research because it can signify the visual difference between coated and uncoated areas. This method expands the histogram of the image and makes a histogram of intensities more distributed. The local and global maximums in the histogram are more scattered. This way, the histogram of the image becomes more balanced via neglecting unpopulated parts of the histogram and stretching out the intensity range. Since this method enhances the global contrast of the image, some of the bright pixels can become too bright. In other words, intensities of the pixels at the right end of the histogram are amplified, which creates shiny noises in some of the bright parts in the image.

By considering L as a representation of a grayscale image's pixel intensities, which is normalized in the intervals of $[0,\ r-1]$, the transformation function can be expressed in equation 1 and equation 2 (Gonzalez and Woods, 2002).

$$s = T(r) \qquad 0 \leq r \leq L \tag{1}$$

$$r = T^{-1}(s) \qquad 0 \leq s \leq 1 \tag{2}$$

Each normalized grey level is confined in the range of [0,1]. If the transformation function T(r) be implemented, the inverse transformation $T^{-1}(s)$ should exist, and the increasing order from value 0 to 1 should result in the output image, and also both the output and input grey levels should be in the same range. So, by definition, the satisfactory assumption of the T(r) are defined as (Gonzalez and Woods, 2002)

- T(r) is single-valued and monotonically increasing in the interval $0 \leq r \leq l$.
- $0 \leq T(r) \leq 1$ for $0 \leq r \leq l$.

Considering an image is denoted as X = {X (i, j)}, in which X (i, j) is the intensity representor of the image at location of (i, j). The image is composing of L discrete gray levels $\{X_0, X_1, \ldots, X_{L-1}\}$. The probability density function (PDF) could be written as P (X_k) (equation 3) (Gonzalez and Woods, 2002; Wang et al., 1999; Szeliski, 2010).

$$P\ (X_k) = \frac{n^k}{n} \tag{3}$$

n^k is the frequency of the level X_k happening in the image X, in which the k is varying from 0 to L-1. n is the total number of pixels or samples in the image. The cumulative probability density function (CDF) or c(x) will be calculated as equation 4 (Wang et al., 1999; Szeliski, 2010; Kim, 1997).

$$c(x) = \sum_{j=0}^{k} p(X_j) \quad (4)$$

The X_k is equal to x and based on dethe finition, the $c(x_{L-1}) = 1$. The transformation function is a function which creates outputs and also in this case, the CDF has been utilized in the transformation function $f(x)$ (equation 5). The CDF (Cumulative Distribution Function) should be multiplied by all the ranges of gray $(x_{L-1} - x_0)$ to obtain the intensity range through all the grey levels (Wang et al., 1999; Szeliski, 2010).

$$f(\mathrm{x}) = X_0 + (X_{L-1} - X_0).\,\mathrm{c}(\mathrm{x}) \quad (5)$$

The result of the histogram equalizer is an image metrics expressed as Y in equation 6 (Wang et al., 1999; Kim, 1997).

$$Y = f(x) = \{f(X(i,j)) \mid \forall X(i,j) \in X\} \quad (6)$$

The intensity range of the pixels is increased so the histogram of the image will be more distributed. Implementation of the Histogram Equalizer divides into three steps (Szeliski, 2010).

- Calculate the histogram of the image
- Compute the sum of the histogram after normalization (histogram calculator)
- Find the resulted data out of input data via transformation function.

3.2.2.2.1. Histogram Equalization Implementation

Since this system has to process coloured images (red-green-blue), the original images are split into three channels and saved as a vector variable (Figure 18).

```
/// split the image into different coloring spaces( here BGR)
vector<Mat> BGR;
split(src, BGR);
```

Figure 18: Splitting an image into blue, green and red channels

The histogram for each channel is calculated as presented in the code in Figure 19.

- **C++:** void calcHist (const Mat* **images**, int **nimages**, const int* **channels**, InputArray **mask**, OutputArray **hist**, int **dims**, const int* **histSize**, const float** **ranges**, bool **uniform**=true, bool **accumulate**=false)

  Parameters:

  The "nimages" is the number of input "image"s as the source arrays should be in certain colour space "channel". Also, a "mask" image can be applied. The parameters of "dim", "histSize", and "ranges" determine the characteristics of the histogram. Details can be found in ("OpenCV", 2017).

The histogram of the image in 8-bit single colour space before and after the application of histogram equalizer is shown in Figure 20.

```
40
41      /// defining the variables in the commands
42      // Establish the number of bins
43      int histSize = 32;
44
45      // Set the ranges ( for B,G,R) )
46      float range[] = { 0, 256 };
47      const float* histRange = { range };
48      bool uniform = true; bool accumulate = false;
49
50      Mat b_hist, g_hist, r_hist;
51
52      ///compute the histogram for each channel
53      calcHist(&BGR[0], 1, 0, mask, b_hist, 1, &histSize, &histRange, uniform, accumulate);
54      calcHist(&BGR[1], 1, 0, mask, g_hist, 1, &histSize, &histRange, uniform, accumulate);
55      calcHist(&BGR[2], 1, 0, mask, r_hist, 1, &histSize, &histRange, uniform, accumulate);
```

Figure 19: Calculating the histogram for each channel

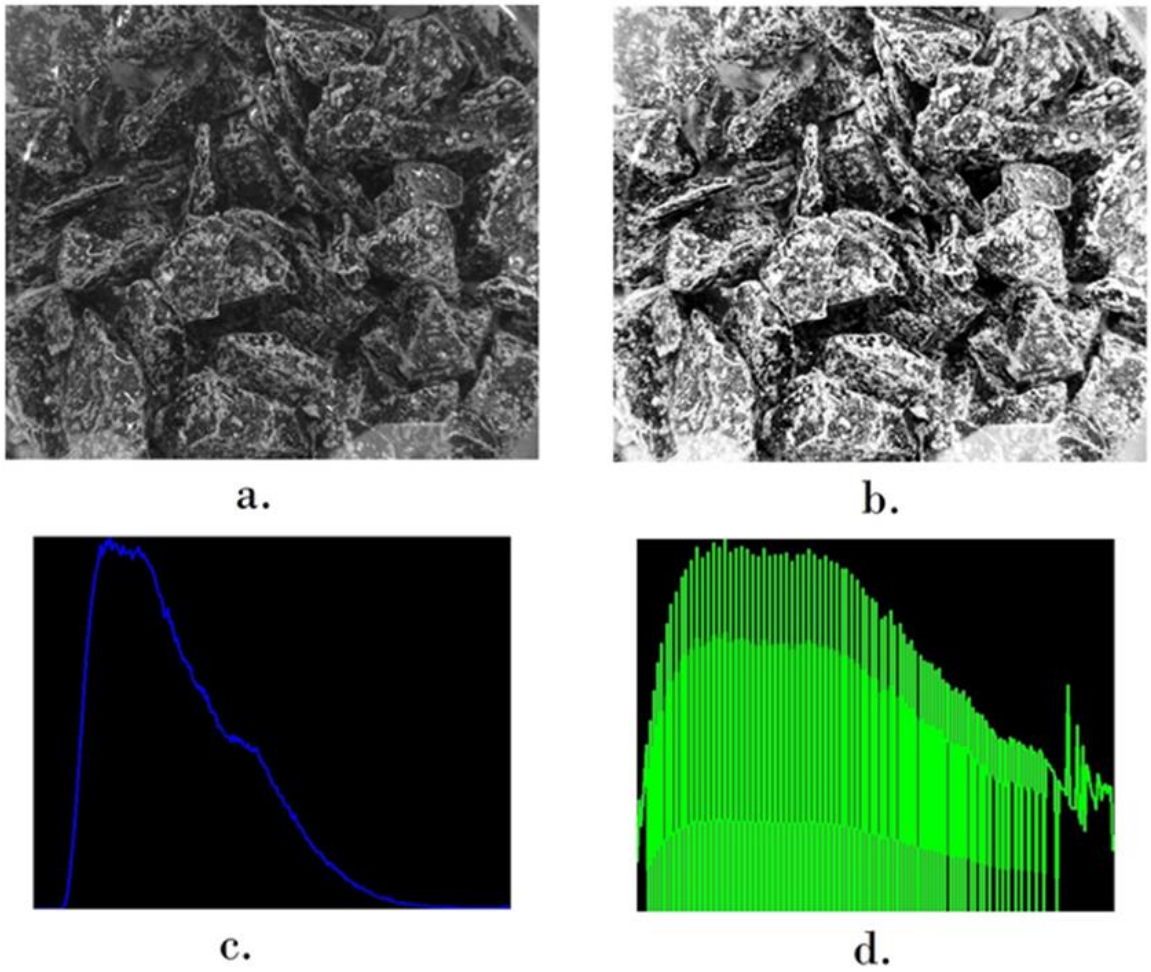

Figure 20: a) Original grayscale image; b) image after histogram equalization; c) histogram of the original image; d) histogram of the processed image

The histogram equalizing is carried out using the *equalizeHist(src, dst)* function, where the command receives a single channel image of *src* and provides the result in the *dst*. Since the global histogram equalization creates some errors in the modification process, a more advanced version of histogram equalization, called Contrast Limited Adaptive Histogram Equalization, was employed for enhancement of the image contrast.

3.2.2.3. Contrast Limited Adaptive Histogram Equalization (CLAHE)

A potential alternative for the contrast enhancement in the image pre-processing is CLAHE. The contrast-limited adaptive histogram equalization is performed in the channel L of CIELAB

colour space to enhance the luminance of the image. The CIELAB colour space is the same as CIE L*a*b* or in short form “Lab”. This colour space includes three channels, which contain values regarding the lightness, green_red and blue-yellow elements and are represented as “L”, “a” and “b” channels, respectively. The Lab is one of the closest colour spaces to the human’s vision, since it is perceptually uniform for the human vision (Lukac and Plataniotis, 2006).

The application of CLAHE deduces the light attenuation and decreases the impact of specular highlights on the objects (Fabio et al., 2014). CLAHE technique tries to enlarge the intensity range of the initial image by increasing the interested features’ contrast. The improvement is gained since the surface between each adjacent structure is excellently drawn (Ancuti et al., 2012).

The gradient of transformation function defines the contrast amplification from a given neighbouring pixel’s value through the application of CLAHE. The gradient is in close relation with the histogram of the image at pixel’s value, as well as the gradient of the neighbouring cumulative distribution function. Prior to the computation of the CDF, CLAHE horizontally cuts the intensity histogram at a certain limit to confine the contrast amplification range (green line in Figure 21). The limit value, which is known as “clip_limit’, restricts the gradient of the transformation function. The neighbouring region size and normalized histogram are the controlling factors affecting the *clip_limit*. After cutting of the histogram on the *clip_limit*, the part above the limit (the blue area on the left image in Figure 21) is distributed equally (the purple area on the right image in Figure 21) in each histogram’s bins. Therefore, after the redistribution, the value of some bins exceeds the *clip_limit* again (the blue area on the right image in Figure 21).

Depending on the histogram of the image, a new larger limit is defined. This iterative process stops when the exceeding values of the bins are smaller than a certain small value (Pizer et al., 1987).

Figure 21: An exaggerated visualization for application of CLAHE on the intensity histogram of an image

An M × M pixel block (or tile) is defined to subdivide the image and perform histogram equalization on each subdivision. To avoid artifacts in the resulting image, either sliding window or deriving the equalization function of blocks with no overlap and using a transfer function to smoothly transit between blocks, could be employed. The later approach is called "Adaptive Histogram Equalization (AHE)" technique which is used in this research (Szeliski, 2010). The regular *AHE* tends to cause some noises due to the overamplification of the contrast at a near-constant area. This problem of noise amplification is restricted by CLAHE (Pizer et al., 1987). The contrast limited version of *AHE* is CLAHE.

3.2.2.3.1. CLAHE Implementation

The code loads an image and creates a matrix variable (Mat) to save the image. Then the image is converted via *cvtColor()*from BGR into Lab. A vector is defined and the Lab version of the image is split into the three channels in the Lab space. Then the CLAHE function is recalled, and the limit of the clipping is determined using the *setClipLimit()* function, and finally, the CLAHE is applied on the lightness channel (L) of the image. Figure 22 compares the differences in the

images before (Figure 22-a) and after (Figure 22-b) application of CLAHE. Figure 23 shows the implementation of the code for CLAHE in C++.

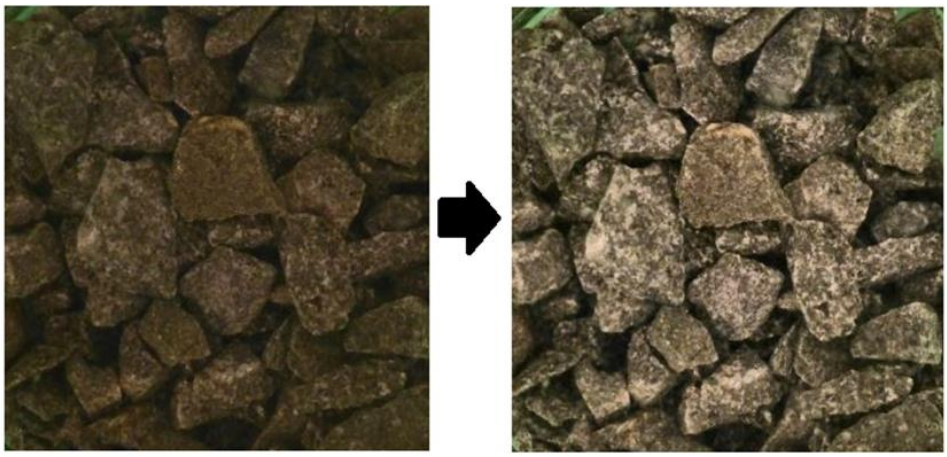

Figure 22: An image a) before applying CLAHE; b) after application of CLAHE

```
14      /// Load an image
15      Mat bgr_image = imread("C:\\Users\\sony\\Desktop\\9.jpg");
16
17      Mat lab_image;
18      cvtColor(bgr_image, lab_image, CV_BGR2Lab);
19
20      // Extract the L channel
21      vector<cv::Mat> lab_planes(3);
22      split(lab_image, lab_planes);  // now we have the L image in lab_planes[0]
23
24                                     // apply the CLAHE algorithm to the L channel
25      Ptr<cv::CLAHE> clahe = createCLAHE();
26      clahe->setClipLimit(2);
27      Mat dst;
28      clahe->apply(lab_planes[0], dst);
```

Figure 23: Implementation of CLAHE using OpenCV in C++

Afterward, the adjusted channel should be merged with the other colour spaces (a and b). The image is merged using the *merge()* command. Finally, the image is converted back into BGR format and both original and adjusted images are available for further processes (the code is provided in Figure 24).

```
30      // Merge the the color planes back into an Lab image
31      dst.copyTo(lab_planes[0]);
32      merge(lab_planes, lab_image);
33
34      // convert back to RGB
35      Mat image_clahe;
36      cvtColor(lab_image, image_clahe, CV_Lab2BGR);
37
38      // display the results
39      imshow("image original", bgr_image);
40      imshow("image CLAHE", image_clahe);
41
```

Figure 24: The separated channels of the image are merged after modification on the L channel

3.2.2.4. Specular Highlight Reconstruction

Digital *inpainting* is used to reconstruct small-size damages (e.g. scratches) in an image. The *inpainting* method is easy to apply, fast and results are proper. The digital *inpainting* is already used in a number of applications, such as removing scratches, disturbed parts, and even a logo from an image. Desired *inpainting* area is one of the main inputs for this function. The information regarding the colours is gathered from the neighbourhood of the *inpainting* boundary and the area of interest is reconstructed with respect to this neighbourhood. *Inpainting* technique enables the isophotes (line of same intensity values on the histogram) to be continued smoothly inside the reconstruction section. Different methods could be applied to achieve this objective (Kandhal, 1992). One group of methods aims to solve a partial differential equation (PDE) on various heuristics and find the distribution of the colour intensities inside the missing part, such as total variational (Chan and Shen, 2000) and curvature-driven diffusion model (Kandhal, 1992). Another type of methods uses a 3×3 window function as a filter. The missing section will be convolved with this filter to find the missing information from diffusion of the known information, i.e. the values of the known neighbourhood (Terre et al., 1993). The inpainting function in OpenCV, which was used in this research project, is based on the latter method. An estimator, based on image histogram gradient, anticipates the smoothness of the curves. The anticipated smoothness is the weighted average in the vicinity of *inpainting* part. By considering the missing pixels as a level

set and also applying fast marching method (FMM), the missing information regarding the image is estimated (Kandhal, 1992). This method is suitable for applying in various problems, such as problems related to the shapes created by shades, arrival time and developing of lithographic in magnification of microchips. The method attempts to follow the movement of a boundary (two or three dimensions) which separates two regions. The assumption is that the boundary moves due to a speed function F in a normal direction. A proper week solution is provided by adding curvature to the speed law with considering related smooth flow. Given an initial position of boundary interface Γ (a closed curve in $\mathbb{R}2$) and a function speed Γ which is in normal direction with speed function F, level set zero for the function could be represented as $\Phi(x, t = 0)$ from $\mathbb{R}2 \rightarrow \mathbb{R}$. The main function is $\Phi(x, t = 0) = \pm d$, where distance between x and Γ is d and assigning positive or negative sin to d depends on the position of the point which if the point is locating inside boundary Γ the sign is positive and if it is placing outside of the boundary the sign is negative and that is how it evolves using chain rule to the equation presented in equation 7 and equation 8.

$$\Phi_t + F|\nabla_\Phi| = 0 \quad (7)$$

$$\Phi(x, t = 0) = 0 \quad (8)$$

This process is time-consuming if it processes all the points. Therefore, points of interest are grouped into three classes, such as alive, landmines, and faraway, which mean inside, near and outside of the boundary, respectively. The computation is only performed on alive points and the boundary evolves when the landmine points are reached and the fast marching is an extreme on-cell version of the mentioned method (Sethian, 1996). The advantages of using this method are a simple implementation, fast processing, relatively accurate results (compared to other methods) and compatibility with different local inpainting methods (Telea, 2004).

3.2.2.4.1. Inpainting Implementation

The image is converted into LAB colour space and split into three channels. Simple thresholding is applied to the channel L to isolate high-intensity specular highlights from the image and keep the remaining pixels in a "mask" (Figure 25-b). The isolated part, i.e. specular highlights, are assigned as white and other pixels are assigned as black (0 value). The thresholding value is considered 230 by practical judgment. The thresholding value could be increased to 235 and the best value should be defined based on trial and error values between 230 to 235. The resulting mask is displayed in Figure 25-b. The code for splitting an image into Lab channels and thresholding is provided in Figure 26 and Figure 27 shows the implementation of *inpainting.* An example of applying *inpainting* function on an image is illustrated in Figure 25.

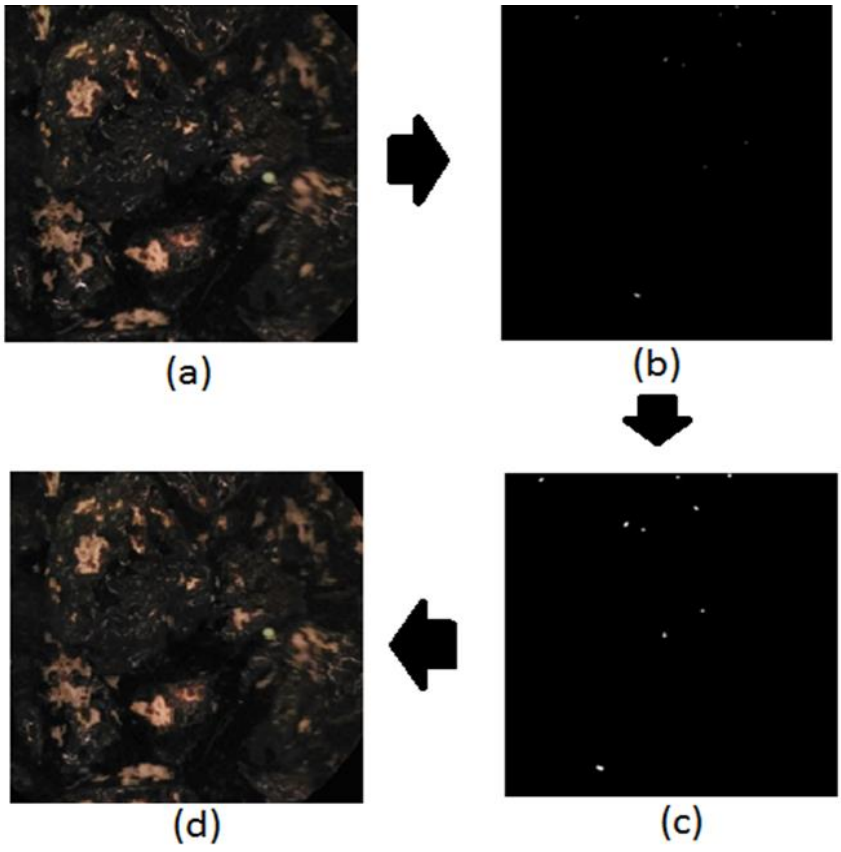

Figure 25: (a) An input image (after CLAHE); (b) A binary mask by thresholding; (c) The binary mask after dilating; (d) An image after inpainting

```
36      vector<Mat> Lab;
37      Mat imgLab;
38      cvtColor(src, imgLab, CV_BGR2Lab);
39      split(imgLab, Lab);
40
41      //imshow("L", Lab[0]);
42      //imshow("a", Lab[1]);
43      //imshow("b", Lab[2]);
44
45      //////////////option to remove small glares
46      medianBlur(src, src, 5);
47
48      //imshow("SRC1", src);
49      Mat fixed_img, temp_img, temp_mask;
50      Lab[0].copyTo(temp_img);
51      threshold(temp_img, temp_mask, 210, max_thresh, THRESH_BINARY);
52      imshow("Mask", temp_mask);
```

Figure 26: The descriptive code for detecting specular highlights

The mask is adjusted by dilating the isolated pixels to ensure that the entire specular parts are considered in the mask (Figure 25-c). Then, the areas of the removed pixels are reconstructed using *inpainting* concerning their neighbourhood values utilizing the input image (Figure 25-a) and the "mask" image., An instance of a reconstructed image is provided in Figure 25-d. The *inpaint()* process is implemented using the OpenCV function as Figure 27.

- void inpaint (InputArray **src**, InputArray **inpaintMask**, OutputArray **dst**, double **inpaintRadius**, int **flags**)

  parameters:

  The input image "src" is *inpainted* and saved in "dst", considering the neighbourhood in the distance of "inpaintRadius" by "flags" method, such as "INPAINT_TELEA" that is discussed.

```
54      Mat element = getStructuringElement(MORPH_CROSS, Size(3, 3));
55      dilate(temp_mask, temp_mask, element, Point(-1, -1), 1, 1, 1);
56      imshow("Mask2", temp_mask);
57      inpaint(src, temp_mask, src, 3, INPAINT_TELEA);
```

Figure 27: The descriptive code in C++ to dilate the detected specular highlight area and inpainting

3.2.3. Clustering of Pixels (choosing the model)

After image enhancement, the pixels of the sample should be clustered to identify the stripped and coated areas. Out of many available clustering methods, K-means is chosen for its various advantages.

3.2.3.1. K-means

The K-means algorithm was initially proposed by Steinhaus in 1956 and then it was used by Lioyd for PCM (pulse code modulation) signal quantization, and thereby, the standard k-means algorithm is sometimes referred as Lioyd and fogy algorithm (Bock, 2007). K-means method for image segmentation operates based on the colour intensity of the pixels. K-means is one of the derivations of the EM (expectation maximization), where isotropic Gaussian assumes to be prior. The classic principle of least squares is a fundamental of the K-means algorithm. The inputs are a set of data points $\{x_1, ..., x_n\}$ and K is the number of types (clusters) in the K-means algorithm. As the algorithm initiates, K centroids $\{c_1, \ldots, c_k\}$ are placed in random locations within the data, and then the following two steps are iteratively followed: Step one, the nearest centroid to each of the data points (x_i) is found, as presented in equation 9, and the then this point is assigned to the related cluster. In the second step, the centroid is recomputed equal to mean of all the points, assigning as the same label (the mathematics are provided in equation 10). Moreover, the new centroids are relocated to new spots. The mentioned steps are continued until none of the points change their cluster. The algorithm reached the converging point at this stage and the iterations will stop. The algorithm is basically aimed to minimize the WCSS (within-cluster sum of squares) as presented in equation 11 (Kandhal and Rickards, 2001).

$$\arg\min D(x_i, c_j) \tag{9}$$

$$c_j(a) = \frac{1}{n_j} \sum_{x_i \to c_j} x_i(a) \quad \text{for a} = 1, \dots, \text{d} \tag{10}$$

$$WCSS = \sum_{\substack{c_i \in k \\ cluster}} \sum_{\substack{j=1\ to\ 4 \\ dimension}} \sum_{\substack{x,y \in c_i \\ object}} (x_{ij} - y_{ij})^2 \tag{11}$$

The $D(x_i, c_j)$ function is the distance of the instance x_i from centroid c_j. The distance could be any distance function, but the Euclidian distance is considered to make sure that algorithm is converging eventually. The parameter a is a particular attribute value. It should be noted that the K-means algorithm is compatible with numeric values and does process characters. Comparing to the other available clustering methods, K-means is fast, although it is computationally hard (NP-hard). The computation time t for the algorithm is calculated using equation 12, which depends on the number of iterations (Kriegel et al., 2017). The Lioyd algorithm's slow computation could be improved through the application of the triangle inequality and caching. The main reason of the slow progress is that the standard algorithm is instantly calculating a large number of distances, which is not required for most of the points, in all iterations.

$$\text{t} = \#\text{iteration} * \text{k} * \text{n} * \text{d} \tag{12}$$

In this equation, #iteration is the number of iterations, n is the number of instances and d is the number of dimensions in the clustering. The Hartigan and Wong (1979) and Wong method in $\mathbb{R}$ is the fastest method but it sometimes fails to converge (Kriegel et al., 2017). The quality of the clustering was meaured by adding up variation within each cluster. It is probable for K-means that it does not reach the best classification (MacKay, 2003). The solution is to monitor the resulting clusters and relating total variance and repeats the algorithm with new initial points (Kriegel et al., 2017)

The K is defined as an input, so it needs to be chosen before the start of the algorithm. Different values for K are used and the total variation for each K is measured. All the results are compared together in order to find the best K (i.e. number of clusters).

The Euclidian distance for two- and three-dimension datasets could be calculated using equations 13 and equation 14, respectively. The same principle could be expanded to the data sets with more dimensions; however, the K-means works better in datasets with low dimensions (Kriegel et al., 2017). x, y and z are different dimensions of the points a and b in the following equations.

$$D(b,a) = \sqrt{(a_x - b_x)^2 + (a_y - b_y)^2} \quad (13)$$

$$D(b,a) = \sqrt{(a_x - b_x)^2 + (a_y - b_y)^2 + (a_z - b_z)^2} \quad (14)$$

The K-means algorithm may have some deficiencies in some cases. Three main drawbacks are consideration of the distance of means from the data points with the same weight in each cluster, the size or shape of the cluster is not fully known, and the algorithm is 'hard'; However, 'soft' is preferable) (MacKay, 2003). The implementing code is provided in Figure 28.

3.2.3.1.1. K-means Implementation

- double kmeans (InputArray **data**, int **K**, InputOutputArray **bestLabels**, TermCriteria **criteria**, int **attempts**, int **flags**, OutputArray **centers**=noArray())

  parameters:

  The k-means receives "K" as a number of clusters and an array of points having N dimensions "data" and saves the processed labels (cluster ID) for each point in "bestLabels". The accuracy of the algorithm is defined as "criteria" and "attempts" representing the number of times that algorithm runs with different initial points.

Each pixel is investigated through the algorithm then based on the processed K-mean's class, the pixel is assigned to the related class. In the end, K classes (e.g. K was defined 3 in this example) could be displayed in individual windows (Figure 28 shows a sample code). An example of classification using K-means (K equal to 3) is illustrated in Figure 29.

```
    Mat labels;
    Mat centers;
// applying K-means function
    kmeans(kmeanPoints, K, labels, TermCriteria(CV_TERMCRIT_ITER | CV_TERMCRIT_EPS, 10, 0.2), 10, KMEANS_PP_CENTERS, centers);

    Vec3b tempColor;

    Mat class0 = Mat::zeros(n, 1, src.type());
    Mat class1 = Mat::zeros(n, 1, src.type());
    Mat class2 = Mat::zeros(n, 1, src.type());

    for (int j = 0; j < n; j++) {
        int cluster_idx = labels.at<int>(j, 0);

        if (cluster_idx == 0) {
            tempColor[0] = centers.at<float>(cluster_idx, 0);
            tempColor[1] = centers.at<float>(cluster_idx, 1);
            tempColor[2] = centers.at<float>(cluster_idx, 2);
            class0.at<Vec3b>(j, 0) = tempColor;
        }
        else if (cluster_idx == 1) {
            tempColor[0] = centers.at<float>(cluster_idx, 0);
            tempColor[1] = centers.at<float>(cluster_idx, 1);
            tempColor[2] = centers.at<float>(cluster_idx, 2);
            class1.at<Vec3b>(j, 0) = tempColor;
        }
        else if (cluster_idx == 2) {
            tempColor[0] = centers.at<float>(cluster_idx, 0);
            tempColor[1] = centers.at<float>(cluster_idx, 1);
            tempColor[2] = centers.at<float>(cluster_idx, 2);
            class2.at<Vec3b>(j, 0) = tempColor;
        }

    }
```

Figure 28: Descriptive code for clustering using K-means classifier

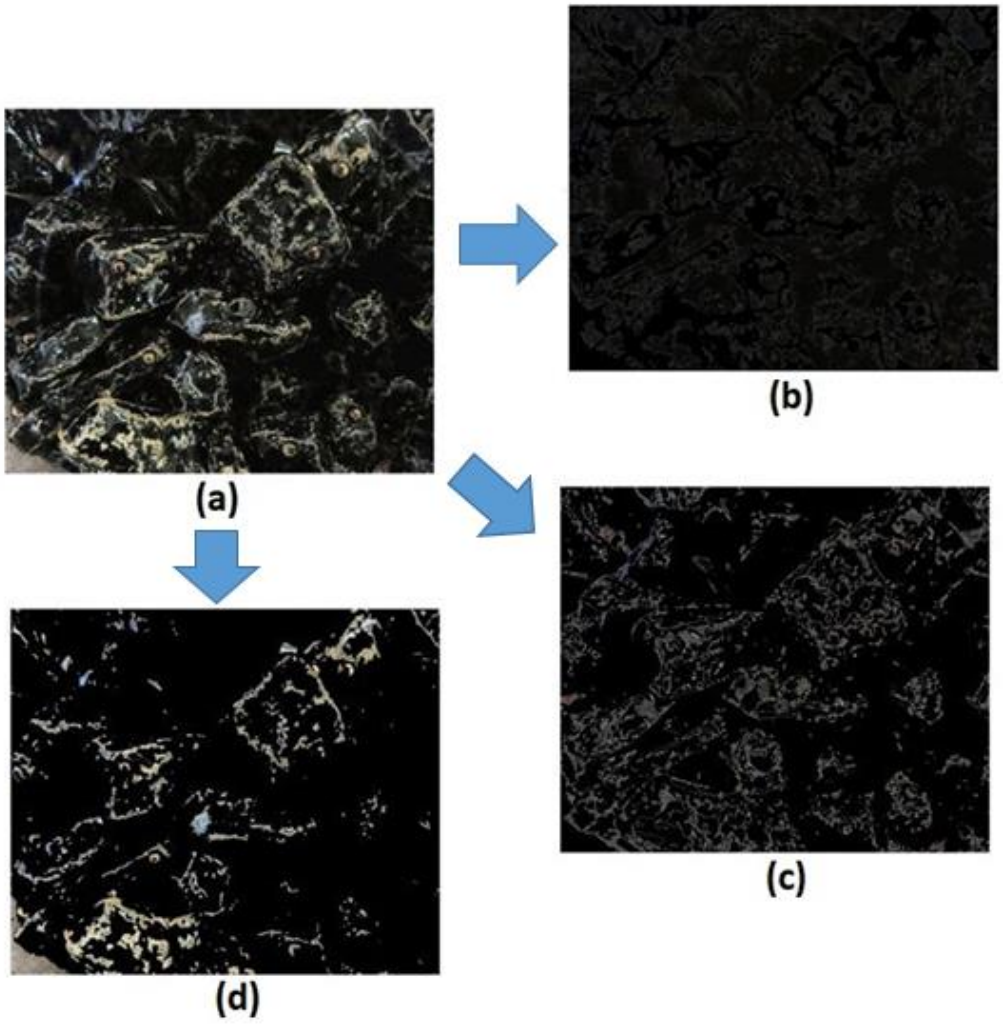

Figure 29: (a) an input image for the K-means algorithm (after applying CLAHE); (b), (c), and (d) are three resulted clusters

Each of the classes has some zero pixels as well as some none zero ones representing points that are clustered in that class. A total number of pixels in each class can be calculated with *countNonZero()* in the code. If the class representing stripped area is identified, the striping percentage can be calculated by dividing a total number of the pixels counted in the stripping class by the total number of pixels in the original enhanced image.

3.2.4. Classification (Model Training)

To overcome the issue of subjective human judgment on the test results, a fully automated code without any interaction of human is required. Hence, there is a need to develop an automated classifier which could identify the clusters that represent stripped areas.

3.2.4.1. Supervised Classifier

By providing positive and negative training samples for the system, the label of each test sample (recognizing the stripping cluster) will be estimated automatically. Depending on the number of the available samples for the training, different supervised machine learning methods could be employed. In the case of having a large number of training samples, some advanced methods, such as deep learning, could be used. In contrast, if the training samples are limited, other methods, such as K-Nearest Neighbor (K-NN), Support Vector Machines (SVM), decision tree, and Naïve Bayes, are practical options for the estimation. In this research, the number of training samples is limited, and therefore the K-NN and SVM methods were used which were trained by the same training sets.

3.2.4.1.1. K-Nearest Neighbors

K-nearest neighbours (K-NN) classification method attempts to recognize patterns and it is one of the basic methods in machine learning (Weinberger and Saul, 2009). The K-NN method consists of different processes. The function extracts a vector of features from the data, which contains two separate vectors of values. The resulted vectors are an input for the classification function (classifier). The classifier compares the features with the provided training set, where it measures k nearest points to the input data (Weinberger and Saul, 2009). Figure 30 shows an illustration of this process.

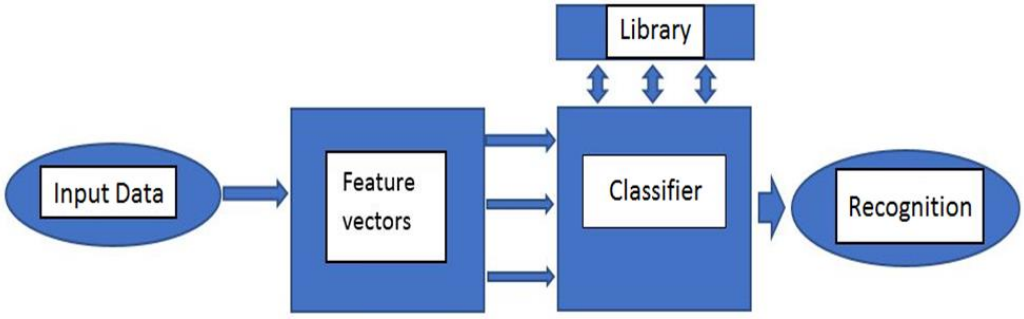

Figure 30: Schematic visualization for the K-NN classifier

The K-nearest neighbours method classifies test data through the K closest neighbours around the data's vector. The closest available data (points) are located by Euclidian distances in most methods (Weinberger and Saul, 2009). Depending on the location of the test data in the feature space, the closest neighbours are detected. Computation of distances affects the performance of K-NN classifier. The algorithm usually uses Euclidean distances, but it does not consider the statistical irregularities deriving from large training labelled-dataset. There are other available types of distances which could be utilized for computing distances. The algorithm can significantly evolve via learning the distance metrics from the training set (Weinberger and Saul, 2009). There are a few distance measurement techniques for K-NN, such as Euclidean, Manhattan, and Minkowski, which are all provided in Table .

Table 2: Different methods of measuring distances between data points

Method	Distance mathematical calculation
Euclidean	$\sqrt{\sum_{i=1}^{n}(x_i - y_i)^2}$
Manhattan	$\sum_{i=1}^{n}\lvert x_i - y_i\rvert$
Minkowski	$(\sum_{i=1}^{n}(\lvert x_i - y_i\rvert)^q)^{1/q}$
n is the # dimensions. x represents datapoint from the dataset. y is the new data point which should be estimated.	

The algorithm uses distances to determine the label of the test sample $Y_j$which the label depends on the majority of labels in the K nearest neighbors in the training data set (labels for $X_i \rightarrow w$ where $i = 0, 1, \dots, K-1$). The distance shall be measured using equation 15. Labels for these K decision-making neighbors in the training set could be defined as decision rules (D(Y$\rightarrow w$)) (Peterson and Coleman, 2008).

$$D(X_i, Y_j) = min_j \{D(X_i, Y_j)\} \quad (15)$$

The accuracy of the classifier depends on the value of K. The value of K could be determined via a trial and error process with different K values.

The K-NN ensures the generalization since it estimates the distances for all the points. Moreover, using Parzen Window in addition to K-NN to improve the performance of estimations detecting the K nearest neighbours over training data which is described with details in Bermejo and Cabestany's (2000) work in the reference (Bermejo and Cabestany, 2000).

3.2.4.1.1.1. K-NN Implementation

Three main steps are required for implementation of the K-NN. First and second steps are designed to train the model using negative and positive samples. The negative samples include non-coated areas of the sample mixtures. In contrast, the positive samples include samples of coated areas. Fourteen positives and fourteen negative samples are provided for training, where the negative samples are extracted from an image of a raw aggregate sample. The code iteratively reduces the size of a circle and uses the circle to crop the image. Histograms for each cropped area are calculated and will be considered as a separate negative training sample. The histograms of all the three channels of the negative samples are stored in a training matrix as "Negative" with the

label “-1”, and the histograms of positive samples are stored in a matrix, named “Positive” with label “+1”. The code for the K-NN is provided in Figure 31.

```
cv::Ptr<cv::ml::TrainData> trainingData;
cv::Ptr<cv::ml::KNearest> kclassifier = cv::ml::KNearest::create();


void knnHistogram(cv::Mat img) {
    vector<cv::Mat> BGR;
    cv::Mat Negative;
    cv::split(img, BGR);

    /// Establish the number of bins
    int histSize = 32;
    int samples = 14;

    cv::Mat temp1(samples, histSize * 3, CV_32FC1);
    temp1.copyTo(Negative);

    /// Set the ranges ( for B,G,R) )
    float range[] = { 0, 256 };
    const float* histRange = { range };

    bool uniform = true; bool accumulate = false;

    cv::Mat b_hist, g_hist, r_hist;
    Mat second_mask;



    for (int i = 0; i < samples; i++) {
        second_mask.setTo(cv::Scalar(0, 0, 0));

        float fraction = (float)i / 20;
        int rad = radius*(1 - fraction);

        circle(second_mask, center, rad, cv::Scalar(255, 255, 255), -1, 8, 0);

        /// Compute the histograms:
        calcHist(&BGR[0], 1, 0, second_mask, b_hist, 1, &histSize, &histRange, uniform, accumulate);
        calcHist(&BGR[1], 1, 0, second_mask, g_hist, 1, &histSize, &histRange, uniform, accumulate);
        calcHist(&BGR[2], 1, 0, second_mask, r_hist, 1, &histSize, &histRange, uniform, accumulate);

        int total = cv::countNonZero(second_mask);

        b_hist = b_hist / total * 100;
        g_hist = g_hist / total * 100;
        r_hist = r_hist / total * 100;

        for (int z = 0; z < histSize; z++) {
            Negative.at<float>(i, 3 * z) = b_hist.at<float>(z);
            Negative.at<float>(i, 3 * z + 1) = g_hist.at<float>(z);
            Negative.at<float>(i, 3 * z + 2) = r_hist.at<float>(z);
        }
    }

```

Figure 31: The code for creating negative training dataset out of a raw aggregate image

Since the training data are recorded in a matrix named’ “trainingdata” in a known order, the first 14 rows are defined for the negative samples with the label “-1”, and the rest are defined for

the positive samples with an assigned label of "+1". The model is trained using the *kclassifier->train (trainingdata)* function. The "vectsize" is considered as 3* histSize, since there are three different colour channels which is multiplied by the size of histogram, i.e. number of bins (as illustrated in Figure 32).

```
68      cv::Mat training_mat;
69      cv::Mat labels;
70      int vectsize = histSize * 3;
71
72      int posNum = 50;
73
74      int num_files = posNum + samples;
75
76      cv::Mat temp4(num_files, 1, CV_32SC1);
77      temp4.copyTo(labels);
78
79      cv::Mat Positive = cv::Mat(50, 32 * 3, CV_32F, positive_data);
80
81      Positive.copyTo(training_mat);
82
83      training_mat.push_back(Negative);
84
85
86      float data;
87      for (int i = 0; i < posNum; i++) {
88          labels.at<int>(i, 0) = 1;
89      }
90
91      for (int i = posNum; i < num_files; i++) {
92          labels.at<int>(i, 0) = -1;
93      }
94
95      K = sqrt(num_files);
96
97      trainingData = cv::ml::TrainData::create(training_mat, cv::ml::SampleTypes::ROW_SAMPLE, labels);
98      kclassifier->setIsClassifier(true);
99      kclassifier->setAlgorithmType(cv::ml::KNearest::Types::BRUTE_FORCE);
100     kclassifier->train(trainingData);
101 }
```

Figure 32: Descriptive code for introducing the positive training data and train the K-NN classifier using the defined training set

Then the K-NN classifier is trained and is used for classification of the histograms of the new clusters. The K-NN calculates K as the square root of the total number of training samples. The classifier searches for the K training data which have the nearest histograms to the histograms of the test sample, and based on the type (positive or negative) of the majority of neighbors, it determines whether the test cluster represent a coated or an uncoated area. (Figure 33 provides the code). Figure 34 illustrates this supervised classification process using a three-cluster K-means.

```
119  void knnResponse(cv::Mat img, cv::Mat mask, int indicator) {
120
121      vector<cv::Mat> BGR;
122      cv::split(img, BGR);
123
124      int histSize = 32;
125
126      /// Set the ranges ( for B,G,R) )
127      float range[] = { 0, 256 };
128      const float* histRange = { range };
129
130      bool uniform = true; bool accumulate = false;
131
132      cv::Mat b_hist, g_hist, r_hist;
133
134      /// Compute the histograms:
135      //calcHist(&BGR[0], 1, 0, Mat(), b_hist, 1, &histSize, &histRange, uniform, accumulate);
136      calcHist(&BGR[0], 1, 0, mask, b_hist, 1, &histSize, &histRange, uniform, accumulate);
137      calcHist(&BGR[1], 1, 0, mask, g_hist, 1, &histSize, &histRange, uniform, accumulate);
138      calcHist(&BGR[2], 1, 0, mask, r_hist, 1, &histSize, &histRange, uniform, accumulate);
139
140      int total = countNonZero(mask);
141
142      b_hist = b_hist / total * 100;
143      g_hist = g_hist / total * 100;
144      r_hist = r_hist / total * 100;
145
146      int length = histSize * 3;
147      cv::Mat temp2(1, length, CV_32F);
148      cv::Mat testMat;
149      temp2.copyTo(testMat);
150
151      for (int i = 0; i < histSize; i++) {
152          testMat.at<float>(0, 3 * i) = b_hist.at<float>(i);
153          testMat.at<float>(0, 3 * i + 1) = g_hist.at<float>(i);
154          testMat.at<float>(0, 3 * i + 2) = r_hist.at<float>(i);
155      }
156
157      cv::Mat matResults(1, 1, CV_32F);
158      kclassifier->findNearest(testMat, K, matResults);
159
160      if (indicator == 0)
161          knnres0 = matResults.at<float>(0, 0);
162      else if (indicator == 1)
163          knnres1 = matResults.at<float>(0, 0);
164      else if (indicator == 2)
165          knnres2 = matResults.at<float>(0, 0);
166      else if (indicator == 3)
167          knnres3 = matResults.at<float>(0, 0);
168
169
170  }
171
```

Figure 33: Descriptive code for labelling the resulted clusters using K-NN

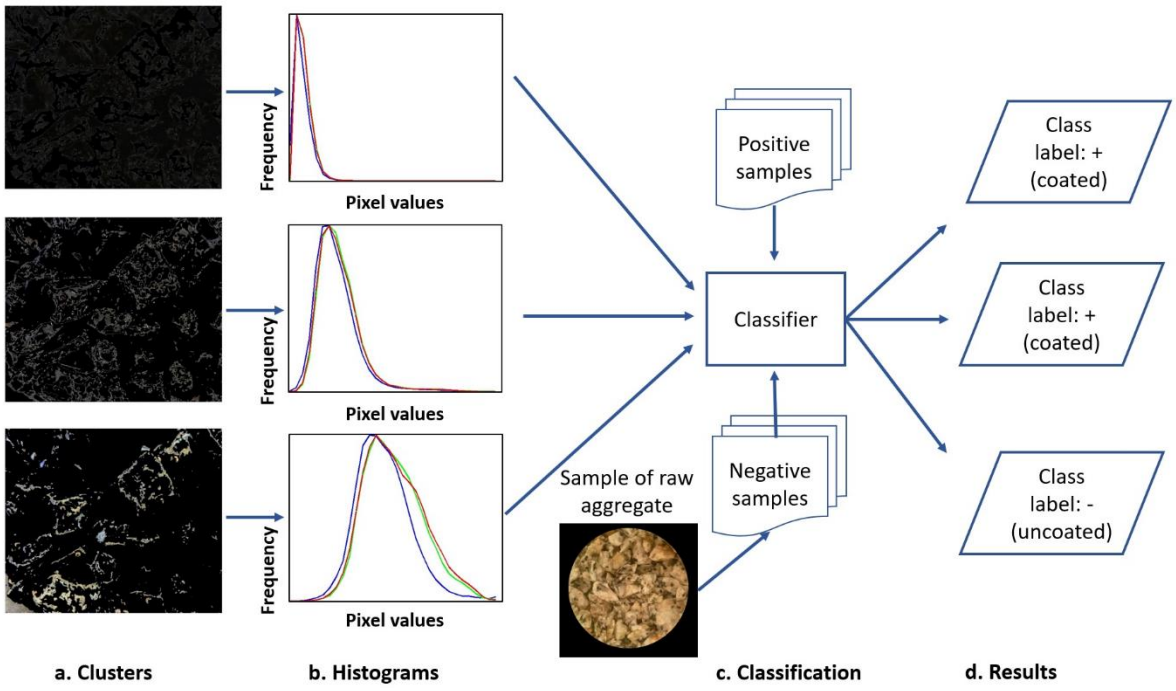

Figure 34: Classification process: a) segmented clusters; b) histogram of clusters' pixel intensities; c) classification

3.2.4.1.2. Support Vector Machine

One of the popular regression and classification methods is support vector machines (SVMs). SVM-based classification typically includes two major steps: training of the classifier using training dataset and predicting test data using the trained classifier (Chang, 2011). OpenCV library includes an implementation of SVM with different kernels, such as linear, Polynomial, Sigmoid, and Radial basis function ("OpenCV library", 2017).

3.2.4.1.2.1. C-support vector classification (C_SVC)

Considering a number of training samples such as $i = 1, \dots, l$, which are labelled in two separate classes, the C_SVC tries to solve a fundamental optimization problem which is presented in equation 16 (Chang, 2011). Equation 16 considers both equation 17 and equation 18, which are the conditions (assumptions). The regularization parameter, named C, is assumed to be always

positive (equation 16) and the link between x_i and higher dimensional spaces (more contributing features in the mentioned optimization problem) is function $\phi(x_i)$. indicator vector $y \in \mathbb{R}^l$ that $y_i \in \{-1,1\}$ and training vectors $x_i \in \mathbb{R}^n$ were used as inputs (Chang, 2011).

$$\min_{\omega,b,\xi} \ \frac{1}{2}\omega^T\omega + C\sum_{i=1}^{l}\xi_i \qquad (16)$$

$$y_i(\omega^T\phi(x_i) + b) \geq 1 - \xi_i \qquad (17)$$

$$\xi_i \geq 0\,, \quad i = 1, \ldots, l \qquad (18)$$

Since ω is a high-dimensional vector of variables (lots of contributing features), a dual problem is provided in equation 19 with the conditions presented in equation 20 and equation 21. After solving the dual problem, an optimal ω could be calculated using equation 22 and the decision function (equation 23) is derived (Chang, 2011).

$$\min_{\alpha} \ \frac{1}{2}\alpha^T\mathrm{Q}\alpha - e^T\alpha \qquad (19)$$

$$y^T\alpha = 0 \qquad (20)$$

$$0 \leq \alpha_i \leq C\ , \ \ i = 1, \ldots, l \qquad (21)$$

Q in equation 19 refers to a $l \times l$ positive semi-defined matrix which can be obtained as $\mathrm{Q}_{ij} = y_i y_j\, K(x_i, x_j)$. Moreover, e in equation 19 was considered as a vector of ones $e = [1, \ldots, 1]^T$ and the kernel function in equation 23 was defined as $K(x_i, x_j) = \phi(x_i)^T\phi(x_j)$ (Chang, 2011).

$$\omega = \sum_{i=1}^{l} y_i\alpha_i\phi(x_i) \qquad (22)$$

$$sgn(\omega^T\phi(x) + b) = sgn(\sum_{i=1}^{l} y_i\alpha_i K(x_i, x) + b) \qquad (23)$$

The target values (the labels for the test data) for data is predicted using decision function resulting from solving the optimization problem. The detailed information regarding SVM technique is available in the reference paper (Chang, 2011).

An OpenCV implementation of SVM in C++ environment is provided in Figure 35. First, the training type was set to C-SVC, and a linear kernel was used to process the data. Second, the

criteria terms were set prior to introduction of training dataset and the training dataset (for memory handling) is also determined.

```
//train for SVM
svm->setType(cv::ml::SVM::C_SVC);
svm->setKernel(cv::ml::SVM::LINEAR);
svm->setTermCriteria(cv::TermCriteria(cv::TermCriteria::MAX_ITER, 100, 1e-6));
svm->train(training_mat, cv::ml::ROW_SAMPLE, labels);
```

Figure 35: Descriptive code for training and defining parameters and type of SVM classifier

Chapter 4: Results and Discussions

4.1. Introduction

This system was created in Visual Studio Community 2015 environment and the functions from open source OpenCV 3.3.0 library were used for image processing and machine learning algorithms (OpenCV, 2017). Performance of the system was evaluated using 125 samples which were prepared according to the Ministry of Transportation Ontario stripping by static immersion test procedure LS-285 (Ministry of Transportation Ontario, 2018). The test samples included two groups: 1) images of 70 loose mixture samples which were prepared at the Lakehead University asphalt laboratory; 2) images of 55 samples which were provided by MTO's Materials Engineering and Research Office.

The images of the samples prepared at Lakehead University were captured using the illumination box (details are provided in Chapter 3), and the MTO's images were captured in ambient room lighting. One of the main objectives was to assess whether using this illumination system improves the lighting condition of captured images, and therefore can reduce the differences of machine-measured results from technician evaluations.

4.2. Experiments

The *retained coating percentage* for each sample was evaluated by expert technicians in MTO's Materials Engineering and Research Office and provided to the research team. Samples in this study had different *retained coating percentages,* which enabled to test the system in different possible scenarios. The technician assessments for the test samples are shown in Figure 36. The *retained coating percentage* for all samples were divided into two separate data sets, including the samples provided by MTO (marked as MTO samples) and the house lab samples which were made

in Lakehead university laboratory (see Figure 36). The blue curve represents manual assessments for the 55 samples provided by MTO and the *retained coating percentages* varied from 5% to 100%. The orange curve demonstrates the 70 samples which were made at Lakehead University Lab, and the *retained coating percentages* were in the range of 20% to 100%. According to the MTO's procedure, the percentages were rounded at 5% intervals. In Figure 36, it could be seen that most of the *retained coating percentages* of the house lab dataset were more than 80% (59 out of 70).

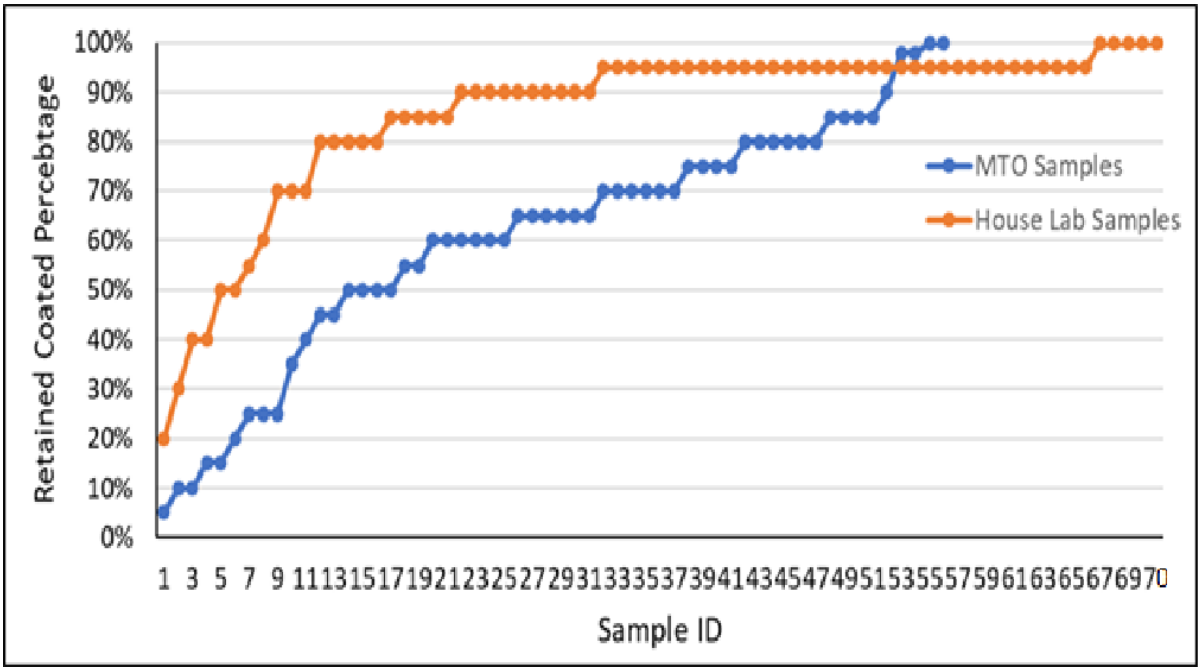

Figure 36: The retained coating percentage for samples in two data sets: a) samples provided by MTO (blue curve) and b) samples provided in the house lab (orange curve)

The effect of capturing images using the illumination box was evaluated by testing the two sets of images: the image set from House Lab (i.e. with controlled lighting) and the image set provided by MTO (i.e. without controlled lighting). In addition, the effectiveness of preprocessing of the images before classification and the performance of the system using different combinations of classifiers were tested. For example, test images were clustered into three and four clusters using

K-means (K=3 or 4), and then the clusters were classified as coated or non-coated by supervised classifiers, including Support Vector Machine (SVM) and K-Nearest Neighbors (K-NN) methods.

4.2.1. Results of the House Lab Samples

To evaluate the effectiveness of performing CLAHE on the images, all the samples were analyzed with and without performing CLAHE and their differences from manual assessments were calculated. The differences of manual assessments with machine-measured results with different combinations of classifiers are illustrated in Figure 37 and Figure 38. Figure 37 presents the differences of machine-measured estimations from technician's evaluations on the images without preprocessing, and Figure 38 shows the differences in the images which were enhanced by CLAHE. The tested combinations include K-means clustering with three and four classes, combined with SVM or K-NN classifiers. In this setting, SVM 3 means SVM classifier combined with K-means with three clusters, K-NN 3 represents K-NN classifier combined with K-means with three clusters, SVM 4 means SVM classifier combined with K-means with four clusters, and K-NN 4 represents K-NN classifier combined with K-means with four clusters. The horizontal axes in Figure 37 and Figure 38 show ranges of differences between machine-measured values using K-NN 3, K-NN 4, SVM 3 and SVM 4 combinations and the manual assessment values. The vertical axes in Figure 37 and Figure 38 represent a population of the samples in each of the related difference ranges.

The differences were divided into five ranges in Figure 37: [0% -5%], (5% -10%], (10% -15%], (15% -25%] and (25% -45%], and the most populated group is the difference range of [0% -5%]. The least populated difference range is (25% -45%], which presents the largest differences in machine-measured results from the manual assessments (evaluated by MTO's skilled technicians).

For example, there were ten samples with the differences of 5 to 10% from the corresponding manual assessments when a combination of K-NN and three-cluster K-means was used.

In Figure 38, the differences between manual assessments and four different combinations of classifiers are presented in four ranges: [0% -5%], (5% -10%], (10% -15%], (15% -25%]. The most populated range is [0% -5%] which contains more samples compared to the same difference range in Figure 37. The biggest differences are in the difference range of (15% -25%], which is the least populated range as well.

These two figures show that the differences are leaning more toward the left side of the figures, which are the smaller differences from manual assessments. Moreover, all ranges in Figure 38, expect the range [0% -5%], contain fewer samples compared to the same ranges in Figure 37, and in particular, the largest difference range, (25% -45%], only exists in Figure 37. These results indicate that application of CLAHE limited the differences to 25%, compared to 45% in the images without preprocessing. Given the findings that the differences tend to be more in the smallest range [0% -5%] in Figure 38, and also the maximum range of differences was smaller in Figure 38, it could be concluded that application of CLAHE on images improves classification and estimation of stripped and coated areas.

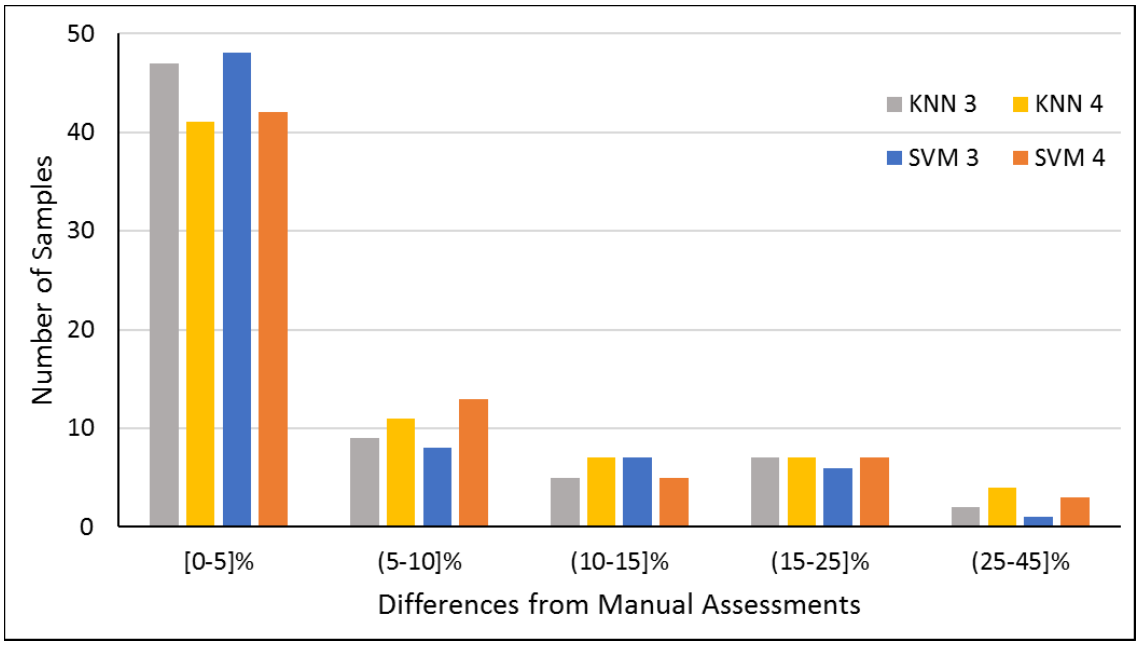

Figure 37: Differences of machine estimations from manual assessments on samples without CLAHE adjustment

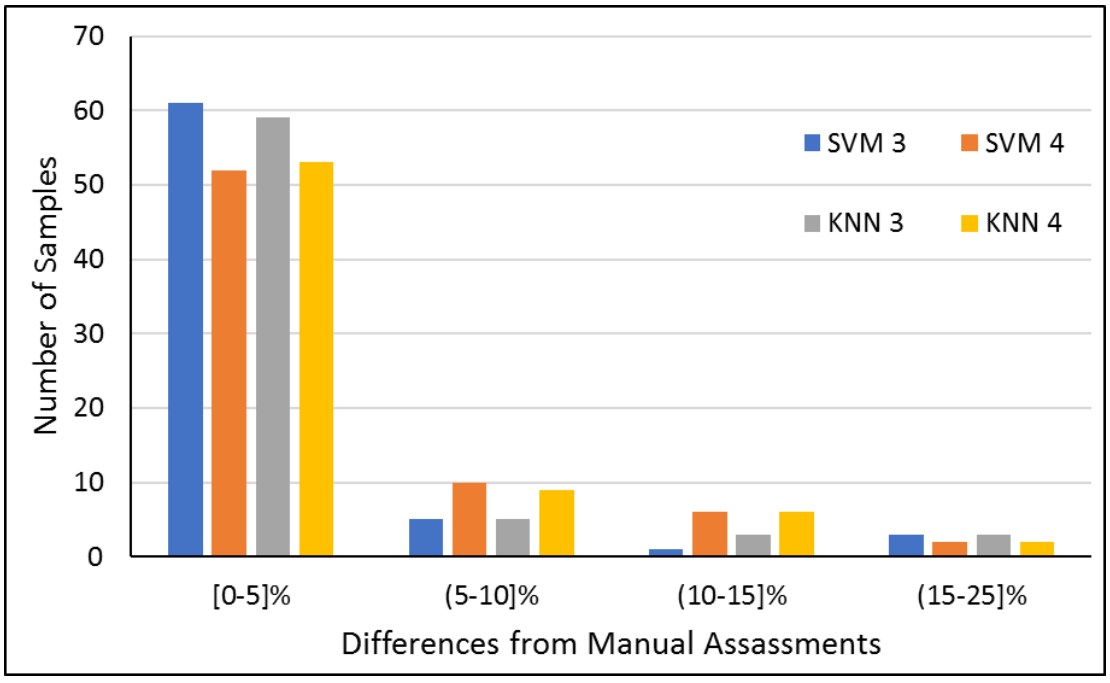

Figure 38: Differences of machine estimations from manual assessments on the samples adjusted by CLAHE

Since the effectiveness of CLAHE was investigated, the results of Figure 38 were used for comparison between different combinations of classifiers. The mean values for the differences

related to SVM3, SVM4, K-NN3 and K-NN4 were 4.507 %, 6.549 %, 4.788 % and 6.408 %, respectively. In addition, the standard deviation of the differences related to SVM3, SVM4, K-NN3 and K-NN4 were 4.939 %, 4.597 %, 5.24 % and 4.643 %, respectively. Combination of three-cluster K-Means with classifiers provided smaller differences, and SVM 3 provided the lowest mean. Based on Figure 38, differences of SVM 3 results from manual assessments are presented as the blue dataset and its most populated range had 61 samples in the range of [0% - 5%], which drastically decreases to 5 samples and then slightly decreases by 1 and increases by 2 in the last range (15% -25%]. The resulted differences related to K-NN3 and SVM3 were identical in 94 % of the test samples (66 out of 70 samples).

4.2.1.1. Wilcoxon Signed-rank test on the Combinations with Three-cluster K-means

The Wilcoxon signed-rank test is a non-parametric statistical hypothesis test which aims at finding a possible significant difference between two paired data sets. Wilcoxon signed-rank test has three initial conditions for the data: data should be paired, chosen randomly, and be in interval scale. All the assumptions are met by the existing data sets. The test initiates with two null hypotheses (the null hypothesis and the alternative). The null hypothesis is that the differences between two paired datasets are symmetric around zero. Through the procedure of the Wilcoxon signed-rank test, the differences between two data sets are calculated and they should be ranked based on the absolute value of the differences. The total sums of positive and negative ranks are calculated and the smaller one will be considered as the variable T. This value should be compared with a critical value, which could be converted to the z distribution and can be obtained through an equation or a critical value table based on the significance level α , which was considered 0.05 in this study (Wilcoxon, 1945). If the T is less than the critical value, the first hypothesis of the

test will be rejected, which means that the differences between the two datasets are not symmetric around zero, and if the T is more than the critical value, the first hypothesis of the test will be satisfied. Detailed information about Wilcoxon signed-rank test is available in (Wilcoxon, 1945).

Wilcoxon signed-rank test was performed in SPSS application on two data sets, including manual and machine-estimated results using K-NN with three-cluster K-means, and the summary of SPSS results are provided in Figure 39. The results indicate the rejection of the null hypothesis in a significance level of 0.05, which means that the differences are not random and it could be presumed that the system tends to overestimate the retained coatings (positive ranks outnumber negative ranks)

Descriptive Statistics of the analysis shows that 70 paired-samples were tested (total N=70), in which there were 24 tie samples (machine and manual estimations were the same) and there were 42 cases that the machine estimations had larger retained coating percentages than the *manual assessments,* and there were four cases where the *manual assessments* were larger than machine-measured estimations (Figure 39).

The Wilcoxon signed-rank test result on *manual estimation* and machine estimated data, resulted from the combination of SVM classifier with three-cluster K-means, also indicates rejection of null hypothesis (see Figure 40). In this combination, the system estimated 41 samples with larger retained coating percentages than the manual estimations, whereas five samples were estimated with lower retained coatings and 24 samples had similar estimations (Figure 40).

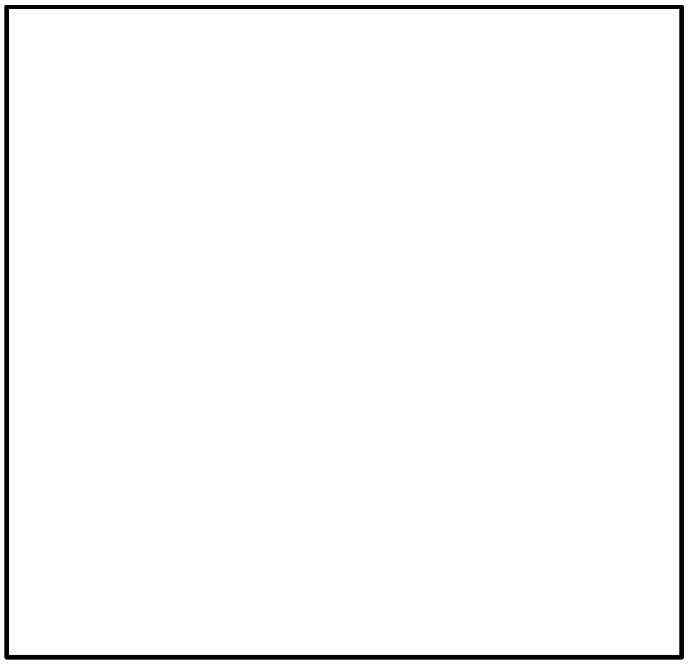

Figure 39: Wilcoxon signed-rank test results (using SPSS) conducted on manual and machine-estimated percentages using K-NN with three clusters

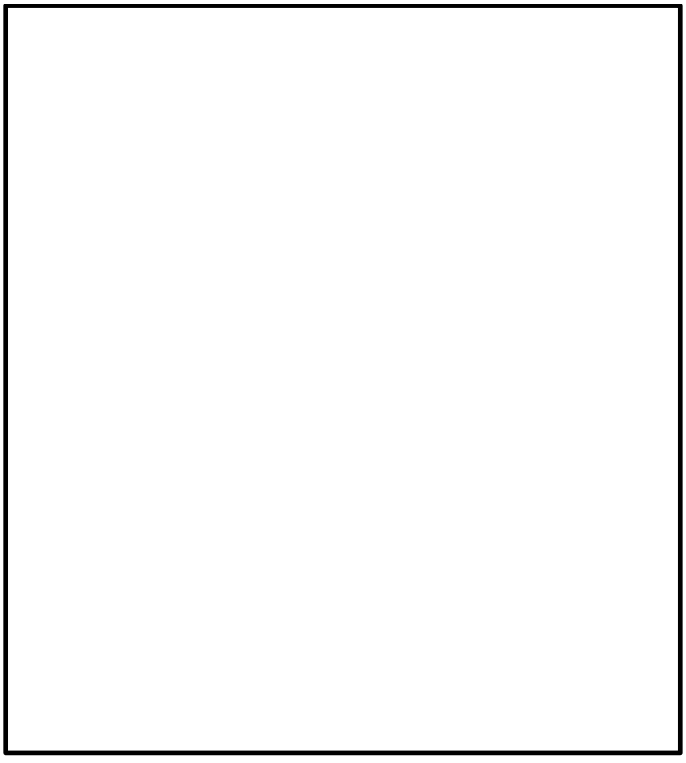

Figure 40: Wilcoxon signed-rank test results (using SPSS) conducted on manual and machine-estimated percentages using SVM with three clusters

Table 3 provides the statistics of the differences between the results of SVM3 and K-NN3, with technician estimations. Mean, Standard deviation, standard error, median, and minimum and maximum differences are presented in Table . In addition, Wilcoxon signed-ranks test results for K-NN3 and SVM3 are available in Table 3. By comparing the differences, it was revealed that the results are more toward the positive ranks, where the machine-estimated retained coating percentages were typically larger than technician assessments.

Table 3: Summary of statistical measures of comparison between manual and machine-measured results for the samples captured using illumination box

	K-NN	SVM
Mean	4.8%	4.5%
Standard Error	0.6%	0.6%
Median	5.0%	5.0%
Standard Deviation	5.2%	4.9%
Minimum	0.0%	0.0%
Maximum	25.0%	25.0%
Count	70	70
Null hypothesis H_0	Rejected	Rejected

The combination of K-NN classifier with three-cluster K-means was selected for further investigations. The average differences of *manual assessments* from machine-measured results in K-NN3 configuration are illustrated in Figure 41 for four different coating ranges. The coating ranges were [0% - 40%], [45% - 55%], [60% - 80%] and [85% - 100%] with average differences between machine-measured and *manual assessments* of 20%, 6.8%, 7.8%, and 3.1%, respectively. The highest differences occurred in the [0% - 40%] coating range with an average difference of

20%, and then the average differences sharply drop to 6.8% for samples in the coating range of [45% - 55%], then slightly increased by 1 % at the coating range [60% - 80%], and decreased to 3.1 % at the coating range [85% - 100%]. The smallest average difference was for the samples with *retained coating percentages* in the range of [85% -100%].

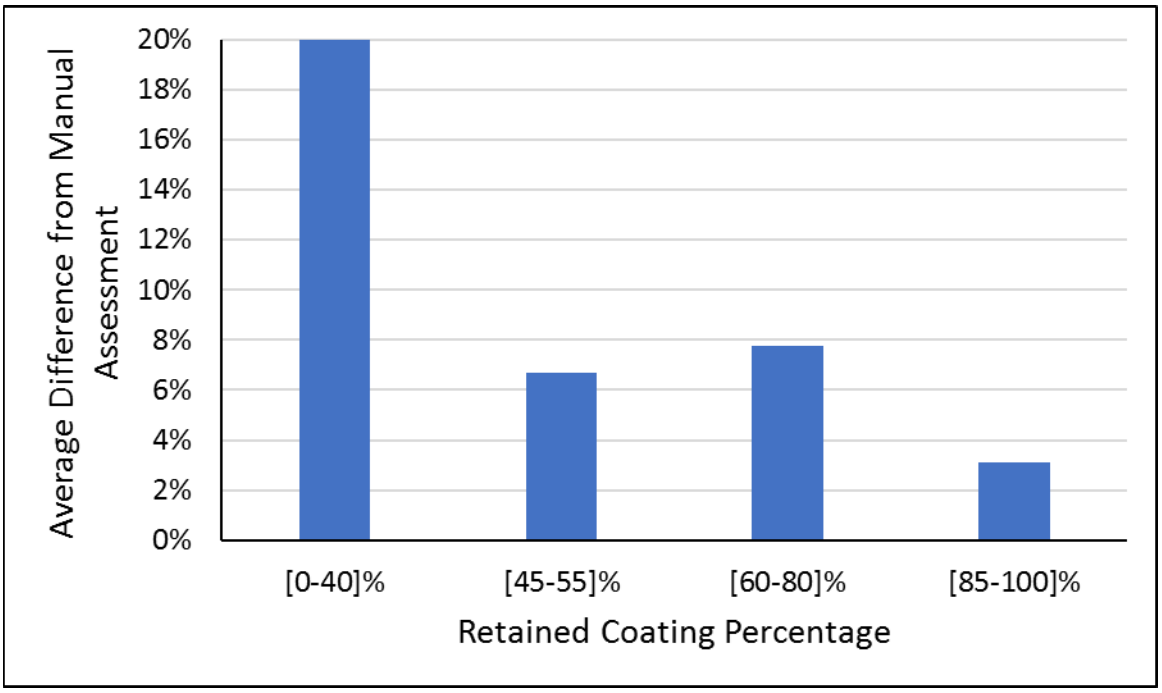

Figure 41: The average differences between manual assessments and machine estimations using K-NN on three classes for different retained coating ranges on the house lab samples

The machine-measured estimations tend to predict the *retained coating percentages* higher than the *manual assessments,* except for the coating range of [60% - 80%], where four out of nine samples were estimated with lower *retained coating percentage* than *manual assessments*. The samples correctly passed or failed by using 65% retained coating as the main criteria (described with detail in Chapter 3 and LS-285 test procedure provided by MTO), although it seems that there were relatively large differences between machine estimations and the *manual assessments* in some ranges, especially the samples with retained coating percentages under the 65% criteria had

the largest differences. For example, the coating range of [0% -40%] had the largest average differences of 20% (Figure 41) were identified under 60 % (failed samples). Moreover, machine-measured estimations were always larger or equal to the *manual assessments,* in the samples with *retained coating percentages* above 85 %.

The performance of the system (using K-NN3) was promising on the samples in the coating range of [60% - 80%], where the system correctly passed the samples and vice versa. However, it is recommended to consider a safe margin of 10% for the samples estimated around the rejection criteria (65% retained coating), because the system had an average difference of 7.8% in the coating range of [60% - 80%]. Thus, manual assessment by an expert should be considered to double-check the machine estimations in the coating percentages of 55%, 60%, 65%, 70 and 75%.

4.2.2. Results of the Samples Provided by MTO

The performance of the system in processing the images captured without illumination box (55 samples which were provided by MTO) was also investigated. The difference between manual assessments and machine estimations for four different combinations of classifiers were studied to find the best machine-measured outcomes, and the results are provided in Figure 42. The vertical axis presents the average difference of manual and machine-measured estimations for the related coating ranges in horizontal axis. The samples are divided into five ranges based on their *retained coating percentage* with a width range of 20 percent, such as [0% - 20%], (20 % -40%], ..., (80% - 100%]. Differences between manual assessment and machine assessments using K-NN and SVM combined with three-clusters K-means (illustrated as blue and orange columns, in Figure 42) behave similarly through all coating ranges. Moreover, they have larger differences compared to the results of K-NN and SVM combined with four-cluster K-means, except in the coating range of (40% ,60%].

By comparing the machine measurements for the MTO samples (Figure 42) and the results on the house lab samples (Figure 38), it was evident that the differences of estimations for the house lab samples (with controlled illumination conditions) were smaller than the differences of estimations for the samples provided by the MTO (room ambient lighting). For example, in the retained coating range of [85% -100%] in (Figure 38), the average differences of manual assessments from machine estimations was 3% for the images captured by the illumination box, whereas the average differences was 10% for the samples provided by the MTO (Figure 42), which the lowest average difference in this range achieved by SVM4.

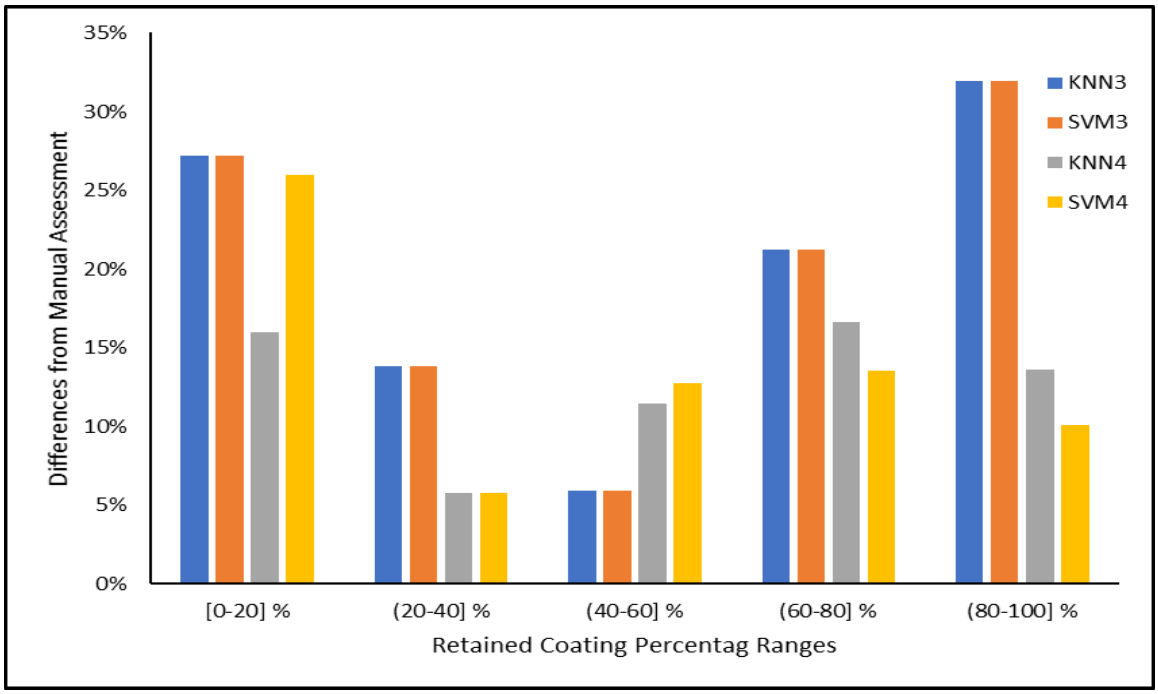

Figure 42: Average difference from manual assessment in different remained coating percentage ranges

Since using a combination of K-NN and four-cluster K-means provides the best results among all combinations of classifiers, a detailed illustration for machine estimation using this combination is provided in Figure 43. The K-NN classification resulted in largedifferences (more than 15%). Although the unsupervised classifier (K-means) classifies the pixels based on their

intensities, the supervised classifiers, such as SVM and K-NN, incorrectly labelled the clusters in many cases, which were due to the poor illumination conditions. Thus, the labelling process was done manually (called semi-automated) as an alternative method to assess the *retained coating percentages,* and the average differences of the new results from technician assessments are illustrated in Figure 43. The differences of semi-manual estimations from manual assessments versus a combination of classifiers using four-cluster and K-NN from manual assessments were illustrated in Figure 43. The blue data set, which represents differences of manual assessments from the results of the semi-manual method started from peak with 22 samples in the difference range of [0% -5%], and experienced a decrease by 8 samples in the difference range of (5% -10%], and remained same in the difference range of (10% -15%], and then has the lowest population in the range of (15% -35%] with only two samples. Also, the differences related to the combination of K-NN and four-cluster K-means were illustrated as orange bars in Figure 43. This data set initiates with 9 samples in the difference range of [0% -5%], and increases to 11 and 17 samples in the next difference ranges of (5% -10%] and (10% -15%], respectively, and then slightly drops by 1 sample in the difference range of (15% -35%]. It can be concluded that the semi-automated estimations tend to shift to the lower differences (left side of Figure 43) and have a low population in the largest differences range (2 samples) compared to the fully-automated method (16 samples). As a result, it is recommended to use semi-automated approach (i.e. manually classify clusters) when an illumination box is not available for capturing an image from the sample.

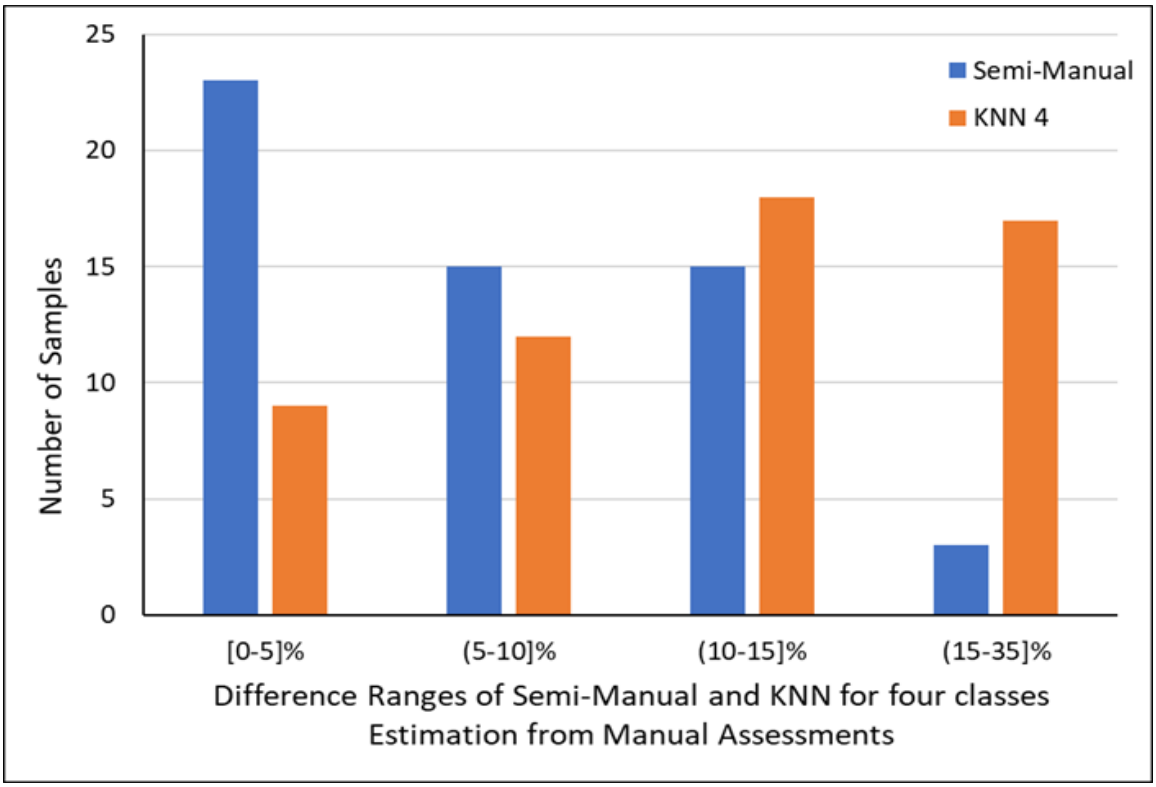

Figure 43: Differences of machine estimations using K-NN and four-cluster K-means from manual assessments versus the differences of the semi-manual method from manual estimations for samples provided by MTO

4.2.2.1. Wilcoxon Signed-Rank test for Semi-Manual Results

The Wilcoxon signed-rank test was performed on semi-manual estimations and MTO technicians' assessments to study whether the differences were symmetrically distributed around zero. The results of the test and descriptive statistics for each data set are provided in Figure 44. The measured percentages were rounded into the closets value of 5% intervals for semi-manual estimations (the manual data set were already in 5% interval scale). The null hypothesis was rejected due to the Wilcoxon signed-rank test, which means that the differences are not distributed

symmetrically around zero and the semi-manual system has a tendency to overestimate the retained coating percentage on the samples.

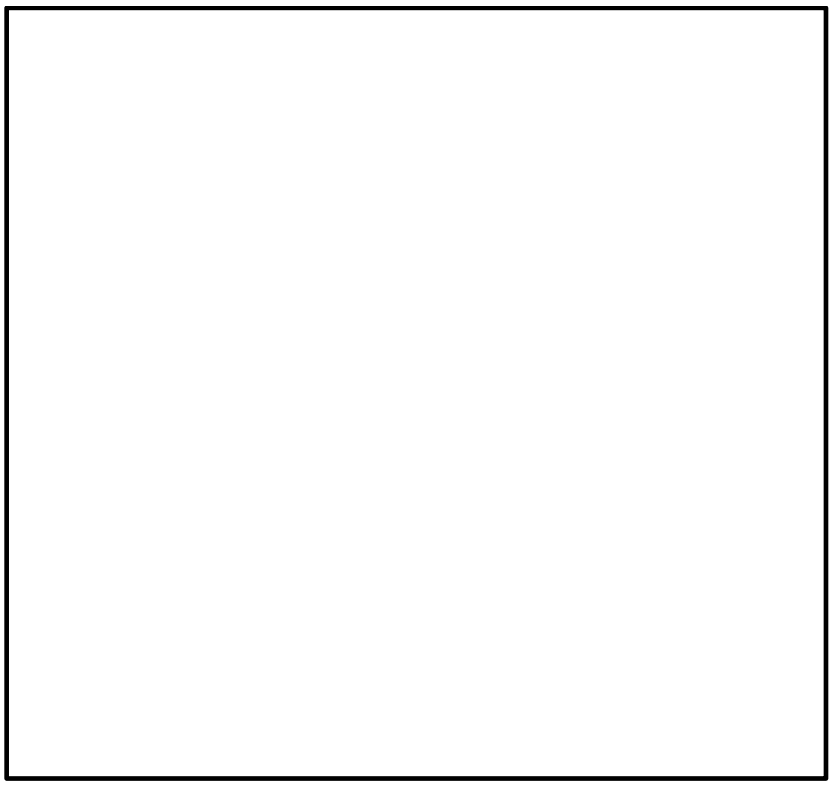

Figure 44: Wilcoxon signed-rank test results in SPSS software which is conducted on semi-manual estimated percentages and manual assessments using K-NN with four classes

By detailed comparison of the machine-measured estimations and semi-manual method's results with the technician assessments, specific trends were observed. Resulted differences for different retained coating ranges are presented in Figure 45 to illustrate the performance of both classification methods (full automated and semi-automated methods) in different *retained coating percentages*. In Figure 45 *retained coating percentages* were divided into 5 separate coating ranges. The blue and the orange bars present average differences of *manual assessments* from the results of semi-automated and fully-automated methods (using combination of four-cluster K-means and K-NN), respectively. As it can be seen in Figure 45, the fully-automated method tends to estimate the *retained coating percentages* with larger differences as the *retained coated*

percentages increase, which means that the K-NN classifier labelled some of the four K-means' clusters incorrectly, especially for samples with high *retained coating percentages*. The best performance of the semi-manual method was for samples in the coating range of [85% - 100%] (Figure 45).

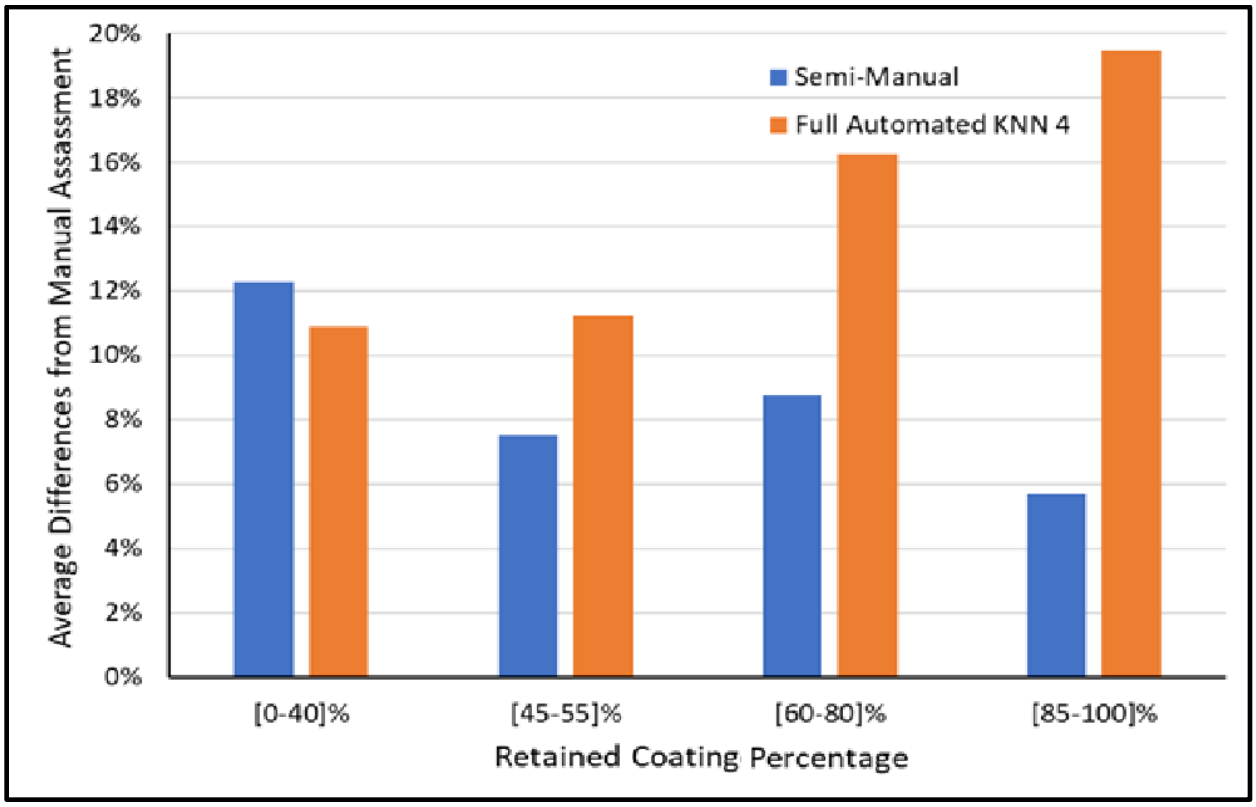

Figure 45: The average differences between manual and machine-measured estimations using K-NN4 versus average differences between semi-manual method results on the samples provided by MTO

The descriptive statistics for differences related to both K-NN 4 and semi-manual methods for samples, which were captured in ambient room lighting, are provided in Table . These data reveal that the semi-manual method is a better alternative for evaluating the retained coated percentage of the images captured in ambient room lighting

Table 4: Summary of the main statistical measures of comparison between manual and machine-measured results for the samples captured in uncontrolled illumination conditions

	K-NN4	Semi-Manual
Mean	15.0%	8.1%
Standard Error	1.1%	0.8%
Median	15.0%	9.0%
Standard Deviation	8.1%	5.8%
Minimum	1.0%	0.0%
Maximum	34.0%	26.0%
Count	55	55

4.3. Discussion

Machine-measured estimations, their differences from the *manual assessment,* and the resulted clusters were analyzed to find the possible causes of errors in the classification process of the *house lab samples* (controlled illumination system), and the shaded areas within the images were found to be a possible cause of error, because they were classified as a coated part (Figure 46). This is mainly due to the dark colour of the shades, which mislead the classifiers, because the colour of the shaded area was close to the coated samples. These undesirable assignments resulted in the largest errors in the evaluations, especially in the samples with low retained coating percentages. In the case of samples with a high percentage of *retained coating*, the shaded areas did not cause major errors, because a large portion of the shaded areas was coated as well. In addition, specular highlights, especially the ones on the surface of the water, were mostly considered as stripped area by the classifiers (Figure 47), which caused large differences from the technician's assessments on the samples captured in ambient room lighting. Figure 48 (left image) shows another example of this problem in one of the samples provided by MTO. This issue was particularly evident in the samples provided by MTO, which were captured under ambient room lighting. The machine-measured estimations for the samples in the coating range of [0% -40%] were significantly affected

by both shadows and surface reflections, which resulted in large differences from *manual assessments* (compared to the other coating ranges). Samples of these undesirable conditions are illustrated in Figure 48. By comparing the results of the test samples from MTO (semi-manual classification was used) and house lab (combination of K-NN and three-cluster K-means was utilized), which had the mean errors of 8.768 % and 4.787 % respectively, it was demonstrated that the illumination box had a positive effect on the performance of the system. This was mainly due to uniform lighting and reduction of specular highlights and shaded areas.

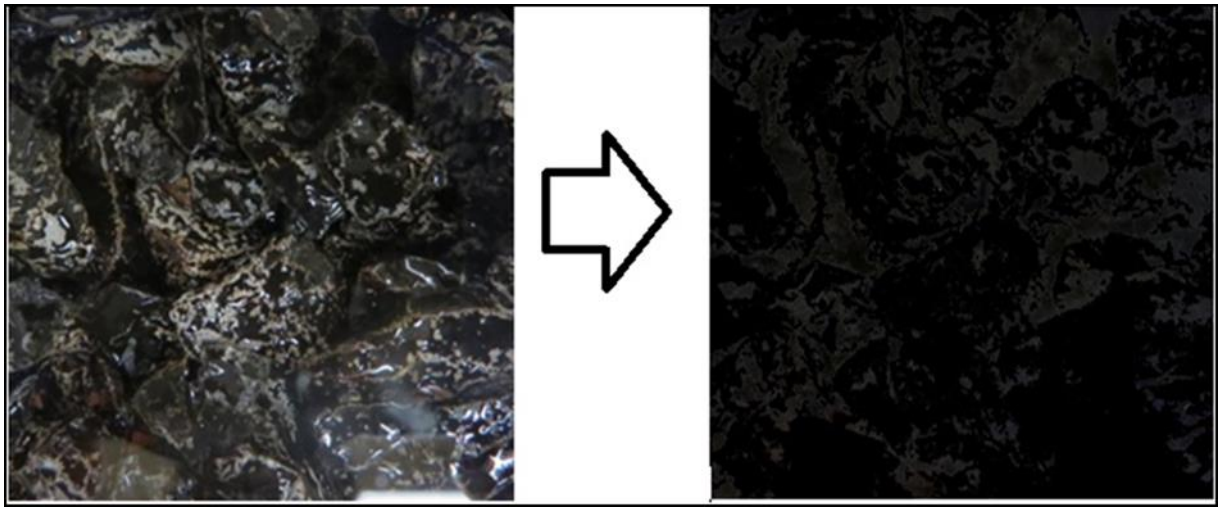

Figure 46: A sample image on the left and the shaded areas between aggregate particles were classified as retained coating areas (right side)

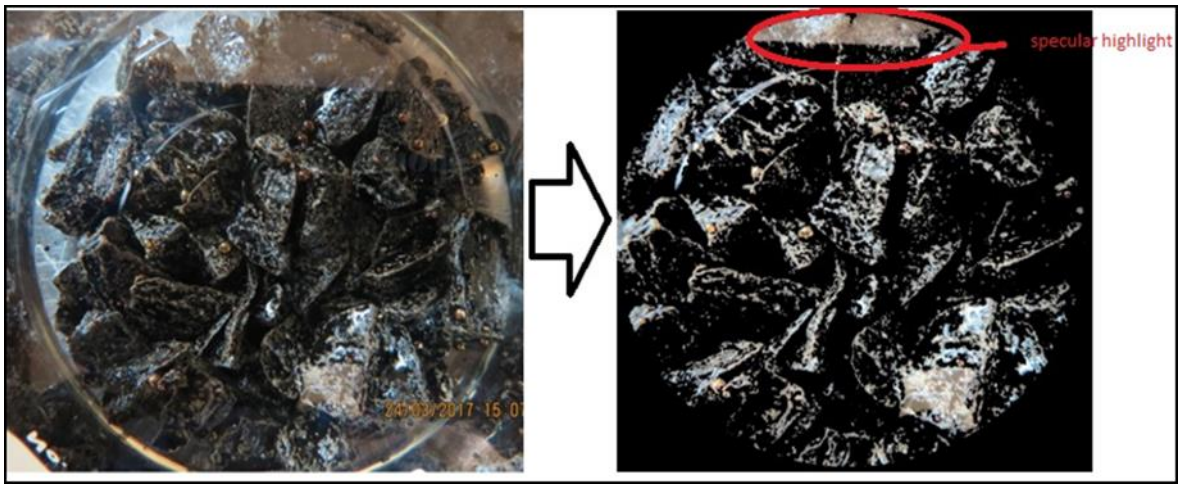

Figure 47: Sample image on the left hand and stripped detected area on the right hand (the

specular highlight was counted as stripped area)

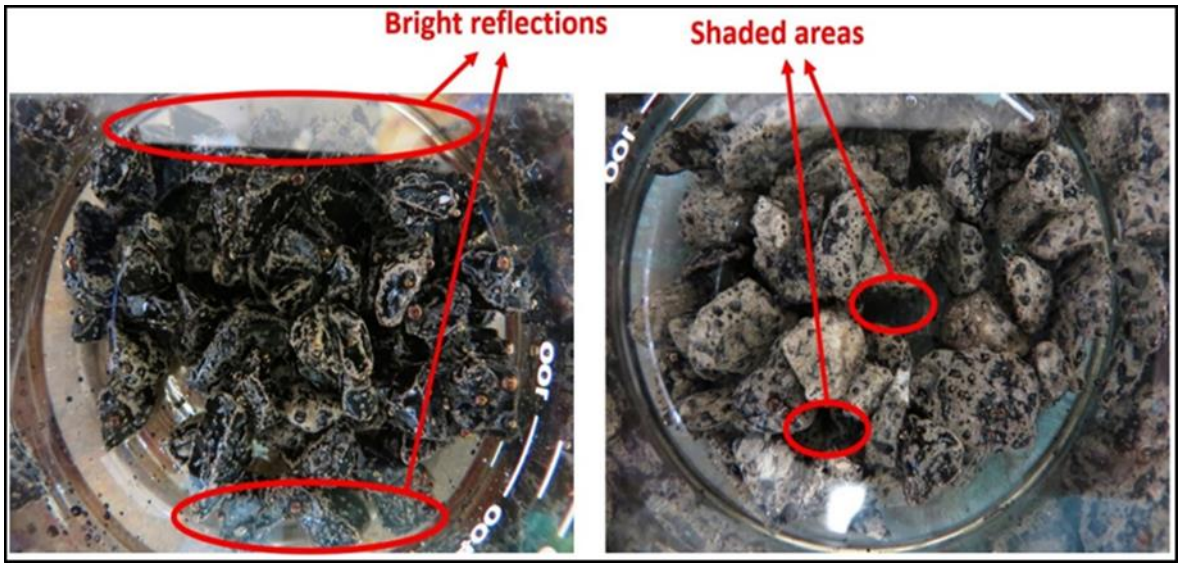

Figure 48: Images which were taken under regular direct lighting.

One of the challenges in similar research projects (Lantieri et al., 2017; Källén et al., 2016) was observed in the mixtures made from the dark or patterned aggregate. The performance of the proposed system was investigated on a variety of aggregate colours. Three aggregate types were used in the samples, which were Dolomitic Sandstone, Granite-Gneiss, and Quartzite, and the estimated results were in similar ranges. For instance, of the machine-measured results on 38 sample images of mixtures with dark aggregate (Dolomitic Sandstone) had a mean difference of 4.565 % with the technician assessment.

Based on the test procedure provided by MTO for the Static Immersion test (LS-285), samples with *retained coating* percentage of less than 65% are rejected. To this end, estimated results for any sample with less than 65% coated area should be less than 65% to be rejected correctly and vice versa. Although the system provides results with some differences near this critical limit (samples in the coating range [60 % -80%]), no test sample was incorrectly rejected or passed. Even in highly stripped samples, which had the largest differences in evaluations, (first two ranges in Figure 41), the maximum diffrence did not cause an incorrect passing of a sample.

Despite these results, it is recommended that any machine-measured percentages with an estimated coating percentage around 65 %, i.e. [55% -75%], to be evaluated by an expert technician.

It is also recommended that if an accurate estimation is required for the sample with low *retained coating percentages* [0% -40%], the manual evaluation is performed by an expert technician, because the performance of this system could have large differences from manual assessments in this range. In addition, while cropping the image in the early stages of the process, specular highlights and shaded areas should be avoided as much as possible to obtain more realistic results.

The preprocessed images, which were captured using the illumination box, had the closest results to the technician assessments. In contrast, the images which were captured in ambient room lighting (samples provided by MTO) were poorly correlated with the *manual estimations*.

There were two main issues in the processing of these images: incorrect clustering by the unsupervised classifier (K-means), and incorrect assignment of labels to some of the clusters by the supervised classifiers. The second issue was due to the lack of proper negative samples and poor contrast of the images. The second problem was the main factor and was due to the lighting conditions. The illumination varied dramatically and created considerable reflections on the surface of the water, as well as notable amount of specular highlights on the coated parts and shaded areas between the mixture particles. These visual noises misled the unsupervised classifier (K-means) to group some pixels from different areas (coated and stripped) into the same cluster, which did not truly represent a separate coated or stripped area.

A semi-manual method was proposed to improve the results in these samples, where the k clusters could be labelled manually by a skilled operator based on the visual comparison of the clusters with the available sample.

Chapter 5: Conclusions and Recommendations

5.1. Summary

A computer vision-based system was developed to automatically evaluate striping in loose asphalt mixtures by static immersion test. The proposed system consists of two parts: first part was the physical lighting improvement using an innovative low-cost illumination box, which provides uniform and non-direct illumination for capturing images from samples; and the second part included development of a program in visual studio 2015 environment using OpenCV library to enhance the test image, classify image's pixels into different clusters, and finally classify each cluster and calculate the *retained coating percentage*. Two sets of test samples, including 55 samples provided by the MTO (captured without controlled lighting conditions), and 70 samples captured in a controlled illumination condition (illumination box) at Lakehead University, were tested using a different combination of classifiers. Moreover, the impact of CLAHE (preprocessing images before classification) was investigated, where the test images were processed with and without CLAHE. Four combinations of classifiers were used in this research, including K-means segmentation using three and four clusters combined with SVM and K-NN classifiers. The mentioned four combinations of classifiers were used to estimate the *retained coating percentage* of 70 samples created in Lakehead University laboratory respect to the MTO's test procedure LS-285 (Ministry of Transportation Ontario, 2018), in different coating ranges.

5.2. Conclusions

Through detailed observation of the results, it was concluded that application of the illumination box positively affected the performance of the system, which could be concluded by comparing the differences between the results on the images captured with (inhouse) and without (MTO) illumination box. Moreover, application of CLAHE decreased the differences between the

machine-measured results and *manual assessments*. In addition, it was observed that using K as 3 in the K-means algorithm provides closer results than utilizing K as 4, in case of the samples created at Lakehead University laboratory.

Moreover, results, which were revealed from SVM, were almost the same as results provided by K-NN. The average, standard deviation and the maximum difference of manual assessments from a combination of three-cluster K-means and K-NN were 4.8 %, 5 % and 25 %, respectively. The results of using a combination of four-clusters' K-means and K-NN showed a better correlation with the MTO technicians' assessments than the other methods for the samples provided by MTO, where the average differences from the manual assessment were 15%, the standard deviation was 8.1 %, and the maximum difference was 35 %. To improve the results for these samples, a semi-manual method, which manually classifies the three clusters, which were resulted from K-means, was used. The average differences related to the semi-manual method, standard deviation and the maximum difference were 8.1 %, 9 % and 25 %, respectively.

The performance of the system is promising in the estimation of *retained coating percentage* (striping evaluation) in loose asphalt mixture, which is immersed inside water, in the sense of removing the subjectivity of the test. This subjectivity is rising mainly due to a human judgment errors in evaluation of striping. This system addresses some of the limitations in previous studies, such as evaluating samples with dark colour aggregates and minimizing the effect of specular highlights and shadows (image noises) without changing the test procedure and samples.

5.3. Suggestions for End-users

- Since the system performs better when the illumination box is utilized, it is recommended to apply such a system to capture an image from a sample.

- The 65 % limit is a critical threshold value, which results in rejection of the samples with lower retained coating percentages. Since this limit is significant in the rejection or acceptance of a sample, the samples with retained coatings in the range of 60% to 70% should be considered as caution zone and these samples should be evaluated manually as well.

5.4. Limitations

The main limitations of the proposed system are provided below.

- The system had poor performance in the assessment of the samples with retained coating percentages between 0 to 40%. Although the system properly rejects the samples in this range, the machine-measured percentages had relatively large differences from manual assessments, and this could be problematic in the cases that require precise evaluations in these coating ranges.
- The skilled technicians are indecisive toward evaluating partially retained coatings, called stained areas, as coated or stripped parts. Similarly, this system has difficulty in evaluation of stained areas due to the colour-similarity of darker colour aggregates and partially retained coatings.
- Analyzing 3D models could provide more accurate results due to higher dimensions and comprehensive coverage of the samples, but the proposed system operates based on the analysis of 2D images.
- Shadows within the sample images negatively affect machine-measured estimations and these areas were mostly considered as coated parts due to their dark colours.
- The background of the samples in some cases could remain in the processed areas which causes inaccuracy in the evaluations.

5.5. Recommendations for Future Work

There are some recommendations for future research projects to advance this system:

- An automated cropping algorithm could be adopted at the initial step for the code to avoid major noises, including shadows and specular highlights.
- Deep learning could be evaluated as a supervised classifier in this system to improve the accuracy of the evaluations because this method has been able to outperform other supervised learning approaches.
- More investigations should be carried out to address the existing problems in the assessment of the stained areas.

References

Al Omari, A. A. M. (2005). Analysis of HMA permeability through microstructure characterization and simulation of fluid flow in X-ray CT images (Doctoral dissertation, Texas AandM University).

Amelian, S., Abtahi, S. M., and Hejazi, S. M. (2014). Moisture susceptibility evaluation of asphalt mixes based on image analysis. Construction and Building Materials, 63, 294-302.

Ancuti, C., Ancuti, C. O., Haber, T., and Bekaert, P. (2012, June). Enhancing underwater images and videos by fusion. In 2012 IEEE Conference on Computer Vision and Pattern Recognition (pp. 81-88). IEEE.

Arambula, E., Masad, E., and Martin, A. E. (2007). Influence of air void distribution on the moisture susceptibility of asphalt mixes. Journal of materials in civil engineering, 19(8), 655-664.

Aschenbrener, T., McGennis, R. B., and Terrel, R. L. (1995). Comparison of several moisture susceptibility tests to pavements of known field performance (with discussion and closure). Journal of the Association of Asphalt Paving Technologists, 64.

ASTM. (1996). Standard practice for effect of water on bituminous-coated aggregate using boiling water.

Atud, T. J., Kanitpong, K., and Martono, W. (2007). Laboratory evaluation of hydrated lime application process in asphalt mixture for moisture damage and rutting resistance (No. 07-1508).

Azari, H. (2010). Precision estimates of AASHTO T283: Resistance of compacted hot mix asphalt (HMA) to moisture-induced damage. National Cooperative Highway Research Program, Transportation Research Board of the National Academies.

Badru, M., and Roberts, F. L. (1988). Stripping in HMA mixtures: State of the art and critical review of test methods.

Bahia, H., and Ahmad, S. (1999). Evaluation and correlation of lab and field tensile strength ratio (TSR) procedures and values in assessing the stripping potential of asphalt mixes (No. WI/SPR-10-99,).

Barrie, P. J. (2000). Characterization of porous media using NMR methods.

Bermejo, S., and Cabestany, J. (2000). Adaptive soft k-nearest-neighbour classifiers. Pattern Recognition, 33(12), 1999-2005.

Bhasin, A., Chowdhury, A., Button, J., and Little, D. (2006a). Evaluation of material property tests to predict moisture susceptibility of HMA. In 10TH INTERNATIONAL CONFERENCE ON ASPHALT PAVEMENTS-AUGUST 12 TO 17, 2006, QUEBEC CITY, CANADA.

Bhasin, A., Masad, E., Little, D., and Lytton, R. (2006b). Limits on adhesive bond energy for improved resistance of hot-mix asphalt to moisture damage. Transportation research record: journal of the transportation research board, (1970), 3-13.

Birgisson, B., Roque, R., and Page, G. C. (2003). Evaluation of water damage using hot mix asphalt fracture mechanics (with discussion). Journal of the association of asphalt paving technologists, 72.

Bock, H. H. (2007). Clustering methods: a history of k-means algorithms. In Selected contributions in data analysis and classification (pp. 161-172). Springer, Berlin, Heidelberg.

Caro, S., Masad, E., Bhasin, A., and Little, D. (2009). Coupled micromechanical model of moisture-induced damage in asphalt mixtures. Journal of Materials in Civil Engineering, 22(4), 380-388.

Caro, S., Masad, E., Bhasin, A., and Little, D. N. (2008). Moisture susceptibility of asphalt mixtures, Part 1: mechanisms. International Journal of Pavement Engineering, 9(2), 81-98.

Chan, T., and Shen, J. (2000). Mathematical models for local deterministic inpainting. UCLA Computational and Applied Mathematics Reports 00-11.

Chandler, J., and Fryer, J. (2013). Autodesk 123D catch: how accurate is it. Geomatics world, 2(21), 28-30.

Chang, C. C. (2011). " LIBSVM: a library for support vector machines," ACM Transactions on Intelligent Systems and Technology, 2: 27: 1--27: 27, 2011. http://www. csie. ntu. edu. tw/~ cjlin/libsvm, 2.

Chen, J. S., Lin, K. Y., and Young, S. Y. (2004). Effects of crack width and permeability on moisture-induced damage of pavements. Journal of Materials in Civil Engineering, 16(3), 276-282.

Chen, Z. (2007). Climate change 2007: the physical science basis. IPCC, NY, USA, 2007, 212-213.

Cheng, D., Little, D. N., Lytton, R. L., and Holste, J. C. (2002). Use of surface free energy properties of the asphalt-aggregate system to predict moisture damage potential (with discussion). Journal of the association of asphalt paving technologists, 71.

Cheng, D., Little, D. N., Lytton, R. L., and Holste, J. C. (2003). Moisture damage evaluation of asphalt mixtures by considering both moisture diffusion and repeated-load conditions. Transportation research record, 1832(1), 42-49.

Cooley, L. A., Prowell, B. D., and Brown, E. R. (2002). Issues pertaining to the permeability characteristics of coarse-graded Superpave mixes. ASPHALT PAVING TECHNOLOGY, 71, 1-29.

Copeland, A., and Kringos, N. (2006). Determination of bond strength as a function of moisture content at the aggregate-mastic interface. In 10th International Conference on Asphalt Pavements. Quebec, Canada. August 12-17, 2006 (pp. 709-718).

Demirkan, H., and Delen, D. (2013). Leveraging the capabilities of service-oriented decision support systems: Putting analytics and big data in cloud. Decision Support Systems, 55(1), 412-421.

El Hussein, H. M., El Halim, A. A., and Kennepohl, G. J. (1993). Assessment of the influence of compaction method on asphalt concrete resistance to moisture damage. Construction and building materials, 7(3), 149-156.

EVS-EN 12697-11:2005 - Estonian Centre for Standardisation. (2019). Retrieved from https://www.evs.ee/products/evs-en-12697-11-2005

Fabio, O., Fabjan, K., Dario, L. R., Jacopo, A., and Stefano, C. (2014). Performance evaluation of a low-cost stereo vision system for underwater object detection. IFAC Proceedings Volumes, 47(3), 3388-3394.

Gonzalez, R. C., and Woods, R. E. (2002). Digital Image Processing. 2nd edn Prentice Hall. New Jersey, 793.

Hamzah, M. O., Kakar, M. R., Quadri, S. A., and Valentin, J. (2014). Quantification of moisture sensitivity of warm mix asphalt using image analysis technique. Journal of cleaner production, 68, 200-208.

Hamzah, M. O., Teh, S. Y., Golchin, B., and Voskuilen, J. (2017). Use of imaging technique and direct tensile test to evaluate moisture damage properties of warm mix asphalt using response surface method. Construction and Building Materials, 132, 323-334.

Hartigan, J. A., and Wong, M. A. (1979). Algorithm AS 136: A k-means clustering algorithm. Journal of the Royal Statistical Society. Series C (Applied Statistics), 28(1), 100-108.

Hum, Y. C., Lai, K. W., and Mohamad Salim, M. I. (2014). Multiobjectives bihistogram equalization for image contrast enhancement. Complexity, 20(2), 22-36.

Källén, H., Heyden, A., Åström, K., and Lindh, P. (2012, January). Measurement of bitumen coverage of stones for road building, based on digital image analysis. In 2012 IEEE Workshop on the Applications of Computer Vision (WACV) (pp. 337-344). IEEE.

Källén, H., Heyden, A., Åström, K., and Lindh, P. (2016). Measuring and evaluating bitumen coverage of stones using two different digital image analysis methods. Measurement, 84, 56-67.

Kandhal, P. S. (1992). Moisture susceptibility of HMA mixes: identification of problem and recommended solutions (No. NCAT 92-1,). National Asphalt Pavement Association.

Kandhal, P. S., Lubold, C. W., and Roberts, F. L. (1989). Water damage to asphalt overlays: case histories (No. NCAT Report No. 89-1). Nashville, Tennessee: National Center for Asphalt Technology.

Kandhal, P., and Rickards, I. (2001). Premature failure of asphalt overlays from stripping: Case histories. Asphalt Paving Technology, 70, 301-351.

Kanitpong, K., and Bahia, H. (2005). Relating adhesion and cohesion of asphalts to the effect of moisture on laboratory performance of asphalt mixtures. Transportation Research Record, 1901(1), 33-43.

Kanitpong, K., and Bahia, H. U. (2003). Role of adhesion and thin film tackiness of asphalt binders in moisture damage of HMA (with discussion). Journal of the Association of Asphalt Paving Technologists, 72.

Karathanassi, V., Iossifidis, C. H., and Rokos, D. (2000). A texture-based classification method for classifying built areas according to their density. International Journal of Remote Sensing, 21(9), 1807-1823.Kassem, E., Masad, E., Bulut, R., and Lytton, R. (2006). Measurements of moisture suction and diffusion coefficient in hot-mix asphalt and their relationships to moisture damage. Transportation research record: journal of the transportation research board, (1970), 45-54.

Kennedy, T. W., Roberts, F. L., and Lee, K. W. (1984). Evaluating moisture susceptibility of asphalt mixtures using the Texas Boiling Test. Transportation Research Record, 968, 45-54.

Kettil, P., Engström, G., and Wiberg, N. E. (2005). Coupled hydro-mechanical wave propagation in road structures. Computers and structures, 83(21-22), 1719-1729.

Kim, J., and Moore, J. R. (2009). Laboratory evaluation of ZycoSoil as an anti-stripping agent on superpave mixtures. Unpublished, Auburn, AL: NCAT.

Kim, S., and Coree, B. J. (2005). Evaluation of hot mix asphalt moisture sensitivity using the Nottingham asphalt test equipment (No. IHRB Project TR-483). Iowa State University. Center for Transportation Research and Education.

Kim, Y. R., Pinto, I., and Park, S. W. (2012). Experimental evaluation of anti-stripping additives in bituminous mixtures through multiple scale laboratory test results. Construction and Building Materials, 29, 386-393.

Kim, Y. T. (1997). Contrast enhancement using brightness preserving bi-histogram equalization. IEEE transactions on Consumer Electronics, 43(1), 1-8.

Kosek, J., Štěpánek, F., and Marek, M. (2005). Modeling of transport and transformation processes in porous and multiphase bodies. Advances in chemical engineering, 30, 137-203.

Kriegel, H. P., Schubert, E., and Zimek, A. (2017). The (black) art of runtime evaluation: Are we comparing algorithms or implementations. Knowledge and Information Systems, 52(2), 341-378.

Kringos, N. (2007). Modeling of combined physical-mechanical moisture induced damage in asphaltic mixes.

Kvasnak, A., and Williams, R. C. (2007). Evaluation of the Interaction Effects between Asphalt Binders and Fillers Using a Moisture Susceptibility Test (With Discussion). Journal of the association of asphalt paving technologists, 76.

Lantieri, C., Lamperti, R., Simone, A., Vignali, V., Sangiorgi, C., Dondi, G., and Magnani, M. (2017). Use of image analysis for the evaluation of rolling bottle tests results. International Journal of Pavement Research and Technology, 10(1), 45-53.

Liu, Y., Apeagyei, A., Ahmad, N., Grenfell, J., and Airey, G. (2014). Examination of moisture sensitivity of aggregate–bitumen bonding strength using loose asphalt mixture and physico-chemical surface energy property tests. International Journal of Pavement Engineering, 15(7), 657-670.

Lu, Q., and Harvey, J. T. (2006, August). Field investigation of factors associated with moisture damage in asphalt pavements. In 10th International conference on asphalt pavements (ISAP), Quebec, Canada (pp. 691-700).

Lukac, R., and Plataniotis, K. N. (2006). Color image processing: methods and applications. CRC press.

Lytton, R. L. (2004). Adhesive fracture in asphalt concrete mixtures. Course Notes.

MathWorks. (2019). "Look-Up Table" <https://www.mathworks.com/help/rptgenext/ug/lookuptable.html?searchHighlight=color%20look%20up%20table&s_tid=doc_srchtitle > (accessed Dec 02, 2017).

MacKay, D. J. (2003). Information theory, inference and learning algorithms. Cambridge university press.

Masad, E. A., Zollinger, C., Bulut, R., Little, D. N., and Lytton, R. L. (2006). Characterization of HMA moisture damage using surface energy and fracture properties (with discussion). Journal of the association of asphalt paving technologists, 75.

Masad, E., Arambula, E., Ketcham, R., Abbas, A., and Martin, A. E. (2007). Nondestructive measurements of moisture transport in asphalt mixtures. Asphalt Paving Technology-Proceedings, 76, 919.

Mehrara, A., and Khodaii, A. (2013). A review of state of the art on stripping phenomenon in asphalt concrete. Construction and Building Materials, 38, 423-442.

Merusi, F., Caruso, A., Roncella, R., and Giuliani, F. (2010). Moisture susceptibility and stripping resistance of asphalt mixtures modified with different synthetic waxes. Transportation Research Record: Journal of the Transportation Research Board, (2180), 110-120.

Ministry of Transportation of Ontario (2018) "Method of test for stripping by static immersion" <https://www.raqsb.mto.gov.on.ca/RAQS_Contractor/RAQSCont.nsf/viewContractorBulletinQualifiedLabsText/8F813018DDFE7AAD852572CE006B7CDA?OpenDocument> (May. 15, 2018).

Mohammad, L. N., Herath, A., and Huang, B. (2003). Evaluation of Permeability of Superpav® Asphalt Mixtures. Transportation research record, 1832(1), 50-58.

Mulsow, C., and Marschke, L. (2011). Multidirektionale reflexionsanalyse zur bestimmung des umhüllungsgrades von bitumenumhüllten gesteinskörpern. Strasse und Verkehr, 98(11), 27.

Nemati, H. R., Steiger, D. M., Iyer, L. S., and Herschel, R. T. (2002). Knowledge warehouse: an architectural integration of knowledge management, decision support, artificial intelligence and data warehousing. Decision Support Systems, 33(2), 143-161.

OpenCV library. (2017). "OpenCV (Open Source Computer Vision Library)." < Retrieved from https://opencv.org/

OpenCV. (2018). "OpenCV: Introduction to Support Vector Machines". < Retrieved from https://docs.opencv.org/3.4/d1/d73/tutorial_introduction_to_svm.htm> (accessed Mar 10, 2019)

Palit, S. K. (2001). An investigation on bituminous mixtures modified with reclaimed crumb rubber (Doctoral dissertation, IIT, Kharagpur).

Palit, S. K., Reddy, K. S., and Pandey, B. B. (2004). Laboratory evaluation of crumb rubber modified asphalt mixes. Journal of materials in civil engineering, 16(1), 45-53.

Paliukaitė, M., Vorobjovas, V., Bulevičius, M., and Andrejevas, V. (2016). Evaluation of different test methods for bitumen adhesion properties. Transportation Research Procedia, 14, 724-731.

Park, J. H., and Koumoto, T. (2004). New compression index equation. Journal of Geotechnical and Geoenvironmental Engineering, 130(2), 223-226.

Peterson, L. E., and Coleman, M. A. (2008). Machine learning-based receiver operating characteristic (ROC) curves for crisp and fuzzy classification of DNA microarrays in cancer research. International Journal of Approximate Reasoning, 47(1), 17-36.

Pizer, S. M., Amburn, E. P., Austin, J. D., Cromartie, R., Geselowitz, A., Greer, T., and Zuiderveld, K. (1987). Adaptive histogram equalization and its variations. Computer vision, graphics, and image processing, 39(3), 355-368.

Pundhir, N. K. S., Kamaraj, C., and Nanda, P. K. (2005). Use of copper slag as construction material in bituminous pavements.

Reinke, G., Glidden, S., Herlitzka, D., and Veglahn, S. (2010). PPA modified binders and mixtures: aggregate and binder interactions, rutting and moisture sensitivity of mixtures. Journal of the Association of Asphalt Paving Technologists, 79.

Ren, Z., and Anumba, C. J. (2004). Multi-agent systems in construction–state of the art and prospects. Automation in Construction, 13(3), 421-434.

Rombi, J. (2014). The use of Sardinian granite by-products from the Sarrabus Gerrei region to be used in road pavement layers (Doctoral dissertation, Universita'degli Studi di Cagliari).

Sasaki, G., Moriyoshi, A., Hachiya, Y., Noriyuki, N. (2006). New test method for moisture permeation in bituminous mixtures. Journal of the Japan petroleum institute, 49(1), 33-37.

Sethian, J. A. (1996). A fast marching level set method for monotonically advancing fronts. Proceedings of the National Academy of Sciences, 93(4), 1591-1595.

St Martin, J., Cooley Jr, L. A., and Hainin, H. R. (2003). Production and construction issues for moisture sensitivity of hot-mix asphalt pavements. In Moisture Sensitivity of Asphalt Pavements-A National SeminarCalifornia Department of Transportation; Federal Highway

Administration; National Asphalt Pavement Association; California Asphalt Pavement Alliance; and Transportation Research Board.

Szeliski, R. (2010). Computer vision: algorithms and applications. Springer Science and Business Media.

Taylor, M. A., and Khosla, N. P. (1983). Stripping of asphalt pavements: State of the art (discussion, closure) (No. 911).

Telea, A. (2004). An image inpainting technique based on the fast marching method. Journal of graphics tools, 9(1), 23-34.

Terrel, R. L., Scholz, T. V., Al-Joaib, A., and Al-Swailmi, S. (1993). VALIDATION OF BINDER PROPERTIES USED TO PREDICT WATER SENSITIVITY OF ASPHALT MIXTURES (WITH DISCUSSION). Journal of the Association of Asphalt Paving Technologists, 62.

Thelen, E. (1958). Surface energy and adhesion properties in asphalt-aggregate Systems. Highway Research Board Bulletin, (192).

Tunnicliff, D. G., and Root, R. E. (1982). ANTISTRIPPING ADDITIVES IN ASPHALT CONCRETE--STATE-OF-THE-ART 1981. In Association of Asphalt Paving Technologists Proceedings (Vol. 51).

Turner, D., Lucieer, A., and de Jong, S. (2015). Time series analysis of landslide dynamics using an unmanned aerial vehicle (UAV). Remote Sensing, 7(2), 1736-1757.

Wang, Y., Chen, Q., and Zhang, B. (1999). Image enhancement based on equal area dualistic sub-image histogram equalization method. IEEE Transactions on Consumer Electronics, 45(1), 68-75.

Wasiuddin, N. M. (2007). Effect of additives on surface free energy characteristics of aggregates and binders in hot mix asphalt (Doctoral dissertation).

Weinberger, K. Q., and Saul, L. K. (2009). Distance metric learning for large margin nearest neighbor classification. Journal of Machine Learning Research, 10(Feb), 207-244.

Wilcoxon, F. (1945). Individual comparisons by ranking methods. Biometrics bulletin, 1(6), 80-83.

Williams, R. C., and Breakah, T. M. (2010). Evaluation of Hot Mix Asphalt Moisture Sensitivity Using the Nottingham Asphalt Test Equipment.

Yuan, J., Dong, W. J., Chen, J. J., Zhang, S., Qian, W. B., and Sun, W. W. (2015). A LED-based measurement system for affinity between bitumen and aggregate. Construction and Building Materials, 81, 298-302.

Appendix

At the following tables the machine-measured results for different combinations of the classifiers are provided. The first table is related to house lab samples and the second table is respect to samples provided by the MTO.

Manual and different machine-measure estimations for house lab samples

ID	Manual	KNN4	KNN3	SVM4	SVM3
1	95%	90%	95%	90%	95%
2	95%	95%	95%	85%	95%
3	95%	100%	95%	100%	95%
4	100%	100%	100%	100%	100%
5	95%	100%	95%	100%	95%
6	95%	100%	100%	100%	100%
7	100%	100%	100%	95%	100%
8	100%	100%	100%	100%	100%
9	95%	100%	100%	100%	100%
10	95%	100%	100%	100%	100%
11	95%	100%	100%	100%	100%
12	90%	95%	95%	95%	95%
13	95%	100%	95%	100%	95%
14	85%	90%	90%	90%	90%
15	70%	85%	80%	85%	80%
16	85%	90%	90%	90%	90%

17	80%	90%	95%	90%	85%
18	50%	55%	55%	55%	55%
19	80%	75%	75%	75%	75%
20	80%	70%	70%	70%	70%
21	95%	100%	100%	100%	100%
22	95%	100%	95%	100%	95%
23	95%	100%	100%	100%	100%
24	95%	100%	100%	100%	100%
25	95%	100%	100%	100%	100%
26	95%	100%	100%	100%	100%
27	95%	100%	100%	100%	100%
28	95%	100%	100%	100%	100%
29	95%	100%	95%	100%	95%
30	95%	100%	100%	100%	100%
31	95%	100%	100%	100%	100%
32	90%	100%	95%	100%	95%
33	90%	100%	95%	100%	95%
34	100%	100%	100%	100%	100%
35	95%	100%	95%	100%	95%
36	95%	100%	95%	100%	95%
37	95%	100%	100%	100%	100%
38	90%	100%	100%	100%	100%
39	90%	95%	95%	95%	95%

40	85%	100%	95%	100%	95%
41	60%	50%	55%	50%	55%
42	70%	65%	65%	65%	65%
43	95%	95%	95%	95%	95%
44	95%	90%	100%	90%	100%
45	95%	100%	95%	100%	95%
46	95%	100%	95%	100%	95%
47	90%	75%	90%	75%	90%
48	90%	85%	95%	85%	95%
49	90%	90%	95%	90%	95%
50	100%	100%	100%	100%	100%
51	90%	95%	95%	95%	95%
52	95%	100%	95%	100%	95%
53	95%	100%	100%	100%	100%
54	90%	95%	95%	95%	95%
55	95%	100%	95%	100%	95%
56	95%	100%	95%	100%	95%
57	95%	100%	95%	95%	95%
58	95%	100%	100%	100%	100%
59	95%	100%	95%	100%	95%
60	95%	100%	100%	100%	100%
61	80%	90%	95%	90%	75%
62	70%	85%	75%	85%	75%

63	85%	90%	85%	90%	85%
64	80%	90%	80%	90%	80%
65	55%	60%	60%	60%	60%
66	40%	55%	60%	55%	60%
67	20%	45%	45%	45%	45%
68	50%	60%	60%	60%	60%
69	40%	55%	55%	55%	55%
70	30%	50%	50%	50%	50%

Manual and different machine-measure estimations for samples provided by MTO

ID	Manual	Semi-manual	KNN4
72	85%	80%	68%
73	85%	76%	82%
74	55%	55%	28%
75	70%	80%	62%
76	65%	70%	70%
77	60%	67%	50%
78	10%	24%	26%
79	10%	24%	29%
80	20%	29%	30%
81	25%	28%	15%
82	35%	33%	69%
83	40%	30%	61%
84	50%	37%	67%
85	65%	65%	44%
86	80%	72%	71%
87	85%	86%	48%
88	70%	72%	46%
89	70%	78%	78%
90	90%	88%	51%
91	100%	100%	78%
92	100%	100%	76%

93	45%	31%	64%
94	60%	54%	43%
95	25%	34%	40%
96	25%	31%	22%
97	65%	64%	34%
98	98%	88%	70%
99	98%	83%	71%
100	75%	65%	77%
101	75%	81%	49%
102	65%	55%	40%
103	70%	58%	46%
104	75%	75%	53%
105	80%	65%	73%
106	70%	74%	69%
107	70%	71%	36%
108	75%	73%	36%
109	80%	75%	39%
110	65%	51%	37%
111	65%	52%	40%
112	80%	65%	34%
113	85%	70%	78%
114	45%	44%	52%
115	50%	51%	74%

116	5%	20%	38%
117	60%	50%	66%
118	60%	53%	37%
119	15%	0%	39%
120	15%	0%	38%
121	60%	70%	77%
122	60%	86%	79%
123	55%	66%	45%
124	50%	39%	43%
125	80%	65%	78%
126	80%	81%	78%
127	50%	40%	41%